AD-A083 221 ORINCON CORP LA JOLLA CA F/G 17/7
A MULTI-TARGET SURVEY. VOLUME II.(U)
DEC 79 N00014-77-C-0296
UNCLASSIFIED OC-R-79-0296-1-VOL-2 NL

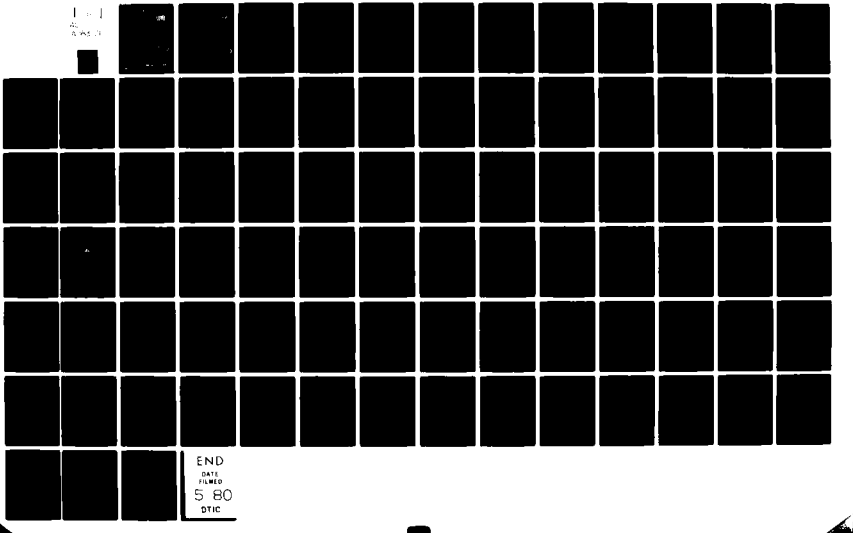

END
DATE FILMED
5 80
DTIC

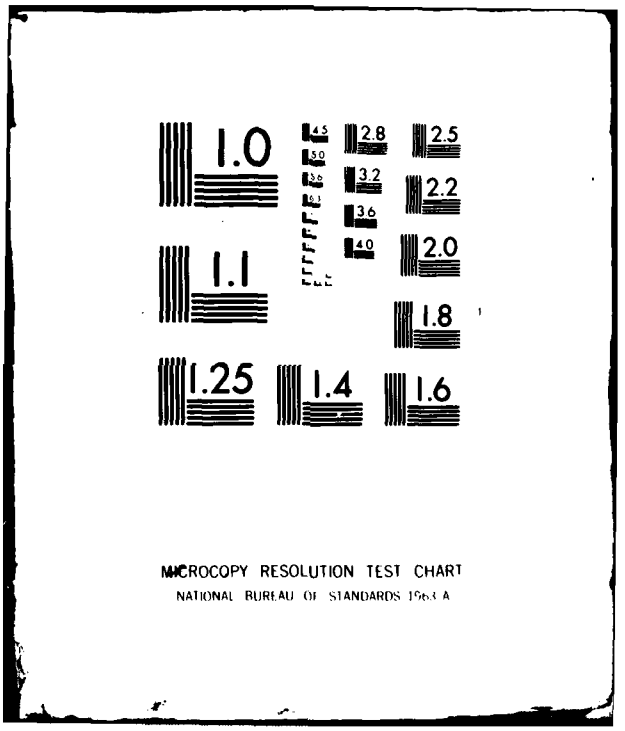
1.0
1.1
1.25
1.4
1.6
1.8
2.0
2.2
2.5
2.8
3.2
3.6
4.0
4.5
5.0
MICROCOPY RESOLUTION TEST CHART
NATIONAL BUREAU OF STANDARDS 1963 A

AD A083221

DTIC
ELECTE
S APR 21 1980 D
B

DISTRIBUTION STATEMENT A
Approved for public release;
Distribution Unlimited

DDC FILE COPY

80 4 17 162

Operations Research INformation CONtrol

ORINCON Corporation
3366 No. Torrey Pines Ct., Suite 320, La Jolla, CA 92037 (714) 455-5530

OC-R-79-0296-1-VOL2
December 1979

LEVEL III

Volume II

AD83220

FINAL REPORT.

A MULTI-TARGET SURVEY. Volume II.

Contract No. N00014-77-C-0296

12 85

Approved for public release;
distribution unlimited

DTIC
ELECTE
APR 21 1980
S D
B

Submitted to:

Office of Naval Research
Department of the Navy - Code 613B:NCM

Arlington, Virginia 22217

394776

80 1 21 002

Operations Research INformation CONtrol

VOLUME II

PUBLICATIONS CREDITED TO
ONR CONTRACT NO. N00014-77-C-0296

CONTENTS:

ACCESSION for
NTIS White Section
DDC Buff Section
UNANNOUNCED
JUSTIFICATION
BY
DISTRIBUTION/AVAILABILITY CODES
Dist. AVAIL. and/or SPECIAL
A

Operations Research INformation CONtrol ORINCON

DOCUMENT 1

A SCORE FOR CORRECT DATA ASSOCIATION IN MULTI-TARGET TRACKING

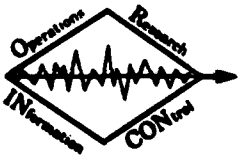

ORINCON

A SCORE FOR CORRECT DATA ASSOCIATION IN MULTI-TARGET TRACKING

D. L. Alspach and R. N. Lobbia
ORINCON CORPORATION
La Jolla, California 92037

SUMMARY

In the real-world multi-target tracking problem, there exists the possibility for many things to go wrong. Typical problems which arise include: too few tracks are formed; too many tracks are formed (false tracks); and inaccurate position, course, and speed estimates are reported. The above difficulties are often the result of incorrect allocation of data to individual tracks. Algorithms, while estimating the motion of a given target, inadvertently mix in clutter and/or measurements from another target. In order for correct allocation of data to a given track to be made, one must have an effective scoring formula; that is, some means of determining how likely a given assignment of data is. To be effective, a scoring formula must produce (on the average) a better score for correct assignments than for incorrect assignments. Information useful in the scoring process includes a priori intelligence data (such as initial target locations), models of target motion, models of the transmission channel, and expected moments of clutter for the sensor gain setting being used. Basically, the score is derived from the residuals which come out of the processing of a batch of data with the extended Kalman filter. This is used to evaluate the likelihood of potential tracks. Although the "likelihood" has an intuitive meaning, the term is used here to mean the probability density function $p(\lambda)$ of the track λ. The expected cost of a given assignment is derived with the theory of extremals being used to obtain the expected cost of adding a clutter point in a track. The resulting expected cost is then shown to behave in a quantitative fashion and this can be visualized from a geometric viewpoint.

1. INTRODUCTION

In the last few years a number of approaches to the problem of tracking multiple targets in a cluttered environment have been published. Some aspects of the problem that have been considered in some subsets of these publications include the problem of false alarms or missing measurements, track initialization, multiple measurement types (MSI) and target classification.

Many of the so-called multi-target trackers described in the open literature really deal only with the problem of one target in clutter. This hypothesis of only one target can greatly restrict the viability of a multi-target tracker to sort out confused situations.

Of the trackers that have been proposed, and in some cases implemented, one can see certain similarities and differences which allow the trackers to be grouped into certain classes. The grouping and certain applications of these groups has led to the following thoughts.

Perhaps the most fundamental aspect of a tracker is how it handles and interacts with the data. The data is after all our handle on the real world and all the information we have about a specific tracking realization is contained in the data. A second fundamental aspect of the multi-target tracking in clutter problem is that of alternate hypotheses. It is possible to derive the probability distribution of tracks and clutter points if one carefully specifies the a priori probability base, i.e., the probabilistic target models, probabilistic measurement models, etc. In very simple cases where one can get the optimal solution, one finds this consists of all possible configurations of the data into the sets. In each configuration each data set represents a possible alternate track or the set of clutter points. A probability measure is assigned to each possible total surveillance region picture. This globally optimal approach is generally not reasonable for implementation and approximate or suboptimal approaches must be considered.

Several approaches focus entirely on the construction of the sets of data (the construction of feasible tracks). It is this latter philosophy that is being addressed in this paper.

Conceptually, using maximum likelihood techniques, various combinations of data are tried and then "scored" using log-likelihood functions. The best fit to the target model gets the lowest score and this is considered to be one of the tracks in the region if no other low score track competes for the same measurements. If two or more targets compete for the same measurements, several situations can occur. These include the possibilities that the two targets are lumped together, one target is rejected, the targets get mixed with track points assigned to clutter and two "bad" tracks reported, or the case that all points are assigned to clutter. It is possible, though perhaps not normal, to find situations where the choice of the best nonoverlapping feasible track does not correspond to a best surveillance picture. This is quite easy to do if the tracks overlap and compete for the same measurements.

Many trackers consider alternate hypotheses as far as assigning measurements to a track. However, once a decision has been made that a measurement belongs with another group of measurements, this decision is not re-examined. Once the decision has been made to assign a piece of data to a "track," that decision is final. This is done because the system usually requires "an answer." Also, there is always new data coming into the tracker allowing new hypothesis tests. In addition, there is a limited amount of computer response. One could say that the hypothesis testing is directed to make a decision on the proper surveillance picture or that the tracker is "decision directed."

In the next section, we will see how effective scoring algorithms are developed—ones which can handle the alternate scenarios posed above. Following this, in Section 3, a refinement to this scoring algorithm is proposed and it is seen that the average cost incurred for assigning measurements to tracks can be visualized from a geometrical viewpoint. In particular, it will be shown quantitatively that there exists a unique number of points (measurements) in a given track that yields an average minimum cost. Incorrectly assigning clutter points to this track and wrongly assigning points to clutter will, on the average, increase the cost in a well-defined manner.

2. SCORING ALGORITHMS

In order for a correct assignment of measurement data to a given track to be made, we must have an effective scoring formula, i.e., some means of determining how likely a given assignment of data is. To be effective, a scoring formula must produce (on the average) a better score for correct assignments than for incorrect assignments. Information useful in the scoring process includes a priori intelligence data (such as initial target locations), models of target motion, and expected amounts of clutter for the sensor gain setting being used. Basically, the score is derived from the residuals which come out of the processing of a batch of data with the extended Kalman filter. This is used to evaluate the likelihood of potential tracks. Although "likelihood" has a useful intuitive meaning, we use the term to mean the probability density function $p(\lambda)$ of the track λ. The concepts we use are well-known, since most of the work in estimation theory pertains to situations where all the observations $Z = \{z_1, z_2, \cdots, z_n\}$ are due to a single target. An obvious example is the stochastic linear system

$$x_{k+1} = A_k x_k + B_k u_k, \qquad k = 0, 1, \cdots, n, \tag{1}$$

$$z_k = C_k x_k + v_k, \qquad k = 1, \cdots, n, \tag{2}$$

with states $\{x_k\} \subset R^x$, observations $\{z_k\} \subset R^z$, process noise $\{u_k\} \subset R^u$ and measurement noise $\{v_k\} \subset R^v$. A_k, B_k, C_k are matrices of appropriate dimension that may vary with time. The initial state x_0 is a Gaussian random vector with covariance P_0, independent of the processes $\{u_k\}$ and $\{v_k\}$, which are themselves zero mean white Gaussian noise with covariances $\{Q_k\}$ and $\{R_k\}$. Under these assumptions, the well known Kalman equations provide minimum variance unbiased estimates $\{\hat{x}_k\}$ of the states based on all past data:

$$\hat{x}_{k+1} = A_k \hat{x}_k + K_k(z_{k+1} - C_{k+1} A_k \hat{x}_k), \tag{3}$$

$$K_k = \bar{P}_k C_{k+1}^t (C_{k+1} \bar{P}_k C_{k+1}^t + R_{k+1})^{-1}, \tag{4}$$

$$\bar{P}_k = A_k P_k A_k^t + B_k Q_k B_k^t, \tag{5}$$

$$P_{k+1} = (I - K_k C_{k+1}) \bar{P}_k, \quad k = 0, 1, \cdots, n. \tag{6}$$

When nonlinear measurements are involved, a simple linearization process (the extended Kalman filter) is used. The equations remain exactly the same, except that the term

$$z_{k+1} - C_{k+1} A_k \hat{x}_k \tag{7}$$

in the first equation above is replaced by

$$z_{k+1} - h_{k+1}(A_k \hat{x}_k), \tag{8}$$

where $h_{k+1}(\cdot)$ denotes the nonlinear relabionship between the measurements and state vector, and the C_k-matrix becomes

$$C_k = \left. \frac{\partial h_k(x)}{\partial x} \right|_{A_k \hat{x}_{k-1}} \tag{9}$$

It is natural to compute the likelihood function $p(\lambda)$ for the track $\lambda \subset Z$ based on the Kalman filter state estimates. The innovations sequence is an integral part of this computation, which is a sequence of the measurement residuals:

$$\delta_{k+1} = z_{k+1} - C_{k+1} A_k \hat{x}_k, \quad k = 0, 1, \cdots, n. \tag{10}$$

The (negative) log likelihood function is given in terms of $\{\delta_k\}$ by

$$c(\lambda) = n\dim(z) \ln 2\pi + \frac{1}{2} \sum_{k=1}^{n} \ln |V_k| + \frac{1}{2} \sum_{k=1}^{n} \delta_k^t V_k^{-1} \delta_k. \tag{11}$$

The covariance matrix for the measurement residual, V_k, can be computed directly:

$$V_k = C_{k+1} \bar{P}_k C_{k+1}^t + R_{k+1}, \quad k = 1, 2, \cdots, n. \tag{12}$$

Each feasible track is the result of a hypothesis test that uses the track likelihood function $p(\lambda)$ (or equivalently, the negative log likelihood $c(\lambda)$) determined from the Kalman filter. Since the density function of the alternative hypothesis (that λ is not a track) is unknown, the decision rule is simply

$$-c(\lambda) = \ln p(\lambda \mid \{\hat{x}_k\}_{k=1}^n) \geq a_n \rightarrow \lambda \in F, \tag{13}$$

$$-c(\lambda) = \ln p(\lambda \mid \{\hat{x}_k\}_{k=1}^n) < a_n \rightarrow \lambda \notin F. \tag{14}$$

Based on the log likelihood decision function, the feasible track set is

$$F = \left\{ \lambda \mid \lambda \text{ Zm } \ln p(\lambda \mid \{\hat{x}_k\}_{k=1}^n) \geq a_n \right\}. \tag{15}$$

Primarily, the only random component of $c(\lambda)$ is

$$\Sigma \delta^t V^{-1} \delta, \tag{16}$$

which for real tracks is a chi-squared random variable with n - dimension (z) degrees of freedom.* Therefore, error probabilities can easily be computed for the hypothesis test to predict the accuracy of feasible track construction. This has a critical impact on the ultimate accuracy of the tracking algorithm, since a real track mistakenly exclused from F cannot be used in the subsequent Bayesian decision process.

*Due to the random nature of the measurement arrival time and of the sensor which senses "the next measurement," the development of V_k is also random in nature but it is hard to compare its meaning from one realization to the next.

Before any new point is added to a partial track, it should pass a coarse test,

$$\|\delta_k\|_\infty \leq \beta_k \tag{17}$$

a fine test,

$$\delta_k^t V_k^{-1} \delta_k < \gamma_k \tag{18}$$

and, finally, the likelihood test. The coarse test checks the magnitude of the maximum component of the vector $\delta_k \in \mathbb{R}^2$ against β_k, and is included because it is computationally cheaper to perform than the fine test. The constants β_k and γ_k can be chosen so that

$$\left\{ z_k \mid \delta_k^t V_k^{-1} \delta_k < \gamma_k \right\} \left\{ z_k \mid \|\delta_k\|_\infty < \beta_k \right\}. \tag{19}$$

One difficulty with this approach is that because of the "deterministic" terms in the likelihood function

$$n\,dm(z) \ln 2\pi + \frac{1}{2} \sum_{k=1}^{n} \ln |V_k| \tag{20}$$

it is difficult to compare some of the tracks of different length. It is also difficult to assess the absolute goodness of a score. Therefore, an alternate score with a more absolute meaning can be defined. This is described in the next section.

3. REFINED SCORING

For track i at stage k define the stagewise chi-squared score

$$S_k^i = (z_k^i - \hat{z}_k^i)^T V_k^{-1} (z_k^i - \hat{z}_k^i). \tag{21}$$

This has the features—if all measurements have been assigned to the correct targets and all filter parameters chosen corfectly—that

$$E\{S_k^i\} = E\{S_k\} = 2 \tag{22}$$

$$E\{(S_k - 2)^2\} = 4 \tag{23}$$

$$\sigma_{S_k} = 2 \tag{24}$$

$$f(S) = e^{-S/2} U(S); \quad \begin{matrix} U(S) = 0, & S < 0 \\ U(S) = 1, & S \geq 0 \end{matrix} \tag{25}$$

where $E\{\cdot\}$ indicates the expected value operator, σ_{S_k} is the standard deviation of S_k, and $f(S)$ is the appropriate density function for a two-dimensional random variable S. Define the cumulative chi-squared score as

$$S^i = \sum_{k=1}^{n_i} S_k^i. \tag{26}$$

For easy evaluation on a single track an evaluation cost that would be quite meaningful would be

$$C_i = \frac{1}{N_i} S^i. \tag{27}$$

For this cost function the statistical parameters are

$$E(C_i) = 2 \tag{28}$$

$$E\left((C_i - 2)^2\right) = 4/N_i \qquad \sigma_{C_i} = 2/N_i^{1/2} \tag{29}$$

$$f_C(y) = \frac{1}{2^{N_i} \Gamma(N_i)} y^{(N_i - 1)} e^{-y/2} U(y). \tag{30}$$

For display purposes the use of C_i as a value measure of a single track makes a great deal of intuitive sense.

Values of $C_i \ll 2$ for reasonable length tracks tend to imply that the filter parameters are set too loose. Thus, by reducing Q_k and/or R_k, one could obtain tighter tracks. Tracks for which $C_i \gg 2$ clearly represent bad data assignment which should not be kept. More precisely, if

$$C_i \rightarrow 2 + \sigma 2/N_i^{1/2} \tag{31}$$

when $\sigma = 3$ (for a 3-sigma case) indicates either that incorrect data has been assigned to the track or that the filter parameters (Q,R) are too small. While

$$C_i < 2 - \sigma 2/N_i^{1/2}, \quad N_i > 3 \text{ for } \sigma = 3 \tag{32}$$

indicates that the filter parameters (Q,R) are set too large.

For a total surveillance region picture of M measurement points and L tracks, one has:

Track No.	Score	Number of Points in Track
1	C_1	N_1
2	C_2	N_2
.	.	.
.	.	.
.	.	.
L	C_L	N_L

The score for the total area should be made up of these scores and the cost for assigning a point to clutter. The number of points in clutter is N_C, the number of points assigned to targets is N_P, and the total number of measurements are M. These are related by

$$M = N_C + N_P \qquad N_P = \sum_{i=1}^{L} N_i \,. \tag{33}$$

A meaningful score could be defined as:

$$S = \sum_{i=1}^{L} N_i C_i + N_C S_C \tag{34}$$

where S_C is a score defined for a clutter point. If all the measurements are correctly assigned to the track:

$$E(S) = 2 \sum_{j=1}^{L} N_i + N_C S_C \tag{35}$$

$$= 2(M - N_C) + N_C S_C \,. \tag{36}$$

If we define the clutter score, S_C, and a total surveillance score as

$$C = \frac{1}{M} S \tag{37}$$

where, if all the measurement points belong to the track,

$$E(C) = \frac{1}{M} E(S) = \frac{1}{M} [2(M - N_C) + N_C S_C] \tag{38}$$

$$E(C) = 2 \frac{M-N_C}{M} + \frac{N_C}{M} S_C \tag{39}$$

so that a plot of the score for a global surveillance region for a real case of N_P measurements assigned to N^* targets with all points assigned correctly and N_C clutter points can be geometrically described by Figure 1.

The curve from N=0, that is, all points assigned to clutter, to $N=N_P$, the correct number of points assigned to clutter, is just a straight line described by:

$$E(S) = \frac{2(M-N_C)}{M} + \frac{N_C}{M} S_C \,. \tag{40}$$

where

N_C varies from M to $M-N_P$.

Beyond the point ($N=N_P$), a clutter point must be assigned to the track (assuming just one track in clutter). The cost to assign a single clutter point to the track can be calculated in the following manner: A given track will project to a given point in measurement space. For example, consider the two-dimensional measurement vector (τ, θ) described in Figure 2.

If a clutter point is added to the track, the increase in score on the track will be given by Equations (21) and (37). The difference is that now the value of the score can be written as

$$C = \frac{S}{M} = \frac{1}{M} \left\{ \underbrace{\sum_{i=1}^{L} N_i C_i}_{\text{assume all track points are properly assigned}} + (N_C - 1) S_C + C_1^c \right\} . \tag{41}$$

Here C_1^c is the cost for assigning one clutter point to the track. C_1^c is a random variable and its distribution depends on the distribution of the clutter points. From Equation (21),

$$C_1^c = (z_k^c - \hat{z}_k^i) V_k^{-1} (z_k^c - \hat{z}_k^i) \tag{42}$$

where z_k^c are the τ, θ points for the clutter point. The distribution of this random variable depends on the random nature of the clutter.

If the distance of the clutter point from the predicted point is assumed to be Gaussian in τ and θ with zero mean, the distance from the predicted point will be Rayleigh distributed and the cost or score C_1^c, the weighted square of the distance (42), will have an exponential density

$$f_{C_1}(c) = \frac{1}{2\sigma^2} e^{-c/2\sigma^2} u(c); \qquad \begin{matrix} u(c) = 0, c < 0 \\ u(c) = 1, c \geq 0 \end{matrix} \tag{43}$$

where σ^2 is a measure of the dispersion of the clutter points with respect to the mid- or tracker-predicted point. The uncertainty, σ, takes into account the unequal variance in τ and θ and is given by:

$$\sigma^2 = \frac{(\text{range of } \theta \text{ in surface})(\text{range of } \tau \text{ in surface})}{\sigma_\theta \sigma_\tau} \tag{44}$$

The score for the closest clutter point to a point predicted by the tracker (closest in the sense of having the smallest score defined by (42)) will be distributed as follows (x = score of the closest point):

$F_x(x)$ = probability that the closest clutter point out of N_C having a score less than or equal to x.

$$F_x(x) = 1 - e^{-x/2\sigma^2} . \tag{45}$$

From the theory of extremals, it is obvious that this distribution is identical to the probability distribution of the event defined below,

$F_x(x)$ = {probability that all of the N_C clutter points have scores less than or equal to x}

or

$F_x(x)$ = 1 - {probability that all N_C clutter points have scores greater than x}

From (43), it follows that the probability that the score of any one of the N_C clutter points being greater than x is given by:

$$e^{-x/2\sigma^2} . \tag{46}$$

Assuming the clutter points are independent of one another, the probability that all of the N_C clutter points have scores greater than x is given by

$$e^{-N_C x/2\sigma^2}$$

and the probability that all of these clutter points have scores less than or equal to x is:

$$1 - e^{-N_C x/2\sigma^2} \tag{47}$$

and density function:

$$f_x(x) = \frac{N_C}{2\sigma^2} e^{-N_C x/2\sigma^2} \quad (48)$$

The expected value of the cost of assigning the closest clutter point to a track is then given by:

$$E(x) = \int_{-\infty}^{\infty} x f(x)\, dx = \frac{2\sigma^2}{N_C} . \quad (49)$$

The expected cost for assigning the next nearest point to a track is

$$\frac{2\sigma^2}{(N_C - 1)} \quad (50)$$

and, finally, the expected cost for adding the k^{th} closest clutter point out of N_C to a track is given by:

$$\frac{2\sigma^2}{N_C + 1-k} . \quad (51)$$

Note that in computing the expected value of the total cost function defined in (41), one must also account for the linear decrease in cost caused by the decreasing weighting coefficient (N_C-k) on S_C when k clutter points are incorrectly assigned to tracks. This amounts to a decrease of S_C/M for every clutter point assigned to a track. Therefore, the net increase in the expected cost by assigning the k closest clutter points out of N_C to tracks is given by:

$$\frac{1}{M}\left\{\sum_{j=1}^{k} \frac{2\sigma^2}{N_C + 1-j} - kS_C\right\} . \quad (52)$$

In effect, this is the sum of an increasing hyperbolic function and a decreasing linear function.

Since, on the average, $\sigma^2 >> S_C$, the shape of the right-hand side of the curve in Figure 1 is concave and monotonically increasing.

Note the two regions of this figure. In one part fewer points are assigned to tracks than actually are available, i.e., too many detections were missed. In the other half of the figure, false alarms or clutter points were assigned to tracks. In both parts of the curve the assumption is made that the data association is done in an optimal manner on the average. Thus, if a clutter point is added to a track, it is the clutter point that lies "closest" to a track of those unassigned. The curve also assumes that all measurements correctly assigned as track points are assigned to the correct track. Wrong assignments of data would, of course, make for even worse scores "on the average."

4. CONCLUSIONS

In the last section, it was shown that the refined scoring algorithm possesses appealing properties from a geometric viewpoint. There exists a unique number of points in a track that results in lower average cost than any other number. Also, the sensitivity of the score to variations in assigned number of track points can be controlled by the clutter score, S_C. This is readily apparent from Figure 1.

This scoring algorithm is therefore a very useful approach in extracting clutter points out of a given target track.

The algorithm is currently being applied to an ocean surveillance problem and the results of this are very encouraging. For a given data set having a false alarm rate of 10^{-4}, i.e., one clutter point in every 10^4 measurements, using the refined scoring algorithm defined in Section 3, we have found that we can effectively decrease this false alarm rate to 10^{-7}. This represents a three-order-of-magnitude decrease and, hence, the detection capabilities of the tracking algorithm have been significantly enhanced.

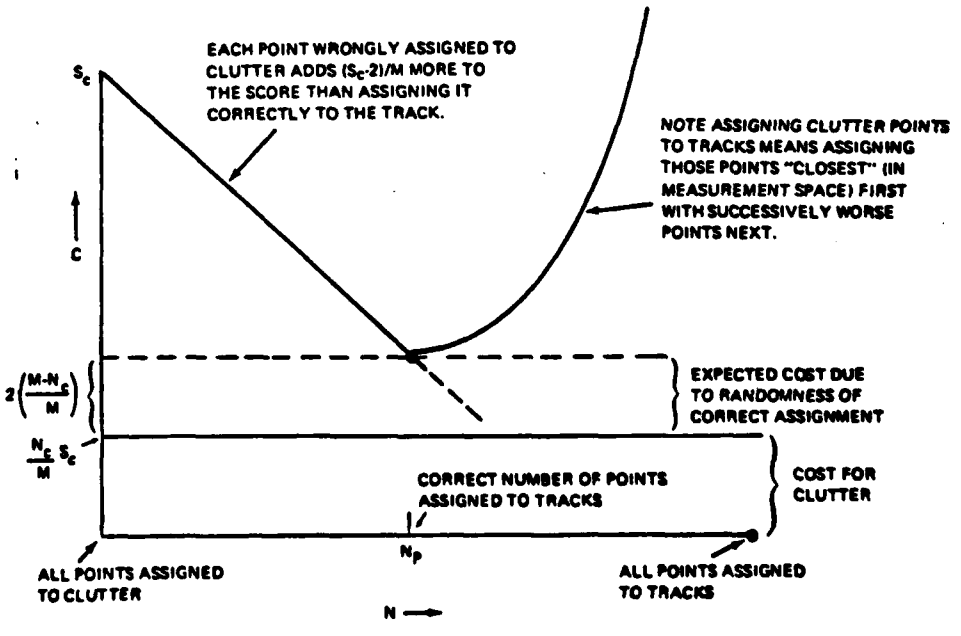

Figure 1. Geometrical description of refined scoring algorithm.

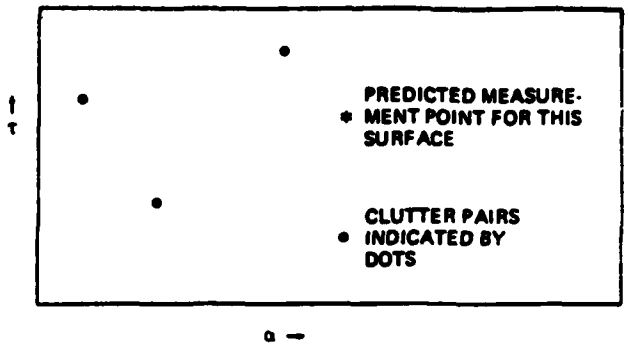

Figure 2. Two-dimensional measurement space.

This work was partially supported by ONR Research Contract No. N00014-77-C-0296.

DOCUMENT 2

SOUND SPEED ESTIMATION AS A MEANS OF IMPROVING TARGET TRACKING PERFORMANCE

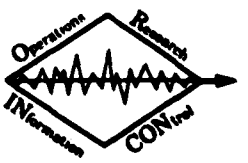

ORINCON

SOUND SPEED ESTIMATION AS A MEANS OF IMPROVING TARGET TRACKING PERFORMANCE

D. L. Alspach
ORINCON Corporation
La Jolla, California 92037

G. Mohnkern
Naval Ocean Systems Center
San Diego, California 92152

R. N. Lobbia
ORINCON Corporation
La Jolla, California 92037

Summary

This paper addresses the issue of target tracking when confronted with a set of sound speed parameters that are partially or completely unknown. It explores the case where these parameters are augmented to the target state in an extended Kalman filter. The filter processes measurements of sound time-of-arrival difference and Doppler difference from a set of spatially displaced sensors.

For scenarios involving up to three sensors it has been found that biased target position estimates and marginal system observability occurs. This is readily verified by propagating the eigenvalues of the information matrix in time. Using this as an analysis tool, a number of geometrical sensor configurations are analyzed.

In general, it is found that with three sensors, the system is, at best, marginally observable for any geometry. However, when using four and more sensors, system observability and estimation performance are markedly improved when two of the sound speed filter parameters are specified to within a close tolerance of their actual values. When attempting to estimate all of the sound speeds (or for that matter (n-1) sound speeds, n = number of sensors), it is again noted, as in the three-sensor case, that system observability and estimation performance become degraded.

1. Introduction

In a target tracking application, one reason for poor estimation performance can be a lack of knowledge concerning the parameters of the mathematical model that relates the target state to the measurements. Since a mathematical model is a necessary ingredient to any target tracker or state estimator, use of incorrect parameters could lead to estimates that diverge from "truth" over a period of time.

It is this problem that is dealt with in this paper. More specifically, it involves a target tracking problem where measurements of time difference and Doppler difference are collected from pairs of spatially displaced sensors. The central issue is that the sound speeds from the target to each of these sensors are partially or completely unknown. These speed parameters appear in the mathematical model relating the target state to the measurements. To avoid biased target tracks, some mechanism should be found to accommodate these parameter uncertainties.

The material in this paper is basically an extension of an earlier work [1] and is more conclusive in terms of the results that were obtained for a number of different geometric scenarios involving sensor placements and target location.

We will start our discussion in Section 2 by describing the mathematical model for the given process and proceed to define an estimator that can accommodate both unknown sound speeds and the target state vector. All of the simulation results will be presented in Section 3. In addition, we will also show how we can assess system observability via the information matrix. This will play a useful role in exploring system observability for a number of different target/sensor geometric scenarios.

From the simulation results it will be seen that a minimum number of sensors are needed and, in addition, two of the sound speeds must be known correctly before accurate estimation of the target state can be achieved.

Finally, in Section 4, a summary of the results and conclusions will be presented.

2. System Definition

One area where the uncertain model parameter problem could arise is depicted in Figure 1. It could equally well apply to tracking of vehicles on the Earth via geophones or any place that the signal does not travel with an infinite effective or known velocity. We have a set of i spatially displaced sensors (distance to target = R_i). If the target generates or reflects sound at time instant, t, because of the sound travel time to each sensor (sound speed = c_i), it will be sensed at each sensor at times $t_1,t_2,\ldots,t_i$. In addition, if the target moves at a velocity, v, the Doppler sensed at each sensor will be different. To estimate the target state, i.e., position, speed, and course, measurements of sound time-of-arrival difference and Doppler difference for a sensor pair i-j (i,j=1,2,3,...,i≠j) can be processed through a Kalman filter. Using spherical geometry, these measurements can be related to the target state by the following equations [1]:

$$\tau_{ij} = t_i - t_j = \frac{R_i}{c_i} - \frac{R_j}{c_j} \tag{1}$$

$$f_{ij} = f_i - f_j = \left(-\frac{\dot{R}_i}{c_i} + \frac{\dot{R}_j}{c_j} \right) f \tag{2}$$

where

$$R_i = \cos^{-1}[\sin x_1 \sin\lambda_i + \cos x_1 \cos\lambda_i \cos(x_2 - \theta_i)] \tag{3}$$

$$\dot{R}_i = \frac{x_3[\sin x_1 \cos\lambda_i \cos(x_2-\theta_i) - \cos x_1 \sin\lambda_i]}{\sin R_i} + \frac{x_4 \cos x_1 \cos\lambda_i \sin(x_2-\theta_i)}{\sin R_i} \tag{4}$$

In the above equations, $x_i, i=1,2,3,4$ represents the target latitude, longitude, latitude rate, and longitude rate, respectively. The latitude and longitude of hydrophone i is λ_i and θ_i. An implicit assumption in (4) is that the sensors are stationary.

Throughout the paper we will take the target state vector to be $\underline{x}^T = [x_1,x_2,x_3,x_4]$. The reason for doing this is that target motion can be described by a linear set of equations. In discrete-time form, the equations for the target dynamics are given by:

$$\underline{x}(k+1) = \underbrace{\begin{bmatrix} 1 & 0 & \Delta t & 0 \\ 0 & 1 & 0 & \Delta t \\ 0 & 0 & 1 & 0 \\ 0 & 0 & 0 & 1 \end{bmatrix}}_{\Phi(\Delta t)} \underline{x}(k) + \underbrace{\begin{bmatrix} w_1(k) \\ w_2(k) \\ w_3(k) \\ w_4(k) \end{bmatrix}}_{\underline{w}(k)} \tag{5}$$

where Δt = sampling interval; i.e., the time between measurements of τ_{ij}, f_{ij}; $w(k)$ is a zero-mean, white noise vector sequence that perturbs the target from otherwise constant course/speed motion; and where

$$E\{\bar{w}(k)\,\bar{w}^T(j)\} = Q_k\,\delta_{kj}\ .$$

It is a simple matter to display speed and course at any time by using the equations below:

$$\text{SPEED} = \sqrt{x_3^2 + x_4^2\cos^2 x_1} \tag{6}$$

$$\text{COURSE} = \tan^{-1}\left(\frac{x_4 \cos x_1}{x_3}\right) \tag{7}$$

Since the measurement model is nonlinear (eq. 1-4), one can implement an extended Kalman filter to track or obtain estimates of the target state vector, $\hat{x}(k)$. This is easily done by linearizing the measurement equations about the most current state estimate, $\hat{x}(k)$, to obtain a linear measurement equation, $H(\hat{x}(k))$. The equations for the filter are standard [2] and are summarized below:

$$\hat{x}(k+1/k) = \phi(\Delta t)\,\hat{x}(k/k) \tag{8}$$

$$P(k+1/k) = \phi(\Delta t)\,P(k/k)\,\phi^T(\Delta t) + Q_k \tag{9}$$

$$\hat{x}(k+1/k+1) = \hat{x}(k+1/k) + k_{k+1}[z(k+1) - h(\hat{x}(k+1)/k))] \tag{10}$$

$$P(k+1/k+1) = [I - k_k H(\hat{x}(k+1/k))]\,P(k+1/k) \tag{11}$$

$$K_{k+1} = P(k+1/k)\,H(\hat{x}(k+1/k))\,[H(\hat{x}(k+1/k))\,P(k+1/k)\,H^T(\hat{x}(k+1/k)) + R_k]^{-1} \tag{12}$$

where

$$z^T(k) = [\tau_{ij}(k),\ f_{ij}(k)]$$

$$h^T(\hat{x}(k+1/k)) = [\hat{\tau}_{ij}(k),\ \hat{f}_{ij}(k)] = \left[\left(\frac{\hat{R}_i}{c_i} - \frac{\hat{R}_j}{c_j}\right),\ f\left(\frac{\dot{\hat{R}}_i}{c_i} - \frac{\dot{\hat{R}}_j}{c_j}\right)\right] \tag{13}$$

R_k = covariance matrix of additive white noise that contaminates $z(k)$

$$H(\hat{x}(k+1/k)) = \left.\frac{\partial h(\bar{x}(k))}{\partial \bar{x}(k)}\right|_{\bar{x}(k)\,=\,\hat{x}(k+1/k)} \tag{14}$$

From (1), (2), (13), and (14) it is easy to see how sound speed, c_i, enters into the measurement model. In [1], it was shown that when incorrect values of c_i were used in the filter model (assuming one did not know the true c_i), the resulting state estimates were found to be biased off from the true target state. In some cases these biases were significant, and consequently the deviation from truth was as significant.

To compensate for this problem, the sound speeds were treated as additional state variables and augmented to the target state. Since the sound speeds were constant over the estimation interval, the state dynamics were simply defined by $\dot{c}_i = 0$. The extended Kalman filter was then implemented for this augmented state vector to generate estimates of both the target state and the unknown sound speeds.

In the next section, we will summarize some of the earlier results that were obtained and then present more exhaustive results that indicate a definite trend occurring.

3. Simulation Results

To examine the effects of estimating unknown sound speeds, we selected a number of different cases involving different target motion scenarios and three-sensor configurations as shown in Figure 2.

The locations of the sensors are defined in Table 1 and the target motion scenarios (cases 1-24) are summarized in Table 2.

Table 1. Location of sensors.

Array	Latitude, λ	Longitude, ℓ
1	5 deg	0 deg
2	-2.5 deg	4.33 deg
3	-2.5 deg	-4.33 deg

Table 2. Target motion scenarios.

Case Number	Starting Position Latitude	Longitude	Speed	Course
1	.5 deg	.5 deg	10 knots	0 deg
2	↓	↓	↓	90 deg
3	↓	↓	↓	180 deg
4	↓	↓	↓	270 deg
5	2.5 deg	0 deg	↓	0 deg
6	↓	↓	↓	90 deg
7	↓	↓	↓	180 deg
8	↓	↓	↓	270 deg
9	-1.3 deg	0 deg	↓	0 deg
10	↓	↓	↓	90 deg
11	↓	↓	↓	180 deg
12	↓	↓	↓	270 deg
13	-1.3 deg	-2.0 deg	↓	0 deg
14	↓	↓	↓	90 deg
15	↓	↓	↓	180 deg
16	↓	↓	↓	270 deg
17	0 deg	2 deg	↓	0 deg
18	↓	↓	↓	90 deg
19	↓	↓	↓	180 deg
20	↓	↓	↓	270 deg
21	0 deg	-4 deg	↓	0 deg
22	↓	↓	↓	90 deg
23	↓	↓	↓	180 deg
24	↓	↓	↓	270 deg

We made the following assumptions:

(a) The covariance matrix of the discrete-time process dynamics was defined by:

$$Q(k) = \begin{bmatrix} q_{33}^2\frac{\Delta t^3}{3} & 0 & q_{33}^2\frac{\Delta t^2}{0} & 0 \\ 0 & q_{44}^2\frac{\Delta t^3}{3} & 0 & q_{44}^2\frac{\Delta t^2}{2} \\ q_{33}^2\frac{\Delta t^2}{2} & 0 & q_{44}^2\,\Delta t & 0 \\ 0 & q_{44}^2\frac{\Delta t^2}{2} & 0 & q_{44}^2\,\Delta t \end{bmatrix}$$

where $q_{33}^2 = q_{44}^2 = (.0091827)^2$ knots/sec is the power spectral density of the random noise perturbing the velocity state equations of the continuous system. This randomness in the target velocity for the continuous system translates both into a position and velocity uncertainty in the equivalent discrete-time model. The values of q_{33} and q_{44} roughly correspond to a standard deviation of .34 nautical miles in position and .6 knot in velocity over a time interval of one hour in the discrete-time model.

(b) The measurement matrix covariance matrix was defined by:

$$R(k) = \begin{bmatrix} r_{11}^2 & 0 \\ 0 & r_{22}^2 \end{bmatrix}$$

(c) Δt=300 sec was the nominal time interval between measurements.

(d) The filter processed measurements from the sensor pairs in a sequential manner starting with sensor pair 1-2, 1-3, 2-3, 1-2, 1-3, ..., etc.

(e) The sound speeds from the target to each of the sensors were chosen as [3]:

c_1 = 4857 ft/sec

c_2 = 4850 ft/sec

c_3 = 4870 ft/sec

We started out by assuming that: first, only one of the three sound speeds was unknown and consequently was estimated along with the target state; second, two sound speeds were unknown and were estimated along with the target state; and third, all three sound speeds were unknown and estimated along with the target state. In all of these cases, it was found that biased estimates were generated by the tracker. A typical example of this is shown in Figures 3, 4, and 5 where an attempt was made to estimate the unknown sound speeds and the target state. The solid curves represent the truth model whereas the dashed curves represent the state estimates. Note the significant biases in latitude and longitude in two of the sound speeds.

Because of these biases, it was decided to examine the observability of the system for all of the cases defined in Table 2. This is easily done with the aid of the information matrix [2]. For the case involving no process noise and state vector a priori information, the information matrix is identical to the inverse of the Kalman filter covariance matrix, $P^{-1}(k/k)$. This matrix must be positive definite for stochastic observability and, provided the above conditions apply, is given in recursive form by:

$$P^{-1}(k/k) = \phi^T(-\Delta t)\, P^{-1}(k-1/k-1) \quad (-\Delta t)$$
$$+ H^T(\bar{x}(k-1))\, R_k^{-1} H(\bar{x}(k-1));$$
$$P^{-1}(0/0) = 0 \qquad (15)$$

where $\phi(\Delta t)$ is the state transition matrix defined in (5), $H(\bar{x}(k-1))$ is the measurement matrix linearized about the state vector $\bar{x}(k-1)$.

To assess the property of stochastic observability, the normalized eigenvalues of this matrix were computed (normalized to one) and plotted as a function of time. Figure 6 shows the results that were obtained for case 11 in Table 2. One of the position eigenvalues becomes ill-conditioned and exhibits a smaller maximum magnitude than the other position eigenvalue by a couple orders of magnitude. This analysis was repeated for all of the other 23 cases and the same general result was obtained, i.e., ill-conditioned behavior of one of the eigenvalues. Because of this and the fact that the state estimates were biased, we concluded that the system was marginally observable for a three-sensor configuration and unknown sound speeds.

As a means of enhancing system observability, it was decided to introduce more than three sensors for target tracking.

We first started with four sensors using different sensor/target motion geometries. Four cases were considered and the geometries are summarized in Figures 7 to 10.

Using the same philosophy as in the threesensor case earlier, we started out by estimating one, two, three, and then four sound speeds. For all of these cases, it was found that we could estimate the target state and up to two sound speeds without obtaining biased estimates, but as soon as we attempted to estimate three or four sound speeds, biases in the estimates again were noted. Marginal system observability again was suspect. To substantiate this we looked at the eigenvalues of the information matrix as a function of time. The functional variations of the eigenvalues were found to be relatively smooth and monotonically increasing for estimation of one or two sound speeds. An example of this is presented in Figure 11. It involved the target/hydrophone geometry defined by Figure 10 where we estimated the target state and two of the sound speeds. However, as we began to estimate three and more sound speeds, the function variation of several of the information matrix eigenvalues becomes progressively more ill-conditioned and lower in absolute magnitude--an indication that the property of system observability has been weakened.

To complete our analysis, we then explored the use of five sensors. Two geometries were selected and are shown in Figures 12 and 13.

Using the same approach as before, we began by estimating, first, one sound speed, then two sound speeds, and so on. Interestingly enough, it was found that one could now estimate up to three sound speeds before biased estimates again occurred.

For all of the above cases involving four and five receiving sensors, the general observation was that one could estimate the target state and up to two sound speeds for the four-sensor configuration, and the target state and up to three sound speeds for the five-sensor configurations.

Of course, these conclusions are based upon a finite set of examples, and to substantiate the above claim more rigorously, one would have to implement a more exhaustive set of examples.

4. Conclusions

In summary, it was first noted that target tracking via extended Kalman filtering tends to produce biased estimates when the sound speeds were uncertain and incorrectly specified in the filter. Attempts to additionally estimate the sound speeds were shown to be of no avail in eliminating these biases--even when applying traditional filter parameter variations that in past applications tended to make the filter more robust to parameter uncertainties.

For this reason the observability of the system was explored in greater detail. With the aid of the information matrix, it was found that the system was marginally observable over the geographical region defined by the three receiving sensors.

Because of this, we therefore took a look at using time-difference and Doppler difference measurements from more than three sensors. In particular we looked at configurations involving four and five receiving sensors.

The results from a finite set of examples have shown that target tracking performance is improved, i.e., very small or nonexistent biases, but estimation of all sound speeds is not possible. Generally speaking, it seems that if we were given n>3 receiving arrays, it would

be possible to estimate the target state and, at most, n-2 of the sound speeds to each of these sensors. The remaining two sound speeds have to be specified a priori for the filter.

Acknowledgments

The authors wish to express their appreciation to J. Hellmer of ORINCON and J. McRoberts of the Naval Ocean Systems Center for their assistance in completing the computer analysis in this paper.

This work was partially supported by the Office of Naval Research under Contract N00014-77-C-0296.

References

1. R. N. Lobbia and D. L. Alspach, "A Case Study in Adaptive Sound Speed Estimation," Twelfth Asilomar Conference on Circuits, Systems, and Components, Pacific Grove, California, November 1978.

2. A. H. Jazwinski, Stochastic Processes and Filtering Theory. New York: Academic Press, 1970.

3. R. Urick, Principles of Underwater Sound. New York: McGraw-Hill, 1967.

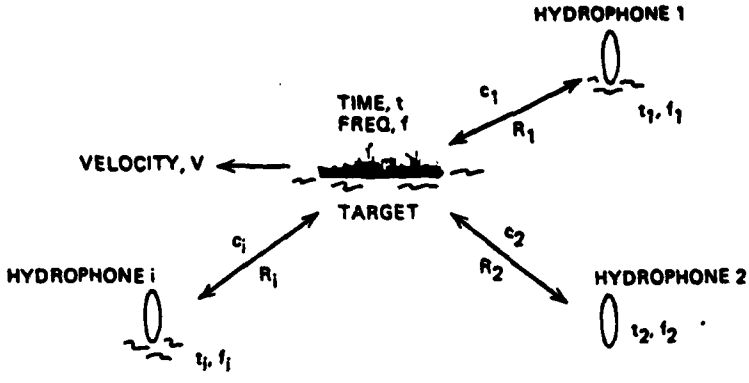

Figure 1.

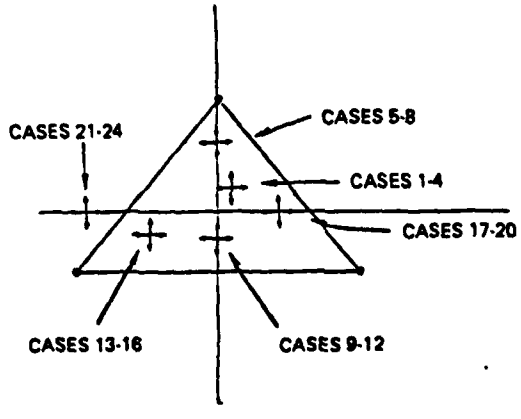

Figure 2. Target motion scenarios for sound speed estimation.

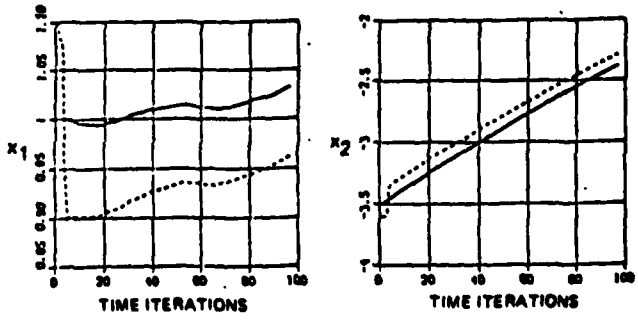

Figure 3. Target state and sound speed estimation (latitude and longitude).

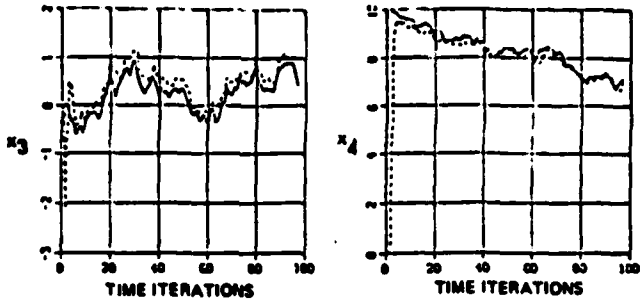

Figure 4. Target state and sound speed estimation (latitude rate and longitude rate).

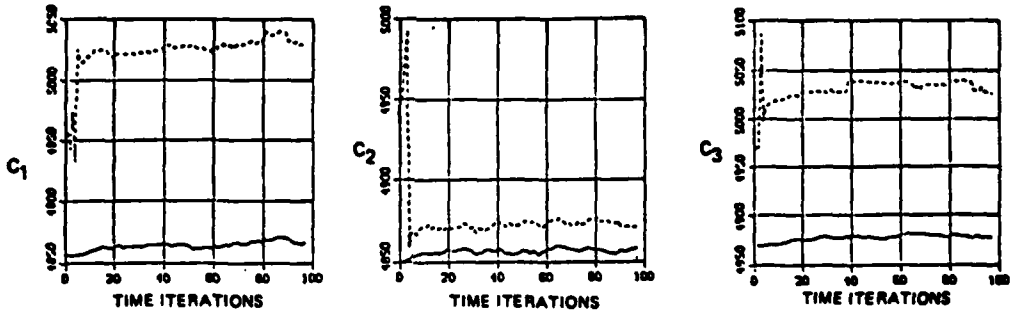

Figure 5. Target state and sound speed estimation (sound speeds).

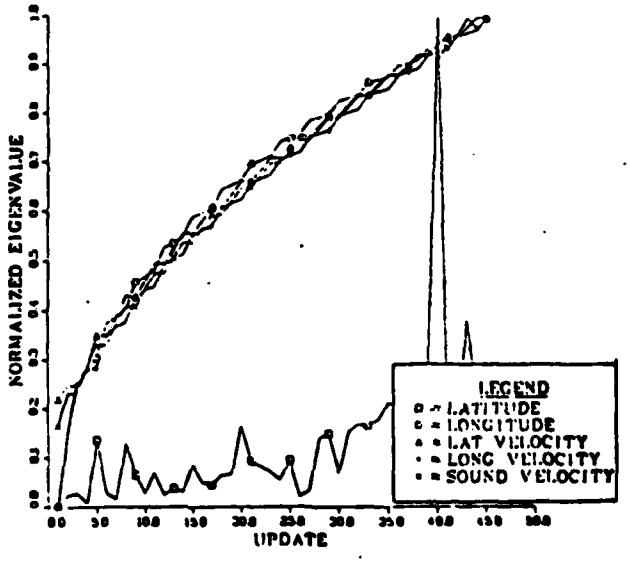

Figure 6. Information matrix eigenvalues--Case 11.

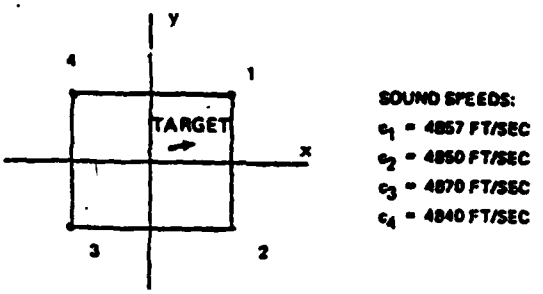

Figure 7. Geometry of four sensors--Case 1.

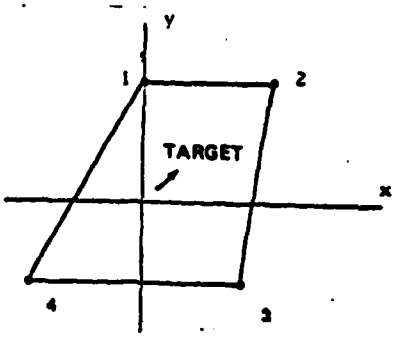

Figure 8. Geometry of four sensors--Case 2.

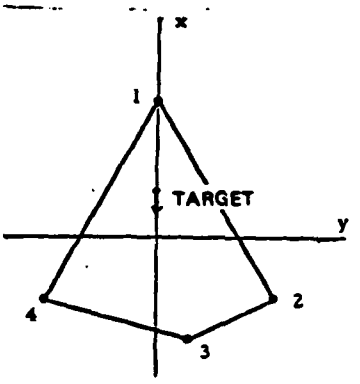

Figure 9. Geometry of four sensors--Case 3.

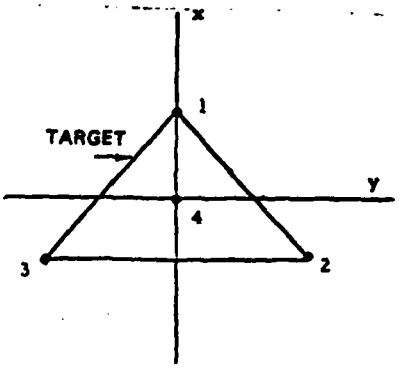

Figure 10. Geometry of four sensors--Case 4.

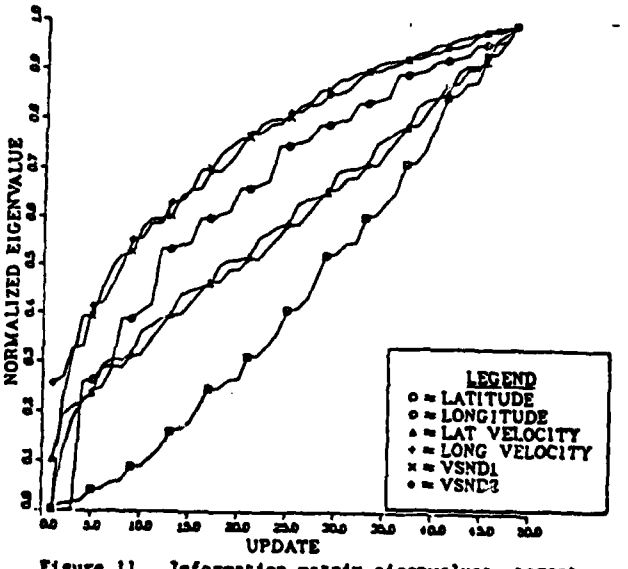

Figure 11. Information matrix eigenvalues--target state and two sound speeds.

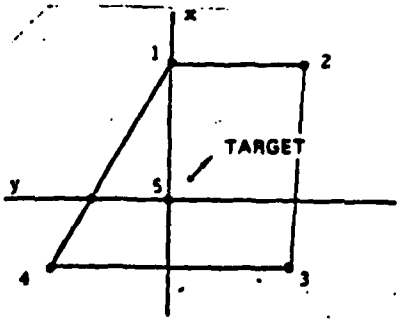

Figure 12. Geometry of five sensors--Case 1.

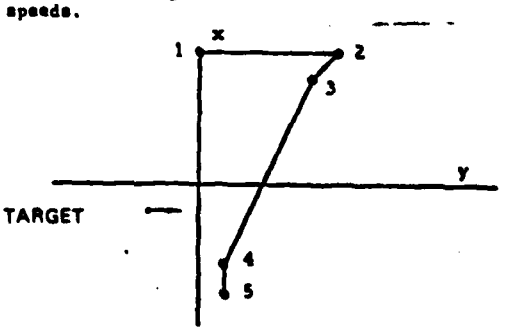

Figure 13. Geometry of five sensors--Case 2.

DOCUMENT 3

MULTIPLE COHERENCE

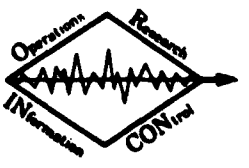

ORINCON

MULTIPLE COHERENCE

Richard Trueblood
AMES Acoustic Research Center
Moffett Field, California

Daniel L. Alspach
ORINCON Corporation
3366 North Torrey Pines Court
La Jolla, California

Summary

The concept of coherence as a measure of the linear relationship between two or more time series is discussed. The definition of coherence in terms of the complex cross power spectral density matrix is given and the relationship between pairwise and multiple coherence and channel signal to noise ratios is discussed. A sample statistic for coherence is given while the details describing the performance which can be obtained from this statistic are contained in a separate report by these authors[1].

1. Introduction

A problem of interest in many different disciplines is that of determining if there is a measurable relationship (physical causality) between two or more time series. In addition, one would often like to obtain a quantitative meaningful measure of the degree of that relationship. This paper describes one possible measure of such a relationship, the coherence.

The most common measure of such a relationship is the pairwise or multiple correlation coefficient. The nature of the correlation coefficient is well documented and will not be discussed here other than to note that it is not a function of frequency and may be affected by linear transformations of either of the time series.

The coherence function (magnitude-squared multiple or pairwise coherence function) is defined as a frequency-dependent quantity that ranges between zero and one[2-11]. This coherence function is zero if the two or more ergodic time series are independent (uncorrelated, if Gaussian) and equal to one at any frequency where there is a linear transformation between the one or more input time series and the output or reference time series.

The situation of interest is shown in Figure 1 where v_i indicates the noise contaminating the signal u(t) in the i^{th} channel. In general, each transmission channel is composed of linear and nonlinear parts (Figure 2). The sum of the output of the nonlinear system (usually a small part of the total transmission), the measurement noise, and the background noise is grouped into the effective noise term $v_i(t)$ (Figure 3).

We are interested in detecting the presence of a common signal u(t) in two or more channels. The input-output relationship indicated in Figure 1.3 can be written as

$$\underline{x}(t) = \int_{-\infty}^{\infty} \underline{g}(\tau)u(t-\tau)d\tau + \underline{v}(t). \quad (n \times 1) \qquad (1.1)$$

Note that because of physical causality requirements $g(\tau)$ is zero for all τ less than zero. In fact, it will be zero for all τ less than some positive time which is the time it takes a signal to travel from the source to a sensor.

The true value of the coherence between time series is generally an unknown quantity. In fact, any measure of the relationship between two or more time series generally must be based on time traces of those series. The functional relationship between the time series and the measure or estimate of coherence is a sample statistic for coherence. The assumption that any one infinite length sample of each series will be enough to allow us to estimate the coherence exactly is made implicitly, and all time series are assumed to be stationary and ergodic. Unfortunately, in practice, one is given only a finite amount of data from each of the time series. In this case the sample statistic is a random variable distributed about the "true magnitude-squared coherence". The density function for the sample statistic in this report is given for a number of specific values of degrees of freedom (N) and number of time series (M) in reference 1.

Based on these density functions, receiver operation characteristic (ROC) curves have been developed. These curves define the probability of detection versus probability of false alarm for a signal of a given true coherence. Curves of probability of detection versus true coherence for fixed levels of probability of false alarm have also been developed for many degrees of freedom and number of sensors up to 10. These are all reported in detail by these authors in reference 1. The fundamental question of the relationship between input signal to noise levels and true coherence for the two channel and multichannel cases of Figure 1 is discussed in this paper.

For a general discussion of the concept of coherence, the reader is directed to reference 5. For a detailed derivation of the distribution of the pairwise and multiple coherence statistic, the reader is referred to reference 7. The densities and derived performance curves in reference 1 are particularly difficult to obtain for low coherence and high values of N (number of samples of the time series), and based on the authors' knowledge are not available elsewhere in the literature.

2. Cross-Power Spectral Density Matrix and Multiple Coherence

Multiple coherence can be most easily defined in terms of the cross spectral density matrix $S_{\underline{xx}}(\omega)$, where the elements of this matrix are defined by

$$S_{ij}(\omega) \triangleq S_{x_i x_j}(\omega) = S^{*}_{ji}(\omega) \qquad (2.1)$$

The crosspower spectral density matrix is of course equivalent to the crosscorrelation matrix. Either of these together with the means of the M jointly gaussian stationary processes, $x_1(t), x_2(t), \ldots, x_M(t)$, completely specifies the joint distribution function of these processes.

Given M finite length time traces, there are *well known techniques for obtaining "sample estimates"* of the cross- and autopower spectral elements. These estimates are used to obtain sample estimates for the multiple coherence between the various time series.

The sample estimate for the cross-power spectral density matrix is a function of the basic data $x_1(t), x_2(t), \ldots x_M(t)$ over some finite time record. It does not require knowledge of any of the characteristics of the transmission channels or of the signal-to-noise ratios of the received signals. The meaning of multiple coherence will be discussed in terms of these quantities in later sections in an attempt to illuminate the subject. Here, however, we will define multiple coherence simply in terms of the crosspower spectral density matrix and its elements.

The multiple coherence between $x_j(t)$ and $x_1(t), x_2(t), \ldots x_{j-1}(t), x_{j+1}(t), \ldots x_M(t)$ is defined by. (reference 5)

$$|\gamma_{j;1,2,\ldots j-1,j+1,\ldots N}|^2 = 1 - 1/\left[S_{jj}(\omega)S^{jj}(\omega)\right], \qquad (2.2)$$

where $S^{jj}(\omega)$ is the jth diagonal element of the inverse of the $S_{\underline{xx}}(\omega)$. The multiple coherence of the jth sensor with respect to the other sensors represents the proportion of the variance (power) of sensor j that can be explained by a linear combination of the remaining sensors in a minimum mean square sense[5].

By reducing this definition to the simple two-channel case we can write

$$S^{-1}_{\underline{xx}}(\omega) = \frac{1}{S_{11}(\omega)S_{22}(\omega) - |S_{12}(\omega)|^2}\begin{bmatrix} S_{22}(\omega) & -S_{12}(\omega) \\ -S^{*}_{12}(\omega) & S_{11}(\omega) \end{bmatrix} \qquad (2.3)$$

so that

$$S^{11}(\omega) = S_{22}(\omega)/[S_{11}(\omega)S_{22}(\omega) - |S_{12}(\omega)|^2]. \qquad (2.4)$$

This gives

$$|\gamma_{1;2}(\omega)|^2 = |\gamma_{2;1}(\omega)|^2 = |\gamma_{1,2}|^2 = \frac{|S_{12}(\omega)|^2}{S_{11}(\omega)S_{22}(\omega)}. \qquad (2.5)$$

This is the mutual or pairwise coherence between channels one and two.

In the three-channel case it is easily seen (writing $S_{ij}(\omega)$ as S_{ij}) that

$$|\gamma_{1;2,3}|^2 = \frac{S_{33}|S_{21}|^2 + S_{22}|S_{31}|^2 - 2R_e(S_{12}S_{23}S_{31})}{S_{11}S_{22}S_{33} - S_{11}|S_{23}|^2} \qquad (2.6)$$

Using the fact that pairwise coherence is defined by equation 2.5 we can write

$$|\gamma_{1;2,3}|^2 = \frac{|\gamma_{1,2}|^2 + |\gamma_{1,3}|^2 - 2R_e(S_{12}S_{23}S_{31})/(S_{11}S_{22}S_{33})}{1 - |\gamma_{2,3}|^2} \qquad (2.7)$$

$$= \frac{[|\gamma_{1,2}|^2 + |\gamma_{1,3}|^2 - 2\,R_e(\gamma_{12}\gamma_{23}\gamma_{31})]}{[1 - |\gamma_{2;3}|^2]}$$

Note that if the crosspower spectral density of channels two and three is zero ($S_{23}=0$), the coherence between these two channels is zero and the multiple coherence of channel one, given two and three is,

$$|\gamma_{1;2,3}|^2 = |\gamma_{1,2}|^2 + |\gamma_{1,3}|^2 \qquad (2.8)$$

3. Pairwise Coherence and Signal-to-Noise Ratios

If $x_1(t)$ and $x_2(t)$ are generated as indicated in Figure 3, equation 1.1 can be written in the frequency domain by Fourier transform as

$$X_1(\omega) = G_1(\omega)U(\omega) + V_1(\omega) \qquad (3.1)$$

$$X_2(\omega) = G_2(\omega)U(\omega) + V_2(\omega). \qquad (3.2)$$

Again assuming the noise terms V_1 and V_2 are independent, the *cross-* and autopower spectral densities can be written as

$$S_{11}(\omega) = G_1(\omega)^2 S_u(\omega) + S_{v1}(\omega) \qquad (3.3)$$

$$S_{22}(\omega) + G_2(\omega)^2 S_u(\omega) + S_{v2}(\omega) \qquad (3.4)$$

$$|S_{12}(\omega)|^2 = G_1(\omega)^2\, G_2(\omega)^2 S_u(\omega)^2. \qquad (3.5)$$

Noting that $|G_1(\omega)|^2 S_u(\omega)$ and $|G_2(\omega)|^2 S_u(\omega)$ are the output signal power spectra at the receiver in channels one and two, we write the magnitude-squared coherence as

$$|\gamma_{1,2}|^2 = \frac{|G_1(\omega)|^2 |G_2(\omega)|^2 S_u(\omega)^2}{\left[|G_1(\omega)|^2 S_u(\omega)+S_{v1}(\omega)\right]\left[|G_2(\omega)|^2 S_u(\omega)+S_{v2}(\omega)\right]} \tag{3.6}$$

Defining the signal-to-noise power in the jth channel as

$$(S/N)_j = \frac{|G_j(\omega)|^2 S_u(\omega)}{S_{vj}(\omega)} \tag{3.7}$$

we can write

$$|\gamma_{1,2}|^2 = \frac{(S/N)_1}{\left[1+\left(\frac{S}{N}\right)_1\right]} \cdot \frac{(S/N)_2}{\left[1+\left(\frac{S}{N}\right)_2\right]} . \tag{3.8}$$

Certain general statements concerning this pairwise magnitude-squared coherence, or just "coherence," can now be made.

The coherence is bounded between zero and one:

$$0 \le |\gamma_{1,2}|^2 \le 1 . \tag{3.9}$$

If the noise-to-signal power goes to infinity in either channel, the coherence will go to zero. This will happen if the signal power in that channel fades to zero. Also, the noise-to-signal power ratio in both channels must go to zero for the coherence to go to one.

An interesting and informative interpretation of the coherence between these two channels can be made in the following manner. Assume one of the channels is noise free ($S_{v2}(\omega) = 0$). This channel then becomes the input signal. The coherence between channels one and two is now given by

$$|\gamma_{1,2}|^2 = \frac{|G_1(\omega)|^2 S_u(\omega)}{|G_1(\omega)|^2 S_u(\omega)+S_{v1}(\omega)} = \frac{(S/N)_1}{1+(S/N)_1} = \frac{S_1}{S_1+N_1} \tag{3.10}$$

This magnitude-squared coherence is the fraction of the power of the output $x_1(t)$ which comes from the signal input passed through a linear system.

Since the transmitted signal is generally not available, it is useful to look at this physical interpretation of coherence from a different point of view. Let us simply take signal $x_2(t)$ as our basic signal and calculate the coherence between $x_1(t)$ and our given signal $x_2(t)$. From equation 2.7, our definition, this will be the same result as if we took signal $x_1(t)$ as our "given" signal. Thus $U(\omega)$ in equation 3.2 is replaced by $X_2(\omega)$:

$$X_1(\omega) = H_{12}(\omega) X_2(\omega) + V_{e12}(\omega) . \tag{3.11}$$

$H_{12}(\omega)$ is the effective linear transfer function between output $x_2(t)$ and output $x_1(t)$. $V_{e12}(t)$ is the effective noise on the transmission channel. It must be noted that $H_{12}(\omega)$ is no longer necessarily a causal system. Now the coherence between channels one and two can be written as in equation 3.10:

$$|\gamma_{1,2}(\omega)|^2 = \frac{|H_{12}(\omega)|^2 S_{22}(\omega)}{\left[|H_{12}(\omega)|^2 S_{22}(\omega)+S_{ve12}(\omega)\right]} \tag{3.12}$$

This two-channel magnitude-squared coherence is the ratio of the power at output $x_1(t)$, which is caused by the "input $x_2(t)$," transmitted over the effective linear transmission channel $[H_{12}(\omega)]$ to the total power in output x_1. Consideration of this effective linear transmission channel allows this physical interpretation of the coherence to be easily carried over to multiple coherence.

4. Multiple Coherence and Signal-to-Noise Ratios

In the case of M channels, a relationship between the input signal-to-noise ratios and the multiple coherence, similar to the one in the last section for two channels, can be derived. The output power spectral density can again be written in terms of this input signal spectral density, the unknown channel transfer functions, and the effective channel noise as

$$S_{ii}(\omega) = |G_i(\omega)|^2 S_u(\omega) + S_{vi}(\omega) \tag{4.1}$$

$$|S_{ij}(\omega)|^2 = |G_i(\omega)|^2 |G_j(\omega)|^2 S_u(\omega)^2, \quad i \neq j \tag{4.2}$$

It should be noted that $|G_i(\omega)|^2 S_u(\omega)$ is the signal power density in the output of the ith channel and $S_{vi}(\omega)$ is the noise power spectral density in the channel. The general power spectral density function can then be written as

$$\underset{\sim}{S_{xx}}(\omega) = S_u(\omega)\, \underset{\sim}{G}^*(\omega)\, \underset{\sim}{G}^T(\omega) + D(\omega) , \tag{4.3}$$

where

$D(\omega)$ is a diagonal matrix with elements $S_{vi}(\omega)$,

and

$$\underset{\sim}{G}^T(\omega) = [G_1(\omega)\, G_2(\omega) \ldots G_M(\omega)] . \tag{4.4}$$

The inverse required to calculate the multiple coherence from equation 2.2 can now be calculated by using the following matrix inversion lemma:

$$\left[A+X^*X^T\right]^{-1} = A^{-1} - A^{-1}X^*\left[1+X^TA^{-1}X^*\right]^{-1}X^TA^{-1} \tag{4.5}$$

Using this lemma, the inverse of the spectral density matrix can be written (assuming all required inverses exist) as

$$\underset{\sim}{S_{xx}^{-1}}(\omega) = D^{-1}(\omega) - S_u(\omega) D^{-1}(\omega)\, \underset{\sim}{G}^*(\omega)\left[1+S_u(\omega)\underset{\sim}{G}^T(\omega)D^{-1}(\omega)\underset{\sim}{G}^*(\omega)\right]^{-1} \cdot \underset{\sim}{G}^T(\omega)\, D^{-1}(\omega) . \tag{4.6}$$

The structure of this inverse can be seen more clearly by noting that

$$S_u(\omega)G^T(\omega)D^{-1}(\omega)G^*(\omega) = \sum_{j=1}^{M} \frac{|G_j(\omega)|^2 S_u(\omega)}{S_{vj}(\omega)} \quad (4.7)$$

This term is the sum of all output signal-to-noise power ratios. Therefore, if, as in the two-channel case, we define

$$(S/N)_i = |G_i(\omega)|^2 S_u(\omega) / S_{vi}(\omega) \quad (4.8)$$

the inverse of the bracketed term in equation 4.6 can be written as

$$\left[1 + S_u(\omega)G^T(\omega)D^{-1}(\omega)G^*(\omega)\right]^{-1} = 1/\left[1 + \sum_{j=1}^{M} (S/N)_j\right] \quad (4.9)$$

With this, the ith diagonal element of $\underline{\underline{S}}_{xx}^{-1}(\omega)$ is given by

$$S^{ii}(\omega) = \frac{1}{S_{vi}(\omega)} \left[\frac{1 + \sum_{j=1}^{M} (S/N)_j - (S/N)_i}{1 + \sum_{j=1}^{M} (S/N)_j}\right] \quad (4.10)$$

Using this and substituting equation 4.10 into equation 2.2, we find

$$|\gamma_{i/1,2,\ldots i-1,i+1,\ldots M}|^2$$

$$= 1 - 1/\ S_{ii}(\omega)\, S^{ii}(\omega)$$

$$= \frac{(S/N)_i \left[\sum_{j=1}^{M} (S/N)_j - (S/N)_i\right]}{\left[1 + (S/N)_i\right]\left[1 + \sum_{j=1}^{M} (S/N)_j - (S/N)_i\right]} \quad (4.11)$$

Several special cases are of interest.

First consider the situation in which the signal-to-noise ratios in all channels are the same:

$$(S/N)_i = (S/N)_j = (S/N) . \quad (4.12)$$

This gives the coherence of channel i with respect to the other M-1 channels as

$$|\gamma_{i:1,2,\ldots i-1,i+1,\ldots M}|^2$$

$$= \frac{(S/N)^2 (M-1)}{[1 + (S/N)]\,[1 + (M-1)(S/N)]} \quad (4.13)$$

Note that for M equal to two as in section 3 the coherence is given by

$$|\gamma_{1;2}| = |\gamma_{2;1}| = \frac{(S/N)^2}{[1 + (S/N)]^2} . \quad (4.14)$$

However, if M becomes very large, the coherence goes to

$$|\gamma_{i:1,2,\ldots i-1,i+1,\ldots M}|^2 \to \frac{S/N}{[1 + (S/N)]} . \quad (4.15)$$

The formal requirement for this to be valid is for the signal-to-noise ratio and number of channels to satisfy the following inequality:

$$(M - 1)(S/N) >> 1 . \quad (4.16)$$

However, based on data from section 3, equation 4.15 is identical to the coherence of two channels when one has an infinite signal-to-noise ratio and the other has a signal-to-noise ratio (at frequency ω) of (S/N). In this sense, a large enough number of weak channels [signal-to-noise ratio of (S/N)] is equivalent to the sum of one noise-free channel and one weak channel.

The second special case for equation 4.11 is when the ith channel has a very large signal-to-noise ratio. Letting $(S/N)_i$ become large in equation 4.11 and keeping all other signal-to-noise ratios equal to (S/N) we find that

$$|\gamma_{i:1,w,\ldots i-1,i+1,\ldots M}|^2$$

$$\xrightarrow[(S/N)_i \to \infty]{} \frac{(M-1)(S/N)}{[1 + (M-1)(S/N)]} . \quad (4.17)$$

Note that for low signal-to-noise ratios, i.e.,

$$(M-1)(S/N) << 1 , \quad (4.18)$$

the coherence goes up linearly with the number of channels each is considered to have the same signal-to-noise ratio as all others, i.e., (S/N). As M becomes larger or as

$$M(S/N) >> 1 , \quad (4.19)$$

this coherence goes to one as it would in the case of two noise-free channels.

Next consider the case where one channel other than the ith channel has a very high signal-to-noise ratio relative to the others:

$$(S/N)_k >> \sum_{j=1}^{M} (S/N)_j - (S/N)_i - (S/N)_k . \quad (4.20)$$

Under these conditions, equation 4.11 is approximately given by

$$|\gamma_{i;1,2,\ldots i-1,i+1,\ldots M}|^2 \frac{(S/N)_i(S/N)_k}{[1+(S/N)_i][1+(S/N)_k]} \quad (4.21)$$

or

$$|\gamma_{i;1,2,\ldots i-1,i+1,\ldots M}|^2 \sim |\gamma_{i;k}|^2, \quad (4.22)$$

as if all other channels were not used. If $(S/N)_i$ is approximately equal to $(S/N)_k$, this means that all weaker channels could be neglected and only the two-channel coherence between the two stronger channels could be used. Also consider the case when all channels including the ith have a much lower signal-to-noise ratio than the kth channel, i.e.,

$$(S/N)_k \gg (S/N)_i = (S/N) \text{ all } i \neq k \quad (4.23)$$

Then, while the coherence of the ith channel given the others is provided by equation 4.21, the coherence of the kth channel given the others is

$$|\gamma_{k;1,2,\ldots k-1,k+1,\ldots M}|^2 = \frac{(M-1)(S/N)_k(S/N)}{[1+(S/N)_k][1+(M-1)(S/N)]}. \quad (4.24)$$

Giving for this case

$$|\gamma_{k;1,2,\ldots,k-1,k+1,\ldots M}|^2 = \frac{(M-1)[1+(S/N)]}{[1+(M-1)(S/N)]} |\gamma_{i;1,2,\ldots,i-1,i+1,\ldots M}|^2. \quad (4.25)$$

For the case of weak signals in the other channels (from equation 4.22):

$$|\gamma_{k;1,2,\ldots k-1,k+1,\ldots M}|^2 = \frac{(M-1)(1+S/N)}{[1+(M-1)(S/N)]} |\gamma_{i;k}|^2 \quad (4.26)$$

Further simplify equation 4.26 to the special case of

$$(M-1)(S/N) \ll 1, \quad (4.27)$$

we have

$$|\gamma_{k;1,2,\ldots k-1,k+1,\ldots M}|^2 \sim (M-1)|\gamma_{i;k}|^2 \quad (4.28)$$

The coherence between the strong signal and the weaker ones goes up linearly with the number of weaker channels. This means that the largest of the M multiple coherence values will be the one in which the largest signal-to-noise ratio channel is used as the reference, which is as expected.

5. A Sample Statistic for Multiple Coherence

The true multiple coherence of a set of time series is a function of the underlying statistics of these processes. The statistics are generally unknown and must be estimated from sample realizations of the processes. The estimates of the basic statistics can then be used to provide estimates of the multiple coherence of the M underlying stochastic processes.

The method of obtaining estimates for true multiple coherence is as follows. Using well documented techniques[1, 3, 4, 5, 6], obtain sample estimates for each element of the crosspower spectral density matrix. From these sample estimates

$$\hat{\underline{S}}_{xx}(\omega) = \begin{bmatrix} \hat{S}_{11}(\omega) & \hat{S}_{12}(\omega) & \cdots & \hat{S}_{1M}(\omega) \\ \hat{S}_{21}(\omega) & \hat{S}_{22}(\omega) & \cdots & \hat{S}_{2M}(\omega) \\ \cdot & \cdot & & \cdot \\ \cdot & & \cdot & \cdot \\ \cdot & & \cdot & \cdot \\ \hat{S}_{M1}(\omega) & \hat{S}_{M2}(\omega) & \cdots & \hat{S}_{MM}(\omega) \end{bmatrix} \quad (5.1)$$

one calculates the sample estimate for multiple coherence in the following manner

$$|\hat{\gamma}_{i;1,2,\ldots,i-1,i+1,\ldots M}|^2 = 1 - 1/[\hat{S}_{ii}(\omega)\hat{S}^{ii}(\omega)], \quad (5.2)$$

where $\hat{S}^{ii}(\omega)$ is the ith diagonal element of the inverse of the M-by-M sample spectral density matrix $\hat{\underline{S}}_{xx}(\omega)$. Details of how to form such estimates are discussed at length in the literature. Since these estimates are random variables there has been considerable study of their distribution. The distributions of these cross- and autopower spectral estimates are known in closed form[7].

The closed-form expression for the multiple-coherence statistic is available[7, 8, 9]. This represents the range of values of the multiple-coherence test statistic and the relative probability of its being in a particular band. All values are of course bounded by zero and one. The density function is conditioned on the total number of different time records, or different stochastic processes, available (p). It is also conditioned on the number of independent samples available from each of the time records (N). Thus the density function of the sample estimate for coherence given the true coherence is given by[9]

$$P_{\frac{\overline{\quad}}{|\gamma|^2}}(y/N, p, |\gamma|^2) = \frac{\Gamma(N)}{\Gamma(p-1)\Gamma(N-p+1)}\left(1-|\gamma|^2\right)^N y^{p-2}(1-y)^{N-p} \; {}_2F_1(N, N, p-1; y|\gamma|^2)$$

$$0 \le y \le 1$$

$$P_{\frac{\overline{\quad}}{|\gamma|^2}}(y/N, p, |\gamma|^2) = 0 \quad y > 1 \text{ or } y < 0. \tag{5.3}$$

In equation 5.3, ${}_2F_1(\,)$ is the hypergeometric function.

This expression for the density function of multiple coherence is both expensive to calculate and generally numerically ill conditioned. Thus to evaluate the density numerically, additional manipulations are required. Great difficulty can be encountered in attempting to use computer library expressions for the hypergeometric function.

For low values of N and p we use a transformation given in reference 12:

$${}_2F_1(N, N, p-1; |\gamma|^2 y) = (1-|\gamma|^2 y)^{p-1-2N} \; {}_2F_1(p-1-N, p-1; |\gamma|^2 y). \tag{5.4}$$

For the cases of interest, (p-1-N) is a negative integer so that a finite series expansion for this latter hypergeometric function is available:

$${}_2F_1(n, N, p-1; |\gamma|^2 y) = (1-|\gamma|^2 y)^{1-1-2N} \sum_{j=0}^{N-p+1} \frac{(-N+p-1)_j^2}{(p-1)_j} \frac{(|\gamma|^2 y)^j}{j!} \tag{5.5}$$

where

$$(p-1)_j = (p+j-1)!/(p-1)! = (p+j-2)(p+j-3)\ldots(p-1) \tag{5.6}$$

$$(-N-p-1)_j = (-N+p-1)(-N+p)\ldots(-N+p-2+j). \tag{5.7}$$

Using these expressions for the hypergeometric function we can write for y between zero and one:

$$P_{\frac{\overline{\quad}}{|\gamma|^2}}(y/N, p, |\gamma|^2) = \frac{\Gamma(N)(1-|\gamma|^2)^N}{\Gamma(p-1)\Gamma(N-p+1)} \frac{y^{p-2}(1-y)^{N-p}}{(1-|\gamma|^2 y)^{2N-(p-1)}} \sum_{j=0}^{N-(p-1)} \frac{[-N+(p-1)]_j^2}{(p-1)_j} \frac{(|\gamma|^2 y)^j}{j!} \tag{5.8}$$

Other expressions for this density valid to large values of N and specific ranges of true coherence $|\gamma|^2$ and y are described in reference 1. There curves of probability of detection versus probability of false alarm are presented as are curves of probability of detection versus true coherence for fixed values of probability of false alarm.

References

1. Trueblood, R.D., and Alspach, D.L., "An Investigation of Multiple Coherence" to be published.
2. Cox, Henry, "Coherence in Multiple Random Processes," paper presented at Sixty-Ninth Meeting of the Acoustical Society of America, Washington, D.C., 2-5 June 1965.
3. Jenkins, G.M., and Watts, D.G., "Spectral Analysis," Hólden Day, California, 1968.
4. Rosenblatt, M. (Ed.), "Symposium on Time Series Analysis," John Wiley and Sons, New York, 1963.
5. Bendat, J.S., and Piersol, A.G., "Random Data, Analysis and Measurement Procedures," Wiley-Interscience, New York, 1971.
6. Enochson, D.L., and Otnes, R.K., "Programming and Analysis for Digital Times Series Data," The Shock and Vibration Information Center, United States Department of Defense, 1968.
7. Goodman, N.R., "Statistical Analysis Based on a Certain Multivariate Complex Gaussian Distribution (An Introduction)," Annals of Mathematical Statistics, Vol. 34, No. 1, pp. 152-177, March 1963.
8. Carter, C.G., "Estimation of the Magnitude-Squared Coherence Functions," Naval Underwater Systems Center Technical Report 4343, 1972.
9. Goodman, N.R., "Measurement of Matrix Frequency Response Functions and Multiple Coherence Functions," Measurement Analysis Corporation Technical Report AFFDL-TR-65-66, June 1965.

10. Munk, W.H., Snodgrass, F.E., and Tucker, M. J., "Spectra of Low-Frequency Ocean Waves," Bulletin, Scripps Institution of Oceanography, Volume 7 (1959), pp. 283-361.

11. Carter, G.C., "Time Delay Estimation," NUSC Technical Report 5335, April 1976 (also Ph.D. dissertation at the University of Connecticut.)

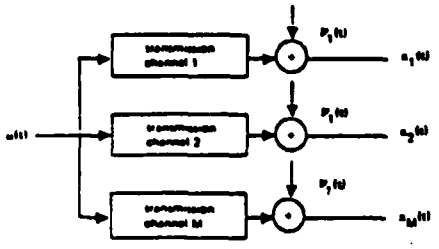

Figure 1. One input-or-output system.

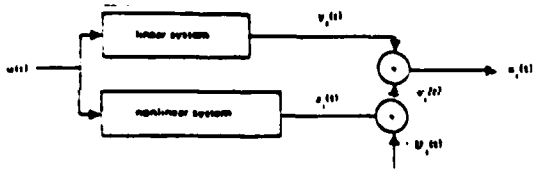

Figure 2. Linear and nonlinear parts of a single channel.

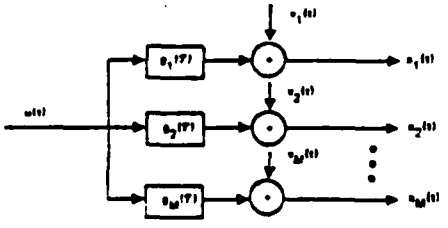

Figure 3. Effective noise with M linear transmission channels.

DOCUMENT 4

A CASE STUDY IN ADAPTIVE SOUND SPEED ESTIMATION

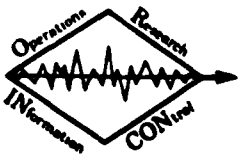

ORINCON

A CASE STUDY IN ADAPTIVE SOUND SPEED ESTIMATION

by

R. N. Lobbia D. L. Alspach

ORINCON Corporation
3366 N. Torrey Pines Ct., Suite 320
La Jolla, CA 92037

ABSTRACT

This paper deals with the problem of sound speed estimation as an aid in improving our knowledge of the position of a drifting sonobuoy. This is accomplished by processing the outputs of a spatially displaced set of hydrophone sensors in an extended Kalman filter. The filter's state vector may be augmented to provide estimates of the sonobuoy's position, velocity, and the sound speed from the sonobuoy to each of the hydrophones.

It is shown that with just time-of-arrival difference and doppler difference measurements, system observability is marginal – directly resulting in biased estimates of the sonobuoy's location. With the additional use of bearing measurements, it is then shown how this enhances system observability and, consequently, estimation performance.

I. INTRODUCTION

In this paper, we are concerned with the accurate location of a sonobuoy over a specified interval of time. It is assumed to be subjected to both random and deterministic forces over this same time period. Because of this, our knowledge of the sonobuoy's location is uncertain and can be in error if we employ conventional dead reckoning methods.

Another approach more accurate than the above would be to place a source emitting a continuous pseudorandom gaussian signal aboard the sonobuoy. A set of three or more passive hydrophones, geographically separated from one another, can then be used to pick up the sonobuoy's signal to provide measurements of sound time-of-arrival difference and doppler difference. As an example, one configuration involving three hydrophones is shown below in Figure 1.

In this figure R_i, i=1, 2, 3 represents the distance from the sonobuoy to each of the hydrophones and c_i, i=1, 2, 3 represents the sound speed to each hydrophone. Note that we are using three distinct sound speeds instead of a single one. This is because sound speed, in a thermally non-homogeneous medium, is related in a complex fashion to such variables as time-of-day, distance between hydrophone and sonobuoy, bearing of hydrophone with respect to sonobuoy, etc.

Now if we consider any pair of hydrophones, pair 1-2 for instance, then we can obtain, through cross-correlation methods, two measurements, time-of-arrival differences and doppler difference, that are related to the sonobuoy's location by the following equations:

$$\tau_{1\text{-}2} = \frac{R_1}{c_1} - \frac{R_2}{c_2} \tag{1}$$

$$\alpha_{1\text{-}2} = \frac{\dot{R}_1}{c_1} - \frac{\dot{R}_2}{c_2} \tag{2}$$

In Equation (1), $\tau_{1\text{-}2}$ represents the sound time-of-arrival difference for the hydrophone array pair 1-2. $\alpha_{1\text{-}2}$ in Equation (2) represents the normalized doppler difference, $\frac{\Delta f}{f}$, where f is the base frequency of the narrowband source.

Using spherical geometry, the distances R_i and time rate-of-change distances $\dot{R}_i$ are related to the sonobuoy's location by the following equations:

$$R_i = \cos^{-1}\left[\sin x_1 \sin\lambda_i + \cos x_1 \cos\lambda_i \cos(x_2 - \theta_i)\right] \tag{3}$$

$$\dot{R}_i = \frac{x_3\left[\sin x_1 \cos\lambda_i \cos(x_2 - \theta_i) - \cos x_1 \sin\lambda_i\right]}{\sin R_i} + \frac{x_4 \cos x_1 \cos\lambda_i \sin(x_2 - \theta_i)}{\sin R_i} \tag{4}$$

where

x_i, i=1, 2, 3, 4 represents the sonobuoy latitude, longitude, latitude rate, and longitude rate, respectively.

λ_i, θ_i represents the latitude and longitude of the i^{th} hydrophone.

In Equation (4) it was assumed that each of the hydrophones was stationary.

Because of the nonlinear feature of the above measurement equations, it is very difficult to solve explicitly for the sonobuoy's state vector (x_1, x_2, x_3, x_4). In the next section, it will be shown how this state vector may be obtained in a recursive manner using an extended Kalman filter.

Following this we will show that when the sound speeds are imprecisely known, then estimates of the sonobuoy's position and velocity become biased. Section 3 then presents a method for augmenting the sound speeds to the sonobuoy state estimate and it is shown that the augmented state becomes marginally observable. This directly results in biased estimates for the sonobuoy's state vector. We then show that the additional use of bearing measurements are seen to enhance system observability to the point where estimation of the sonobuoy state vector becomes unbiased.

Finally, in Section 4, we will summarize our results.

Operations Research INformation CONtrol ORINCON

2. ESTIMATION OF SONOBUOY STATE VECTOR

It is apparent from Equations (1) to (4) that it would be difficult to solve for the sonobuoy state vector in terms of the measurement τ_{i-j}, α_{i-j}. A recursive approach may be sought that avoids this difficulty. The approach we use here involves application of an extended Kalman filter.

In order to implement this filter, we need in addition to the measurement Equations (1) to (4), a model for the dynamics of the system. This is easily obtained when we assume a constant speed and constant course drift and, in addition, a random perturbation to account for modeling uncertainties, environmental forces, etc. In discrete-time form, the equations for the system dynamics are given by:

$$\underline{x}(k+1) = \underbrace{\begin{bmatrix} 1 & 0 & \Delta t & 0 \\ 0 & 1 & 0 & \Delta t \\ 0 & 0 & 1 & 0 \\ 0 & 0 & 0 & 1 \end{bmatrix}}_{\Phi(\Delta t)} \underline{x}(k) + \underbrace{\begin{bmatrix} 0 \\ 0 \\ w_3(k) \\ w_4(k) \end{bmatrix}}_{\underline{w}(k)} \tag{5}$$

where

$$\underline{x}(k) = \begin{bmatrix} x_1(k) \\ x_2(k) \\ x_3(k) \\ x_4(k) \end{bmatrix} \quad \text{is the sonobuoy state vector}$$

Δt = sampling interval

$w_3(k)$, $w_4(k)$ are zero mean, random, white noise sequences

$E\{\underline{w}(k)\underline{w}^T(j)\} = Q_k \delta_{kj}$; δ_{kj} is the Kroneker Delta.

If we linearize the measurement equation about our most recent estimate of the state, $\hat{\underline{x}}(k)$, to obtain a linear measurement matrix, $H(\hat{\underline{x}}(k))$, we can then implement the extended Kalman filter in real time. In vector-matrix form, these equations are recursively given by [3];

$$\hat{\underline{x}}(k+1/k) = \Phi(\Delta t)\,\hat{\underline{x}}(k/k) \tag{6}$$

$$P(k+1/k) = \Phi(\Delta t)\,P(k/k)\,\Phi^T(\Delta t) + Q_k \tag{7}$$

$$\hat{\underline{x}}(k+1/k+1) = \hat{\underline{x}}(k+1/k) + K_k\,[z_k - h(\hat{\underline{x}}(k+1/k))] \tag{8}$$

$$P(k+1/k+1) = [I - K_k\,H(\hat{\underline{x}}(k+1/k))]\,P(k+1/k) \tag{9}$$

$$K_k = P(k+1/k)\,H(\hat{\underline{x}}(k+1/k))\,[H(\hat{\underline{x}}(k+1/k))\,P(k+1/k)\,H^T(\hat{\underline{x}}(k+1/k)) + R_k]^{-1} \tag{10}$$

Equations (6) and (7) represent predictions of the state estimate and covariance to time (k+1), whereas Equations (8) through (10) update the state estimate and covariance to account for a new measurement. In the latter set of equations, the measured vector is given by $z_k^T = [\tau_{i-j}(k), \alpha_{i-j}(k)]$, where $h(\cdot)$ represents the nonlinear dependence of z_k on $\underline{x}(k)$ defined by Equations (1) through (4). R_k is the covariance matrix of an additive white-noise measurement sequence. $H(\underline{x}(k+1/k))$ is the measurement equation that is linearized about the most current state estimate and is defined by:

$$H(\hat{\underline{x}}(k+1/k)) = \left.\frac{\partial h(\underline{x}(k))}{\partial \underline{x}(k)}\right|_{\underline{x}(k) = \hat{\underline{x}}(k+1/k)}$$

This linearization was found to accurately describe the functional characteristics of the nonlinear measurement model as $H(\cdot)$ was relatively insensitive to variation in $\hat{\underline{x}}(k)$.

These equations were implemented in the case where we knew the sound speeds to each hydrophone. Under these circumstances, the resulting estimation performance was seen to be excellent.

However, for the case involving unknown sound speeds, the estimation performance degrades rapidly when we use incorrect values for the sound speeds in the Kalman filter. An example of this is shown in Figures 2 and 3 for a case involving an average sonobuoy drift velocity of 1 knot and course of 45 degrees. In Figure 2, the solid curves represent motion of the truth model and the dotted curves represent estimates of the sonobuoy state as provided by a Kalman filter. The measurements were assumed noisy with a standard deviation in τ and α of .1 second and 1×10^{-5}, respectively. The estimation error and a priori/a posteriori standard deviations are presented in Figure 3. A set of three hydrophones were configured essentially as vertices of an equilateral triangle with the sonobuoy starting near the center of this triangle. The truth model sound speeds were set at: c_1 = 4857 ft/sec, c_2 = 4957 ft/sec, and c_3 = 4757 ft/sec around nominal values from Urick [1]. The filter used an incorrect value of 5000 ft/sec for all three speeds and no attempt to estimate them was made. It is clear from Figure 2 that significant biases in estimated position and speed develop.

In the next section, we will see how the use of bearing measurements enhances system observability and allows unbiased estimation of the sonobuoy state vector.

3. SOUND SPEED ESTIMATION

Because of the biases that develop when we use incorrect sound speeds in the Kalman filter, it was felt that estimation of these sound speeds in addition to the sonobuoy states would eliminate the biases. This is done simply by augmenting the sound speeds to the original four element sonobuoy state vector. The assumption was made that the sound speed was constant and unknown over a sufficiently long time interval. Its state equation is then given by:

$$\dot{c}_i = 0; \quad i = 1, 2, 3 \tag{11}$$

Implementation of the extended Kalman filter for the augmented state vector is therefore rather simple and straightforward and will not be presented here.

Upon implementing the augmented state filter, it was found that biases still developed in the sonobuoy states and sound speeds for a number of scenarios involving different starting positions, speeds, courses, etc. For this reason, the observability of the linearized, augmented state system was explored using the information matrix [2]. In the situation involving no process noise and state vector a priori information, the information matrix is equal to the inverse of the Kalman filter covariance

Operations Research INformation CONtrol ORINCON

matrix, $P^{-1}(k/k)$. This matrix must be positive definite for stochastic observability and, provided the above conditions apply, is given in recursive form by:

$$P^{-1}(k/k) = \Phi^{T}(-\Delta t)\, P^{-1}(k-1/k-1)\, \Phi(-\Delta t) + H^{T}(\hat{x}(k-1))\, R_k^{-1}\, H(\hat{x}(k-1)); P^{-1}(0/0) = 0 \quad (12)$$

where $\Phi(\Delta t)$ is the state transition matrix defined in (5), $H(\hat{x}(k-1))$ is the measurement matrix linearized about the state vector $\hat{x}(k-1)$.

To assess the property of stochastic observability, the normalized eigenvalues of this matrix were computed (normalized to one) and plotted as a function of time. Figure 4 shows the results that were obtained for the case involving one unknown and constant sound speed. One of the sonobuoy position eigenvalues becomes ill-conditioned and exhibits a smaller maximum magnitude than the other position eigenvalue by a few orders of magnitude. This analysis was repeated for a number of different sonobuoy starting positions and headings, and the *same general result was obtained, i.e., ill-conditioned behavior* of one of the eigenvalues. Because of this and the fact that the state estimates were biased, we concluded that the system was marginally observable.

As a means of improving the property of system observability, we introduced an additional measurement of bearing to use in the Kalman filter. We assumed that it was contaminated by additive white noise with a standard deviation of .1 degree. These *measurements defined the bearing of the sonobuoy with respect* to each hydrophone, and are normally available as outputs from the same set of hydrophones without introducing additional sensors.

The Kalman filter was then rerun with these additional measurements and the sonobuoy tracking performance was found to be very good. Figures 5, 6, 7, and 8 summarize the results of one case where we estimate the four sonobuoy states and three sound speeds. In Figure 5, convergence of the sonobuoy state estimates to their true values is seen to be very rapid. Noise was introduced in the sound speed truth model to add more realism to the problem and this variation is reflected by the variation in sound speed of the truth model as shown in Figure 6. Figures 7 and 8 present estimation error and standard deviations of the sonobuoy states and sound speeds. These errors are seen to fall well within the $\pm$ two-sigma value as one would expect for unbiased estimation. A number of other cases were also run and are not presented here because of space limitations. For these other cases it was found that tracking performance was as good as before and all of the earlier noted biases in the state estimates, when processing only time-delay and doppler difference measurements, had disappeared.

4. CONCLUSIONS

To summarize the above results, we saw that to estimate the sonobuoy position and velocity accurately we need to also estimate the sound speeds to each hydrophone when they are unknown. With the aid of the information matrix we found that the linearized system was marginally observable when attempting to estimate both the sonobuoy states and sound speeds.

Because the linearized measurement model accurately represented its nonlinear counterpart, we concluded that the nonlinear system was also marginally observable. This was also reflected by the biased estimates of sonobuoy position when implementing the Kalman filter.

Finally, by incorporating and additional independent measurement (bearing) the system observability was enhanced considerably and we were then able to track the sonobuoy's motion quite accurately.

Although not reported in the last section, we also looked at the use of time-delay and doppler difference measurements of more than three hydrophones (as opposed to time delay, doppler difference, and bearing measurements of just three hydrophones) as a means of improving system observability. In general, it was found that if one had n hydrophones with n unknown sound speeds from the sonobuoy to each hydrophone, then we could at most estimate the sonobuoy state vector and (n-1) sound speeds; one of these sound speeds had to be known exactly when implementing the Kalman filter.

At the present time, we are continuing research in this area of sonobuoy state and sound speed estimation to more fully explore the sensitivity of the estimation process to geometrical placement of the hydrophones, time between measurements, etc.

ACKNOWLEDGMENTS

The authors wish to express their appreciation to Dr. W. Marsh and Dr. G. Mohnkern of the Naval Ocean Systems Center (NOSC) for their support and helpful suggestions during the course of this research, and to J. Hellmer and J. McRoberts (NOSC) for their assistance in completing the computer analyses in this paper.

REFERENCES

[1] R. J. Urick, *Principles of Underwater Sound for Engineers*, McGraw Hill, 1967

[2] A. H. Jaywinski, *Stochastic Processes and Filtering Theory*, pp. 231-234, Academic Press, 1970

[3] J. S. Meditch, *Stochastic Optional Linear Estimation & Control*, McGraw-Hill, 1969

This work was partially supported by the Office of Naval Research under Contract N00014-77-C-0296.

Operations Research INformation CONtrol ORINCON

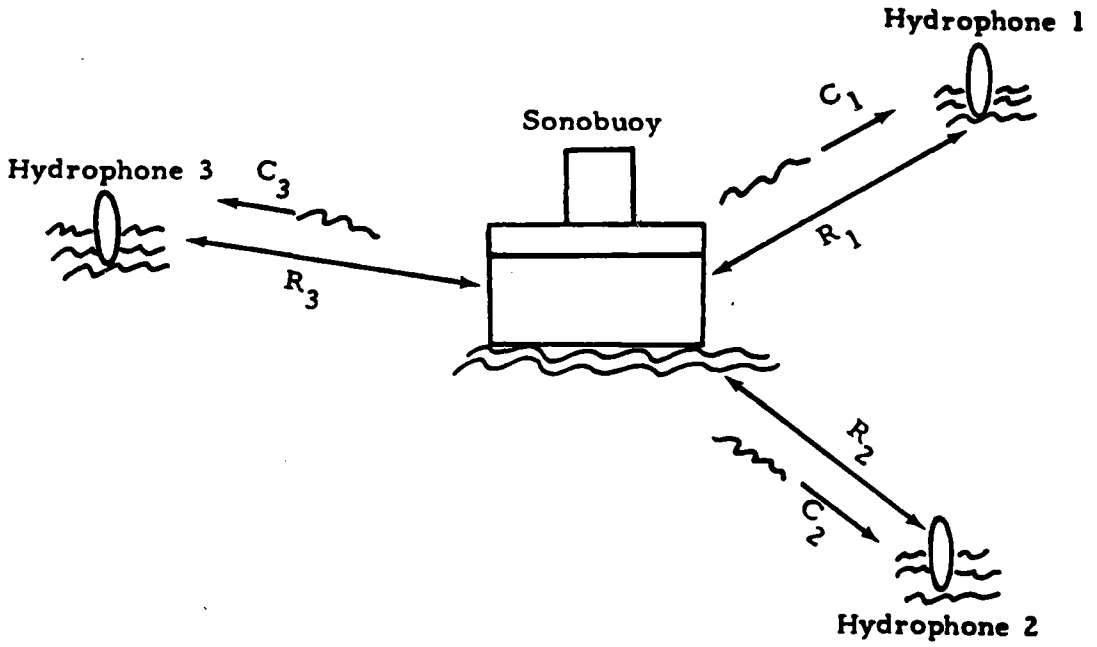

Figure 1. Hydrophone/sonobuoy geometry.

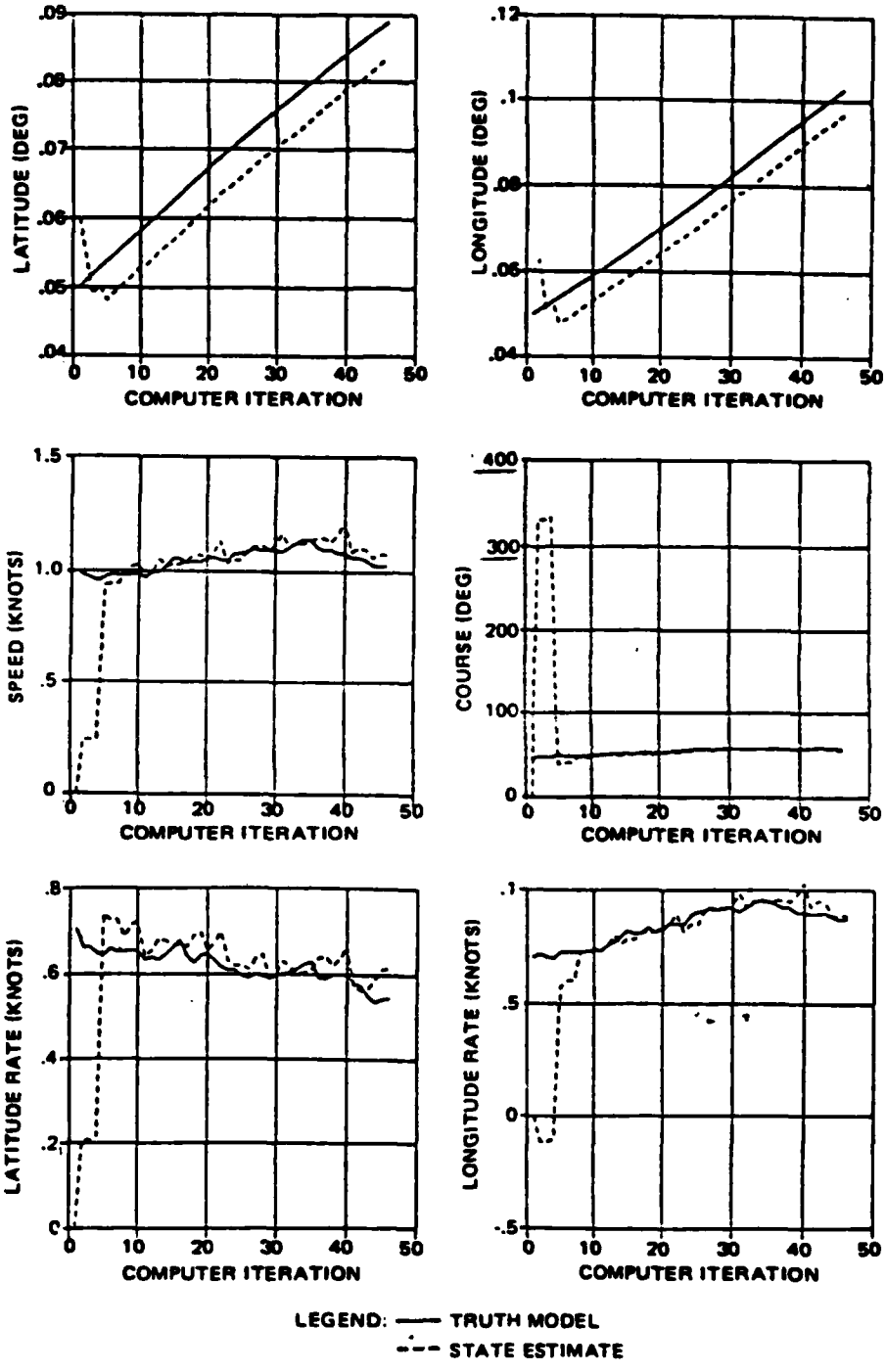

Figure 2. Estimation of sonobuoy states using incorrect sound speeds.

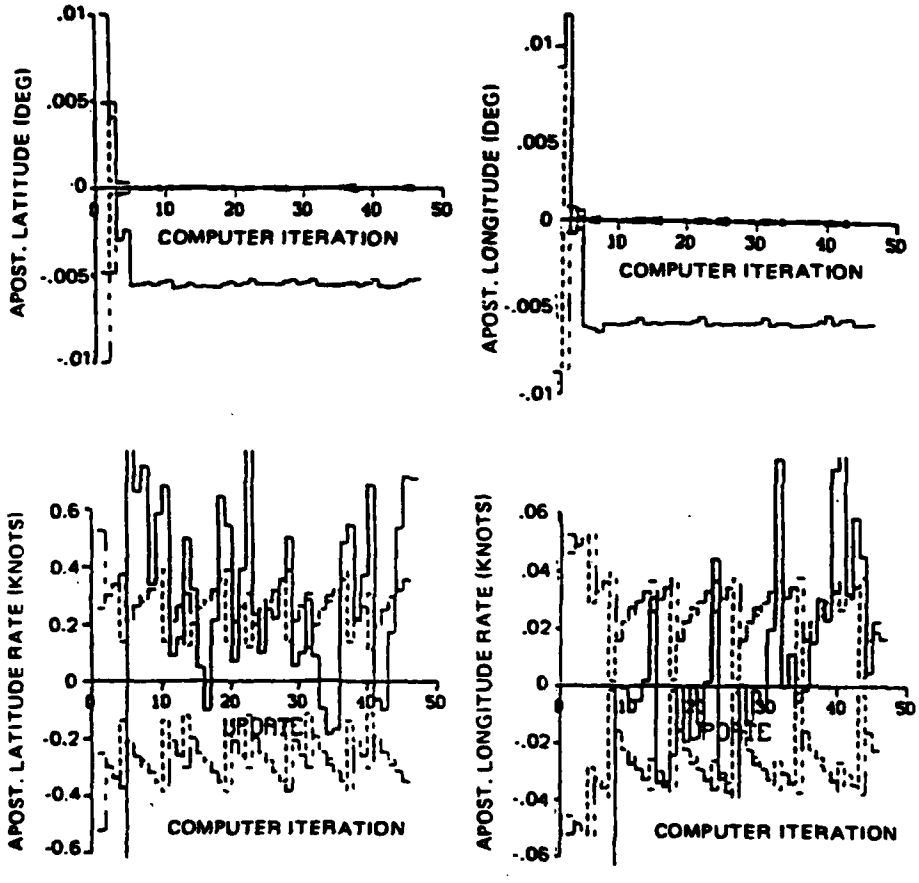

LEGEND:
DASH – APOST. STD. DEV.
SOLID – STATE ERROR
CHNDOT – APRIOR STD. DEV.

Figure 3. Sonobuoy estimation error and standard deviation—incorrect sound speeds.

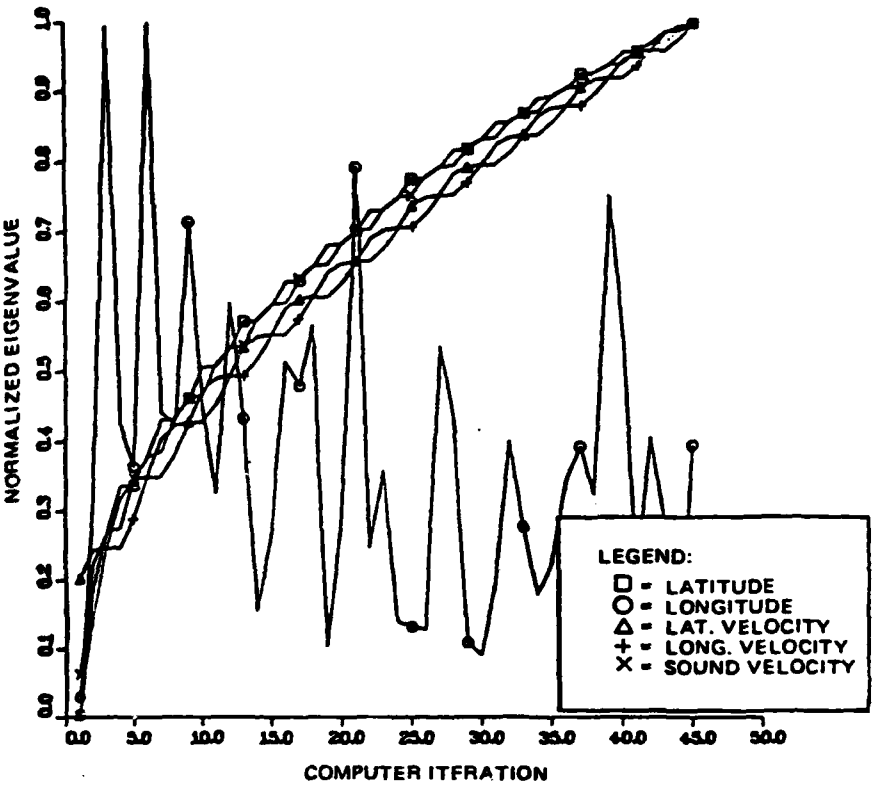

MAX:LAT. = 6.223+02 LONG. = 8.598+00

MAX.LAT. RATE = 3.189+01
:LONG. RATE = 2.767+01

SOUND SPEED = 1.420+00

COURSE = 90

Figure 4. Normalized eigenvalues of the information matrix.

ORINCON

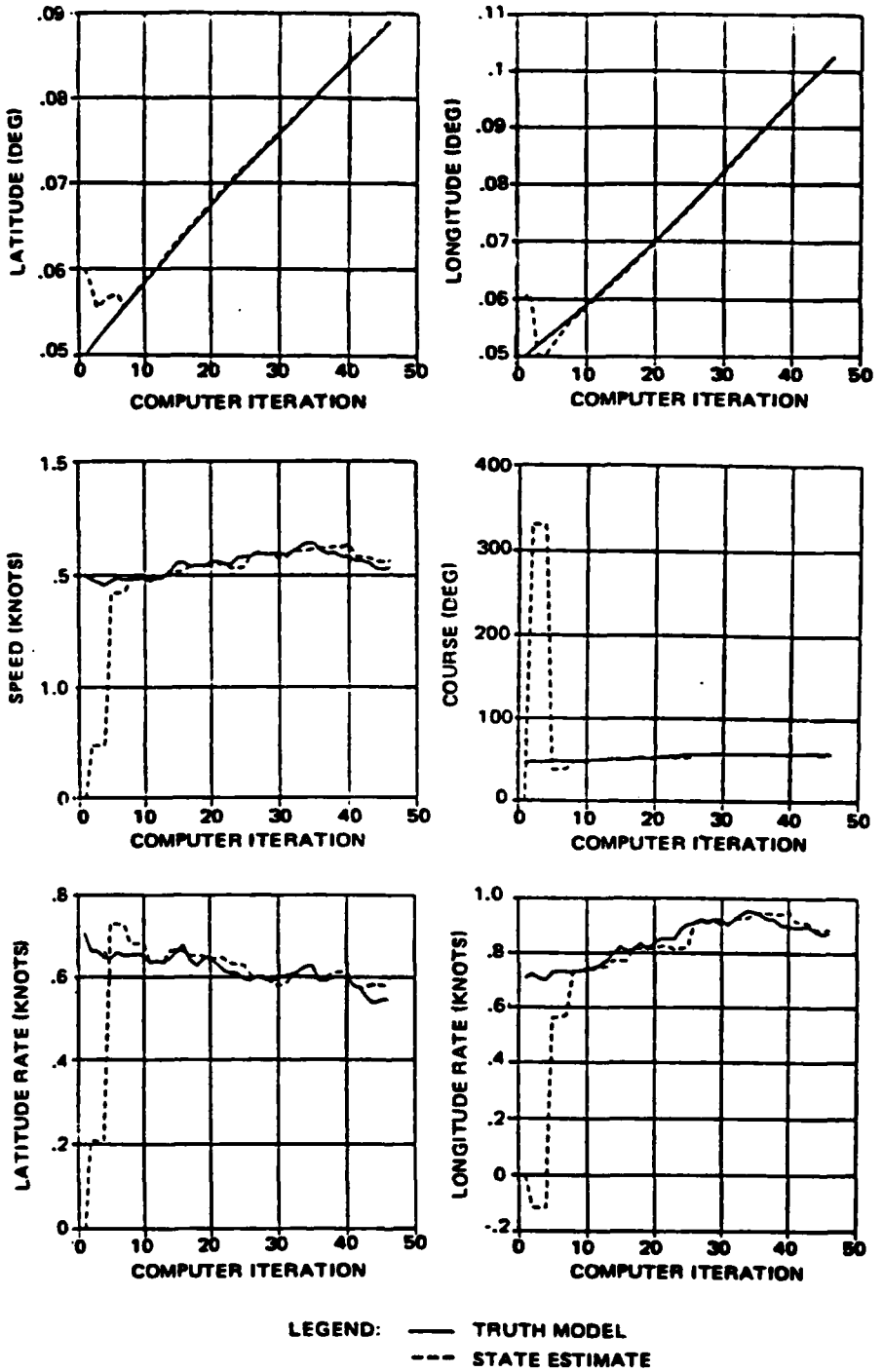

Figure 5. Estimation of sonobuoy states.

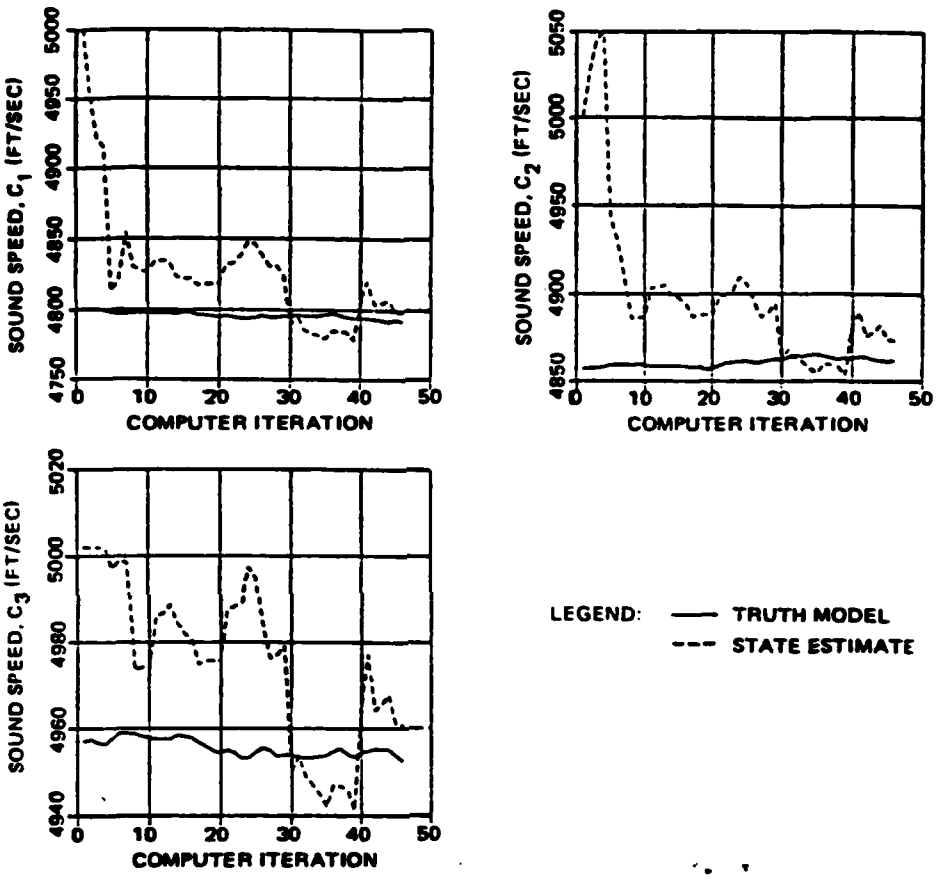

Figure 6. Estimation of sound speeds.

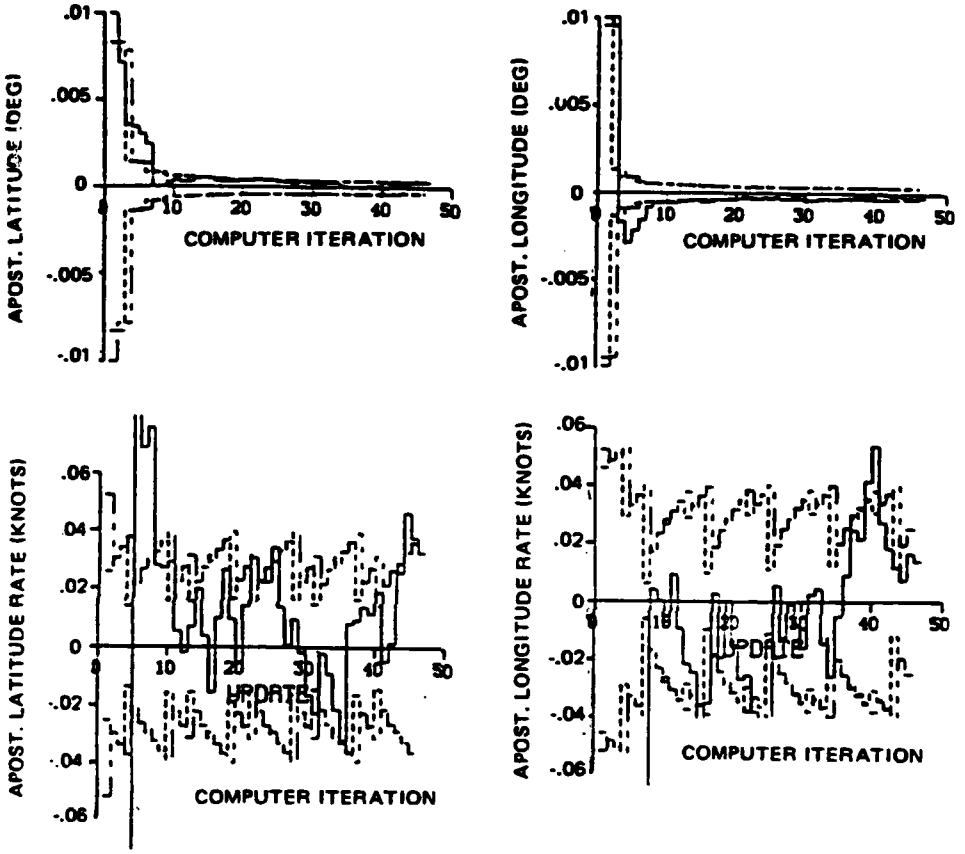

Figure 7. Sonobuoy estimation error and standard deviation.

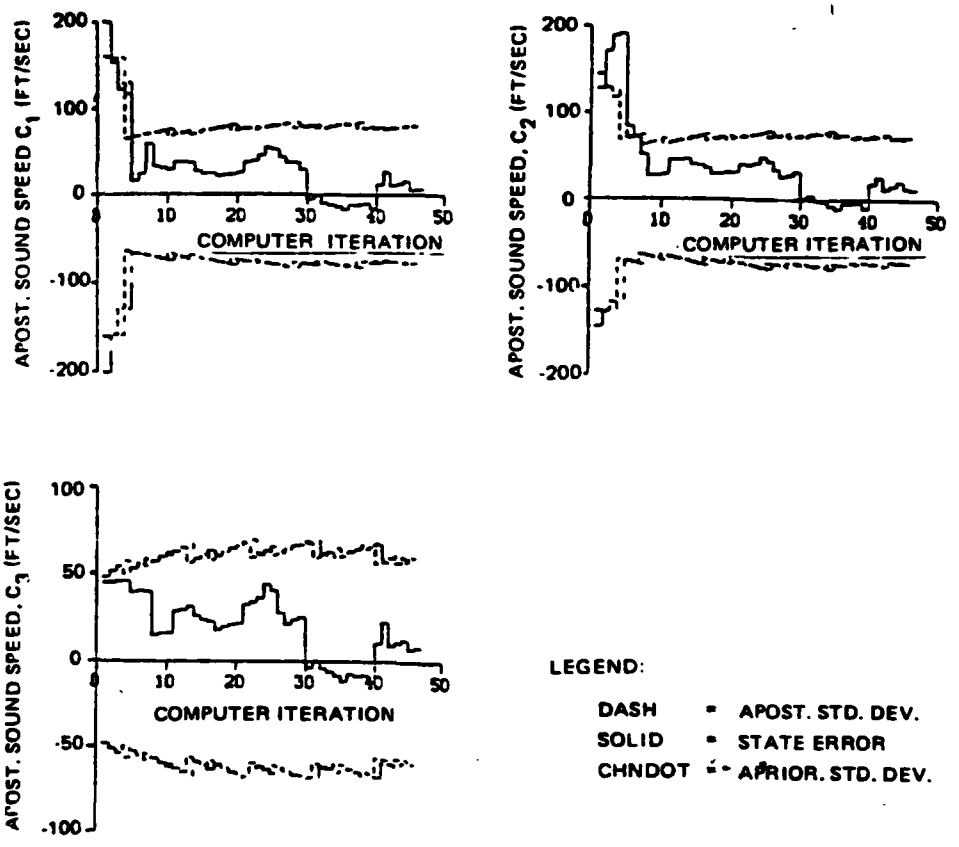

Figure 8. Sound speed estimation and standard deviation.

DOCUMENT 5

DATA ASSOCIATION ALGORITHMS FOR LARGE AREA SURVEILLANCE

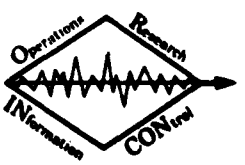

ORINCON

This work was supported by the Office of Naval Research
under Contract N00014-77-C-0296.

DATA ASSOCIATION ALGORITHMS FOR LARGE AREA SURVEILLANCE

ORSA/TIMS Meeting

May, 1978

Dr. Charles L. Morefield*

and

Christian M. Petersen**

*1745 Collingwood Drive, San Diego, CA 92109

**8571 Villa La Jolla, #D, La Jolla, CA 92037

1.0 OVERVIEW OF INTERSENSOR CORRELATION FOR OCEAN SURVEILLANCE

In a typical large-area ocean surveillance situation, data is generated by many different sensors due to the presence of various surface ships, aircraft, etc. If the data collected by the sensors is overlaid in a common coordinate system, then a picture such as that shown in Figure 1-1 below results. The underlying assumption of the picture is that each individual sensor has formed a picture of the surveillance area based only on its own data. In some cases, this may require the solution of a multitarget tracking problem [1] at the sensor level. In Figure 1-1, for example, sensor S2 must discriminate and track the two closely spaced targets T1 and T2.

When the multitarget tracking problem is solved separately for each individual sensor, a somewhat redundant view of the surveillance area may result. The different data collection systems S1, S2, ..., may report on the same target. When this situation arises, the final step in the process of forming a complete picture of the surveillance area is to perform intersensor correlation. Referring again to Figure 1-1, we see that target T1 is seen by sensors S1 and S2. The tracks of T1 produced by the two sensor systems will not overlay exactly--thus the requirement for some sort of decision process (automatic or manual) to accomplish intersensor correlation.

This paper is devoted exclusively to automatic (i.e., computer) algorithms for carrying out the tasks associated with intersensor correlation. One particular algorithm (the "k-track clustering" algorithm) is discussed in some detail in order to highlight the fundamental combinatorial structure of large area surveillance.

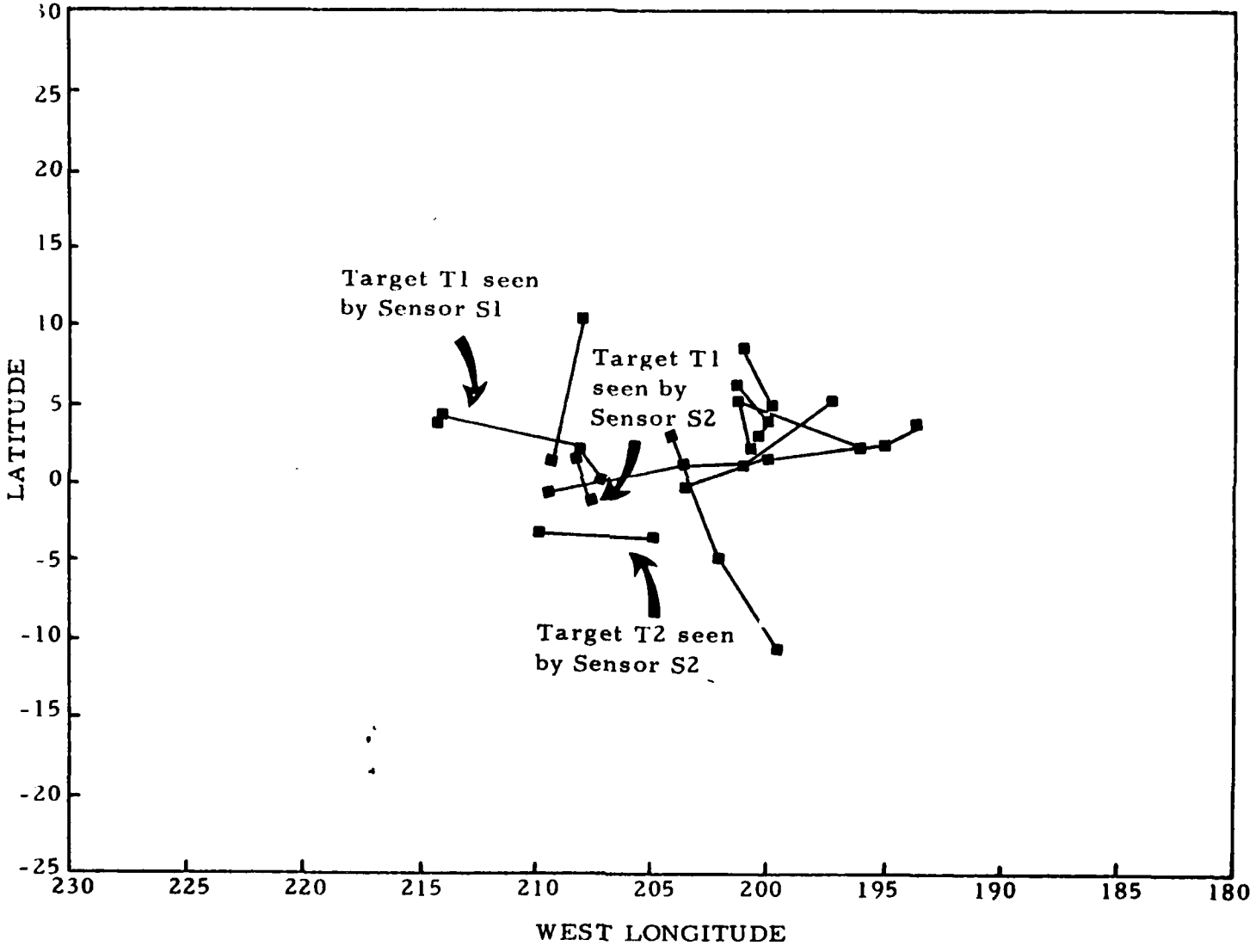

Figure 1-1. Typical multisensor view of a large ocean area.

The working definition of Multisource Interaction (MSI) adopted in this paper is one which is effectively decoupled from the problems of sensor allocation and sensor-level multitarget tracking. By that we mean that the sensors' fields of view are controlled by a separate process, and that the multitarget tracking problem is solved on a sensor-by-sensor basis. The responsibility of MSI data processing is then to carry out intersensor correlation for various track file data bases. The MSI issues addressed herein arise due to the partitioning of a large surveillance data base into smaller, more manageable segments. As Figure 1-2 indicates, data is generated by many sensors due to objects present in several spatial sectors during some specified time interval. If the multitarget tracking problem is solved separately for each individual sensor (see [1]), then track estimates for objects in the surveillance area become consolidated first at the level of individual sensors. This is indicated schematically in Figure 1-2 as the consolidation of the raw sensor measurements (data bases A, B, C) into a "sensor-level" data base D that consists of a complete track file for that specific sensor.

The final step in the process of forming a complete picture of the objects present in the surveillance area is the solution to the intersensor correlation problem. At this level of the MSI data processing hierarchy, the track files D, E, F belonging to the different sensor systems are compared to determine the correlation between tracks in separate data bases. As indicated in Figure 1-2, the output of an intersensor correlation algorithm is an entry (or entries) into a master data base G that consists of track files on an object-by-object basis for the entire surveillance volume. If the intersensor correlation problem is solved correctly, the master data base will contain a complete list of object tracks, without duplication, and in

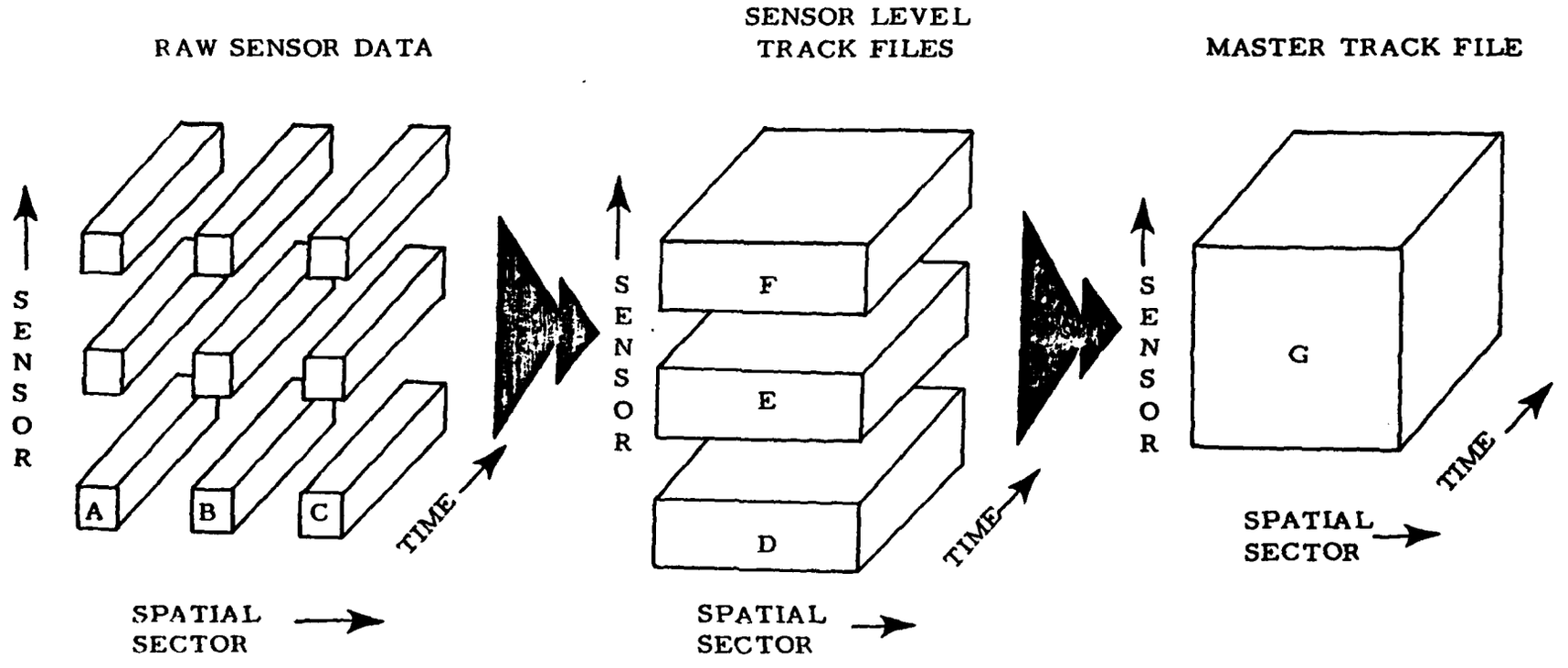

Figure 1-2. Overview of MSI Hierarchical Information Processing.

a single, common coordinate system. (The coordinate system utilized in the algorithm described in Section 2. is latitude, latitude rate, longitude, longitude rate.)

1.1 Description of the Intersensor Correlation Problem

The multitarget tracking data processing done at the sensor level, using algorithms such as those discussed in [1], produces track files consisting of object state vectors and (sometimes) estimation error covariance at specific points in time.

Typically, the sensor level track files will contain information such as that shown below in Table 1-1.

Table 1-1. Typical information content of an MSI Data Base.

Data / Track	State Vector	State Vector Error Covariance	Object Name	Sensor I.D. Number
1	$^{3}\hat{x}^{1}(t_1)$, $^{3}\hat{x}^{1}(t_2)$	$^{3}P^{1}(t_1)$, $^{3}P^{1}(t_2)$	QUEEN MARY	3
2	$^{8}\hat{x}^{2}(t_3)$	Unknown	Unknown	8
3	$^{6}\hat{x}^{3}(t_4)$, $^{6}\hat{x}^{3}(t_5)$, $^{6}\hat{x}^{3}(t_6)$	$^{6}P^{3}(t_4)$, $^{6}P^{3}(t_5)$, $^{6}P^{3}(t_6)$	Unknown	6

The notation used in Table 1-1 is defined as follows:

$\hat{{}^{j}x}^{i}(t_k)$ ~ sensor level track file estimate of the state at time t_k of a target seen by sensor j. The individual tracks are denoted by the index i.

${}^{j}P^{i}(t_k)$ ~ the sensor level track file error covariance matrix of the measurement $\hat{{}^{j}x}^{i}(t_k)$.

It is often the case that the $(\hat{x}, P)$ data recorded in the data base is itself generated by a tracking filter of some kind. Referring again to Figure 1-2, recall that the $(\hat{x}, P)$ records are associated with sensor level track files (D, E, F). Thus, $(\hat{x}, P)$ records are created by processing the raw sensor data for <u>one</u> sensor with a filter to produce a chain of target track points.

Because of the diversity of sensors that are operating in a large area surveillance system, the time points t_k at which the object states (latitude, longitude, etc.) are estimated may not coincide. Furthermore, the number of time points per object and even the state vector coordinate system where the sensor-level multitarget tracking problem is resolved will differ for the various sensors' track files. The diverse nature of the sensor-level track files introduces an added degree of complexity into the intersensor correlation problem.

Based on these last comments, a more accurate definition of intersensor correlation might be as follows: to cluster together those tracks corresponding to the same object, and to produce a composite estimate of each object's motion in a single coordinate system common to all sensors.

1.2 Algorithms for Intersensor Correlation

There are two basic components of any intersensor correlation process: a similarity measure to quantify the "distance" between tracks, and a clustering criterion to carry out the actual correlation of tracks. Since the tracks to be clustered together are in fact samples from a stochastic process, similarity measures can be based theoretically upon the distance between stochastic processes. In essence, we simply process the data from different track files with a single Kalman filter; the residuals from the filter are then used to measure the "distance" between the tracks.

The clustering criteria used to determine the intersensor correlations can range from various forms of pairwise correlators to the more sophisticated k-wise correlation to be discussed below. As an example of a simple pairwise clustering criterion, consider the following:

Step 1. Compute the similarity S_{ij} between all pairs of tracks

Step 2. If S_{ij} is greater than a preset threshold δ, then Track i and Track j are declared to be the same object ($i \leftrightarrow j$)

Step 3. If $i \leftrightarrow j$, and $j \leftrightarrow k$, then $i \leftrightarrow k$ (i.e., all three tracks are the same ship).

A little reflection upon the algorithm presented above will indicate to the reader that an iterative application of Step 3 will produce a complete picture of the correlations in any particular data base. It is also clear that the algorithm is vulnerable to at least one type of cascading error. This is shown below in Figure 1-3, which contains four targets (T1, T2, T3, T4) on parallel courses. If S_{12}, S_{23}, S_{34} are all greater than δ, then the pairwise algorithm outlined above will declare all four sensor-level track files to be the same ship.

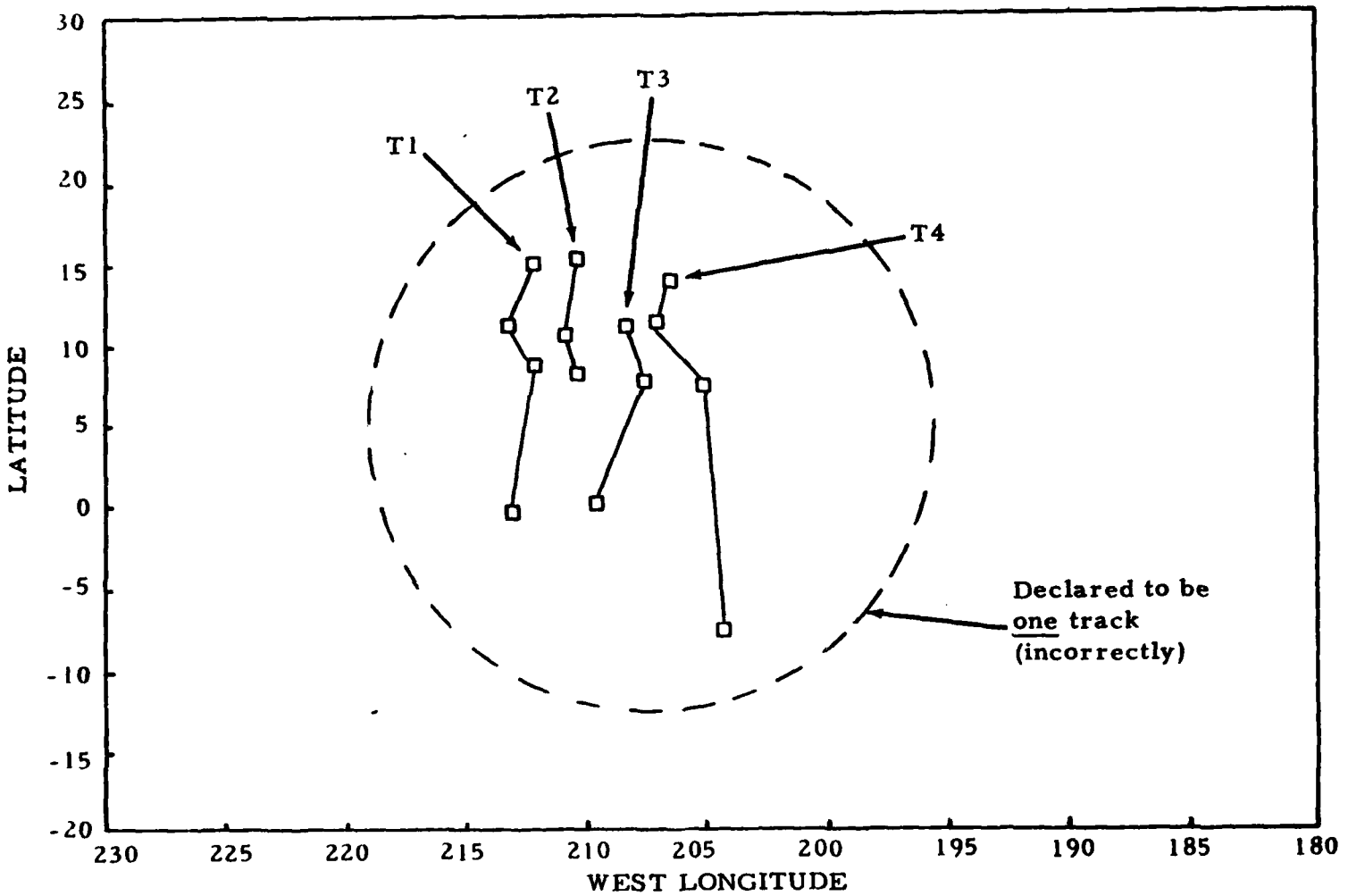

Figure 1-3. Cascading errors in a simple pairwise intersensor correlation process.

The object of these last remarks is to illustrate that simple automatic algorithms for intersensor correlation may have hidden difficulties, and that there is some merit in working with the more complex decision processes discussed in the following sections.

1.2.1 Track File Similarity Measure

This section will describe a simple technique for measuring the similarity between different tracks in an MSI data base. For example, in Table 1-1 above, a fundamental question that the analyst might wish to ask is the following: how similar is track #1 (QUEEN MARY) to track #3? The basic technique we employ is illustrated in Figure 1-4 below. First, the points t_1, t_2, t_3, t_4, t_5, t_6 are ordered in terms of increasing time. Following this, the sensor-level state vectors are input to a Kalman filter, and the residual sequence is monitored.

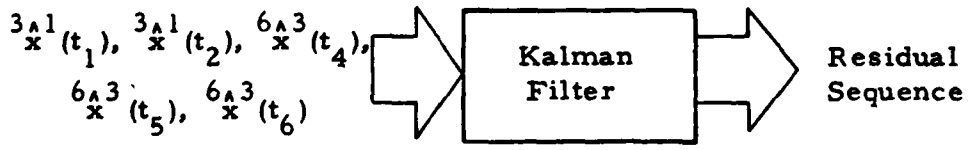

Figure 1-4. Measuring the similarity of different track files.

When testing the similarity of two tracks i and j, it is necessary that the test be carried out in a coordinate system common to both tracks. Since the tracks i and j come from different sensor-level track files, it is possible that they are represented as vectors $\hat{x}$ of different form. As a simple example, the state of track i might be represented as latitude/longitude only, while track j might be represented as latitude, longitude, course, and speed.

In the algorithm described in this paper, sensor-to-sensor track correlation is carried out for all tracks in a single, common coordinate system. We assume that target motion is adequately modeled by a stochastic difference equation of the form

$$y(k+1) = \varphi(k+1, k)\, y(k) + v(k), \quad k = 0, 1, \ldots, \tag{1}$$

where

- $y(k)$ ~ vector describing object state at time t_k (latitude, latitude rate, longitude, longitude rate)
- $\varphi(\cdot, \cdot)$ ~ state transition matrix model (for "straight-line" motion)
- $v(k)$ ~ noise model compensating for inaccuracies in modeled track motion (e.g., small random course changes)

The state vectors $\hat{x}$ from the track files are treated as if they are "measurements" of actual target motion; the error covariance matrices P of the state vectors are treated as though they are "noise" in the measurements. Using this pseudo-measurement, we have:

$$^{j}\hat{x}^{i}(k) = c^{j}(y(k), k) + {}^{j}w^{i}(k) \tag{2}$$

where

- $y(k)$ ~ actual target state at time t_k
- $c^{j}(\cdot, \cdot)$ ~ observation equation for j^{th} sensor
- $^{j}w^{i}(k)$ ~ "measurement" noise with covariance $^{j}P^{i}(t_k)$

Using the $\hat{x}$ as inputs, a Kalman filter can be used to estimate the true ship motion y(k) under the assumption that the inputs $\hat{x}$ from the various sensor-level track files are due to the same ship. As the Kalman filter operates, residuals r(k) are produced whose magnitude can be predicted, using the covariances P from the track files and the covariances of v(k) in Equation (1) above. In particular, the covariance matrix $\Delta(k)$ of the residuals can be computed.

If the observed variance of the residuals r(k) compares favorably with their predicted value $\Delta(k)$, then the sensor-level tracks whose state vectors were used to compute the residual sequence $\{r(k)\}$ are said to be "similar."

Note that in the two-track case, if the vectors for the two tracks i and j being tested for correlation are in the same coordinate system and at the same time point, then we could alternatively use euclidean distance as a similarity measure, for example

$$\text{distance } (i,j) = \| {}^{k}\hat{x}^{i}(t) - {}^{\ell}\hat{x}^{j}(t) \|^{2} \tag{3}$$

$$S_{ij} = \exp(-\text{distance } (i,j)) \tag{4}$$

However, the tracks we deal with from the various MSI files are often not in the same coordinate system and not at the same time point. Therefore, we resort to the Kalman filtering technique described above to compute distance between tracks.

Each potential correlation ω is the result of a hypothesis test that uses a likelihood function $p(\omega)$ determined from the motion model Equation (1). For example, if Track #1 and Track #3 from Table 1-1 are to be tested to determine their similarity, then

$$\omega = \left\{ {}^{3}\hat{x}^{1}(t_1),\ {}^{3}\hat{x}^{1}(t_2),\ {}^{6}\hat{x}^{3}(t_4),\ {}^{6}\hat{x}^{3}(t_5),\ {}^{6}\hat{x}^{3}(t_6) \right\}$$

is a 2-track correlation and the likelihood function is found by computing a sequence of estimates $\hat{y}(t_i)$ of ship position using Equations (1) and (2) and ω. The rule that decides that tracks $i_1, i_2, i_3, \ldots$ are correlated is then

$$S_{i_1 i_2 i_3 \ldots} = \ell n\, p\left(\omega \mid \{\hat{y}(t_k)\}\right) \geq \delta . \tag{5}$$

Based on the log likelihood decision function, the set of potential correlations is

$$D = \left\{ \omega \mid \ell n\, p\left(\omega \mid \{\hat{y}(t_k)\}\right) \geq \delta \right\} . \tag{6}$$

As noted above, the actual computation of $S_{i_1 i_2 i_3 \ldots}$ is carried out by a Kalman filter, using the innovations sequence

$$r(k) = {}^{j}\hat{x}^{i}(k) - c^{j}(\varphi(k, k-1)\,\hat{y}(k-1),\ k) . \tag{7}$$

The negative log-likelihood function is given in this case by

$$-\ell n\, p(\omega) = \frac{1}{2} \sum_{k=1}^{n} \dim\left({}^{j}\hat{x}^{i}(t_k)\right) \ell n\, 2\pi + \frac{1}{2} \sum_{k=1}^{n} \ell n\, |\Delta(k)| .$$

$$+ \frac{1}{2} \sum_{k=1}^{n} r(k)^{t}\, \Delta(k)^{-1}\, r(k), \tag{8}$$

where $\Delta(k)$ is the covariance of $r(k)$ computed by the Kalman filter and $\dim({}^{j}\hat{x}^{i}(t_k))$ is the dimension of ${}^{j}\hat{x}^{i}(t_k)$.

The summation $\Sigma r(k)^t \Delta(k)^{-1} r(k)$ is a chi-squared random variable, as are its individual terms $r(k)^t \Delta(k)^{-1} r(k)$. The remaining terms in Equation (8) are deterministic. As a result, the similarity test Equation (5) can be written in the form of the following cumulative chi-square test:

$$\sum_{k=1}^{n} r(k)^t \Delta(k)^{-1} r(k) \leq \chi_c^2 . \qquad (9)$$

Note that χ_c^2 is a function of the number of individual measurements in the correlation.

The actual construction of the complete set of potential correlations D is accomplished through the use of a depth first backtracking algorithm. By this we mean that as many tracks as possible are added to a potential correlation before backtracking occurs. When backtracking occurs, all points associated with the track being stripped out of the correlation are removed.

1.2.2 Discriminating Between Correct and Incorrect Correlations

Because of the statistical nature of the decision process (9) used to construct the potential correlation file D, some tracks may be included in more than one correlation. It may be difficult to decide which correlation is correct (if any) based only on the similarity measure. The Bayesian decision process is structured to alleviate this difficulty by evaluating only complete pictures of the surveillance area. The potential correlations in D are matched together in every way possible until the best possible "global" picture of the area is found. The basic constraint operable at each stage in this combinatorial decision problem is that a track can be used in at

most one correlation. The actual optimization problem is the following:

maximize $\Sigma S_{i_1 i_2 i_3 \cdots}$ subject to the constraint that tracks are only used once

(10)

The mathematical form of the problem is as follows:

$$\max \; d^t \nu \tag{11}$$

subject to

$$B\nu \leq \mathbf{1} \tag{12}$$

$$\nu \text{ binary} \tag{13}$$

where d is a vector of similarity measures $S_{i_1 i_2 i_3 \ldots}$, ν is a binary vector denoting which elements of D were selected, B is a matrix of zeros and ones chosen to enforce the constraint mentioned in (10), and $\mathbf{1}$ is a vector of ones.

1.2.3 Integer Programming Methods

Problem (11) – (13) is a 0-1 integer program that can be solved using implicit enumeration techniques. The basic idea of these techniques is to minimize through the use of appropriate tests the extent to which the Bayesian decision tree must be examined before a solution of (11) – (13) is found. The actual technique employed in the algorithm is discussed in some detail in [1]. Since the combinatorial structure of the Bayesian decision process is the same for both k-track correlation and the multitarget tracker discussed in [1], the algorithm can be used without modification.

2.0 NUMERICAL RESULTS

This chapter will discuss some of the characteristics of the k-track correlation process as it is actually applied to data. Table 2-1 below summarizes a set of two test cases that were analyzed. Runs #1 and 2 were synthetic data cases in which intermittent, noisy track reports were made on six ships. The synthetic data test cases will be discussed in some detail to illustrate the basic structure of the MSI correlation problem.

Table 2-1. Summary of numerical results using k-track correlation algorithm.

Run No.	Data File	Parameter File	Number of Potential Correlations	Time Required for Potential Correlations (sec.)	Number of Correlations Selected	Time Required by Integer Program (sec.)	Number of Individual Track Reports in Data Base	Number of Data Points
1	ORT1A	PAR1A	11	5.7	3	<.1	10	30
2	ORT1B	PAR1B	26	7.4	3	.3	10	30

2.1 Description of Simulated Data Bases

The truth model for Runs #1 and 2 is contained in Figure 2-1 and Tables 2-2 and 2-3 below. The actual data bases (ORT1A and ORT1B) used in Runs #1 and 2 are contained in Tables 2-4 and 2-5.

The situation modeled in data bases ORT1A and ORT1B is one in which six simulated ships are seen and reported by a fictitious suite of MSI sensors on different occasions within a 60-hour time period. The ships are assumed to hold constant latitude rate/longitude rate courses for the entire 60 hours. The sensors that are brought to bear on the situation are of two types, as indicated in Table 2-6. Type 1 sensors measure latitude, longitude, and their time derivatives. Type 2 sensors measure latitude and longitude only.

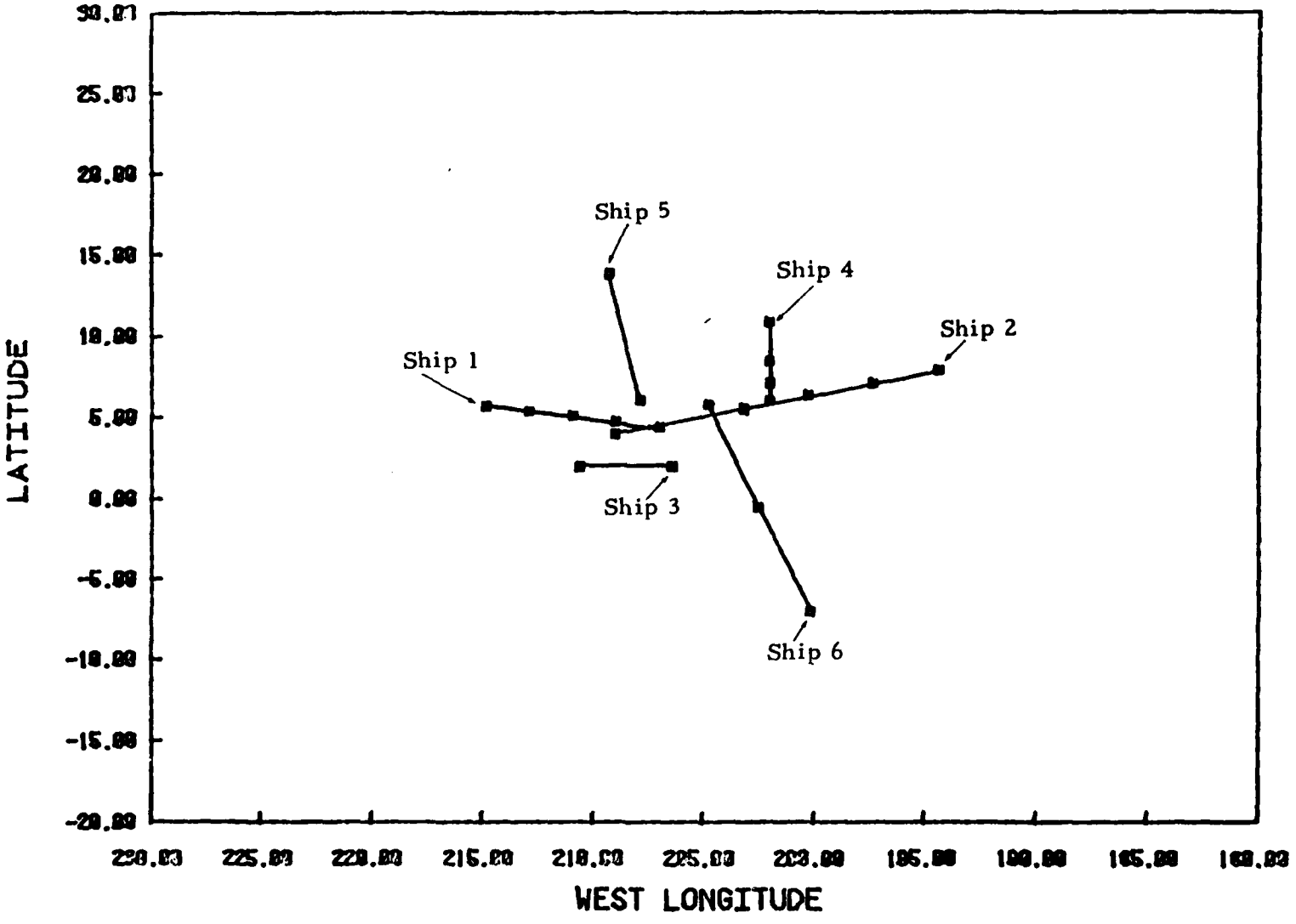

Figure 2-1. Six-ship simulation scenario (truth model).

Table 2-2. Summary of 6-ship simulation.

Ship	Initial N. Lat. (deg.)	Initial E. Long. (deg.)	Course (deg.)	Speed (knots)	Number of Sensors Detecting Ship and Forming Track Report
1	4	155	280	10	2
2	4	151	75	15	3
3	2	155	270	7	1
4	6	158	0	6	2
5	1	153	350	13	1
6	9	154	160	17	1

Table 2-3. Truth model for Runs #1 and 2.

DATA POINT NUMBER	SHIP NUMBER (TRUTH)	TRACK FILE NUMBER	MOVEMENT INFORMATION				
			TIME	NORTH LAT	LATITUDE RATE	EAST LONG	LONGITUDE RATE
1	1	1	43200.0	4.3473	0.8039E-05	153.0251	-0.4572E-04
2		1	129600.0	5.0419	0.8039E-05	149.0726	-0.4577E-04
3		2	43200.0	4.3473	0.8039E-05	153.0251	-0.4572E-04
4		2	86400.0	4.6946	0.8039E-05	151.0494	-0.4575E-04
5		2	172800.0	5.3892	0.8039E-05	147.0948	-0.4580E-04
6		2	216000.0	5.7365	0.8039E-05	145.1159	-0.4582E-04
7	2	3	86400.0	5.5529	0.0000E+00	156.8159	0.0000E+00
8		3	129600.0	6.3294	0.0000E+00	159.7294	0.0000E+00
9		3	172800.0	7.1058	0.0000E+00	162.6472	0.0000E+00
10		4	0.0	4.0000	0.1797E-04	151.0000	0.6724E-04
11		4	86400.0	5.5529	0.1797E-04	156.8159	0.6739E-04
12		4	129600.0	6.3294	0.1797E-04	159.7294	0.6749E-04
13		4	172800.0	7.1058	0.1797E-04	162.6472	0.6760E-04
14		5	86400.0	5.5529	0.1797E-04	156.8159	0.6739E-04
15		5	129600.0	6.3294	0.1797E-04	159.7294	0.6749E-04
16		5	172800.0	7.1058	0.1797E-04	162.6472	0.6760E-04
17		5	216000.0	7.8823	0.1797E-04	165.5700	0.6772E-04
18	3	6	43200.0	2.0000	0.0000E+00	153.5991	0.0000E+00
19		6	172800.0	2.0000	0.0000E+00	149.3966	0.0000E+00
20	4	7	0.0	6.0000	0.2778E-04	158.0000	0.0000E+00
21		7	172800.0	10.8000	0.2778E-04	159.0000	0.0000E+00
22		8	0.0	6.0000	0.2778E-04	158.0000	0.0000E+00
23		8	43200.0	7.2000	0.2778E-04	158.0000	0.0000E+00
24		8	86400.0	8.4000	0.2778E-04	158.0000	0.0000E+00
25		8	172800.0	10.8000	0.2778E-04	158.0000	0.0000E+00
26	5	9	86400.0	6.1210	0.5927E-04	152.0950	-0.1051E-04
27		9	216000.0	13.8025	0.5927E-04	150.7187	-0.1076E-04
28	6	10	43200.0	5.8050	-0.7396E-04	155.1728	0.2706E-04
29		10	129600.0	-0.5849	-0.7396E-04	157.5022	0.2692E-04
30		10	216000.0	6.9740	-0.7396E-04	159.0342	0.2712E-04

Table 2-4. Synthetic MSI data base for Run #1 (data base ORT1A).

	MOVEMENT INFORMATION				
	TIME	NORTH LAT	LATITUDE RATE	EAST LONG	LONGITUDE RATE
1	43200.0	4.1492	0.9206E-05	152.9049	-0.4658E-04
2	129600.0	5.0456	0.8344E-05	149.2870	-0.4341E-04
3	43200.0	4.2937	0.5911E-05	152.9590	-0.4638E-04
4	86400.0	4.8076	0.8067E-05	151.0732	-0.4574E-04
5	172800.0	5.5932	0.9221E-05	146.9504	-0.4462E-04
6	216000.0	5.8718	0.5875E-05	145.1482	-0.4542E-04
7	86400.0	5.5847	0.0000E+00	156.9793	0.0000E+00
8	129600.0	6.5455	0.0000E+00	159.5486	0.0000E+00
9	172800.0	6.9731	0.0000E+00	162.6776	0.0000E+00
10	0.0	3.8903	0.1803E-04	150.9037	0.6873E-04
11	86400.0	5.4676	0.1771E-04	156.6906	0.6771E-04
12	129600.0	6.1707	0.1763E-04	159.5567	0.6677E-04
13	172800.0	7.2429	0.1972E-04	162.5593	0.6782E-04
14	86400.0	5.3501	0.1733E-04	156.6992	0.6804E-04
15	129600.0	6.2073	0.1607E-04	159.6627	0.6680E-04
16	172800.0	6.9876	0.1758E-04	162.7621	0.6848E-04
17	216000.0	7.7721	0.1728E-04	165.5123	0.6816E-04
18	43200.0	1.8336	0.0000E+00	153.6828	0.0000E+00
19	172800.0	1.8522	0.0000E+00	149.4227	0.0000E+00
20	0.0	6.1539	0.2936E-04	158.1071	-0.6317E-06
21	172800.0	10.6991	0.2757E-04	157.9753	0.1652E-05
22	0.0	6.0474	0.2727E-04	158.0660	-0.4371E-06
23	43200.0	7.2062	0.2697E-04	158.1080	-0.3568E-05
24	86400.0	8.3819	0.2803E-04	158.1236	0.6289E-06
25	172800.0	10.8695	0.2667E-04	158.0033	-0.9170E-06
26	86400.0	5.9870	0.5672E-04	151.9055	-0.1170E-04
27	216000.0	13.7665	0.6102E-04	150.7840	-0.1249E-04
28	43200.0	5.8855	-0.7186E-04	155.1613	0.2583E-04
29	129600.0	-0.6172	-0.7366E-04	157.4634	0.2694E-04
30	216000.0	-6.9056	-0.7588E-04	159.7972	0.2731E-04

Table 2-5. Synthetic data base for Run #2 (data base ORT1B).

	MOVEMENT INFORMATION				
	TIME	NORTH LAT	LATITUDE RATE	EAST LONG	LONGITUDE RATE
1	43200.0	2.3662	0.1931E-04	151.8230	-0.5395E-04
2	129600.0	5.0791	0.1099E-04	151.2165	-0.2292E-04
3	43200.0	3.8109	-0.1254E-04	152.3634	-0.5202E-04
4	86400.0	5.8242	0.8303E-05	151.2872	-0.4569E-04
5	172800.0	7.4293	0.1946E-04	145.6509	-0.3447E-04
6	216000.0	7.0897	-0.1288E-04	145.4386	-0.4188E-04
7	86400.0	5.8711	0.0000E+00	158.4497	0.0000E+00
8	129600.0	8.4906	0.0000E+00	157.9215	0.0000E+00
9	172800.0	5.7781	0.0000E+00	162.9507	0.0000E+00
10	0.0	2.9031	0.1850E-04	150.0369	0.8164E-04
11	86400.0	4.6994	0.1543E-04	155.5623	0.7047E-04
12	129600.0	4.7428	0.1469E-04	158.0031	0.6056E-04
13	172800.0	8.4769	0.3482E-04	161.7687	0.6976E-04
14	86400.0	3.5248	0.1175E-04	155.6485	0.7361E-04
15	129600.0	5.1084	-0.4343E-06	159.0629	0.6081E-04
16	172800.0	5.9240	0.1422E-04	163.7965	0.7615E-04
17	216000.0	6.7804	0.1130E-04	164.9938	0.7198E-04
18	43200.0	0.3364	0.0000E+00	154.4359	0.0000E+00
19	172800.0	0.5223	0.0000E+00	149.6579	0.0000E+00
20	0.0	7.5385	0.4305E-04	159.0714	-0.6106E-05
21	172800.0	9.7906	0.2576E-04	157.7525	0.1597E-04
22	0.0	6.4738	0.2285E-04	158.6602	-0.4225E-05
23	43200.0	7.2620	0.2001E-04	159.0805	-0.3449E-04
24	86400.0	8.2195	0.3025E-04	159.2360	0.6079E-05
25	172800.0	11.4950	0.1706E-04	158.0335	-0.8865E-05
26	86400.0	4.7811	0.3463E-04	150.2000	-0.2200E-04
27	216000.0	13.4423	0.7618E-04	151.3719	-0.2750E-04
28	43200.0	6.6095	-0.5367E-04	155.0578	0.1522E-04
29	129600.0	-0.9081	-0.7107E-04	157.1149	0.2712E-04
30	216000.0	-6.2626	-0.9251E-04	159.4644	0.2897E-04

Table 2-6. Sensor characteristics for simulated MSI data bases.

Run Number	Data Base	Sensor Type	Measurement Standard Deviation*				Detection Probability
			Latitude (deg^2)	Longitude (deg^2)	Latitude Rate $(deg/hr)^2$	Longitude Rate $(deg/hr)^2$	
1	ORT1A	1	.1	.1	.12E-5	.12E-5	.5
		2	.1	.1	Not measured	Not measured	.5
2	ORT1B	1	1.	1.	.12E-4	.12E-4	.5
		2	1.	1.	Not measured	Not measured	.5

*Measurement noise is modeled as a zero-mean uncorrelated Gaussian process with the indicated standard deviation.

The individual track files are contained in both synthetic data bases. As Table 2-6 indicates, the only difference in data bases ORT1A and ORT1B is the measurement accuracy of the sensors. The simulated sensor accuracy in data base ORT1A is ten times greater than that in ORT1B.

The test cases involving simulated data were run on a DEC 10 computer.

2.2 Problem Structure for Simulated MSI Scenarios

The basic structure of the k-track correlator is that of an integer program that operates on a set of potential correlations to select the most accurate picture possible of the surveillance area.

The set of potential correlations for Run #1 selected by the backtracking Kalman filter process described in Section 1.2.1 is shown in Figures 2-2 through 2-12. Each figure indicates the track file data points involved in that particular correlation. Although the parameter file setup allowed as many as ten tracks to be correlated simultaneously, the various tests employed during the backtracking process selected only 2- and 3-track correlations.

Three basic types of errors can occur in the process of forming potential k-track correlations:

Type 1 Error: the tracks included in the correlation are correct (in that they correspond to the same ship), but not all tracks from the same ship were included.

Type 2 Error: the correlation includes tracks from more than one ship.

Type 3 Error: failure to detect a true correlation.

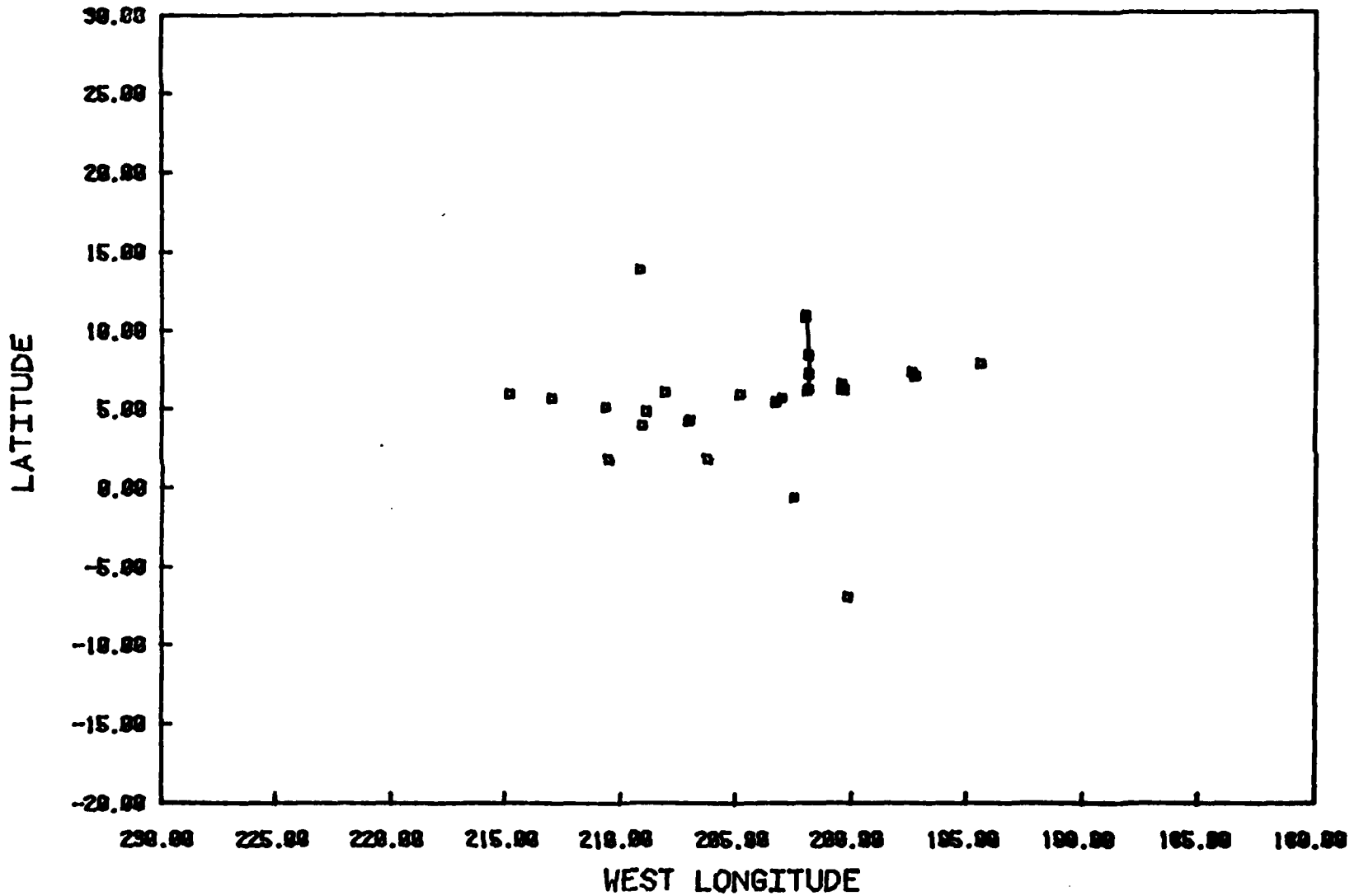

Figure 2-2. Potential correlation #1 (ORT1A/PAR1A).

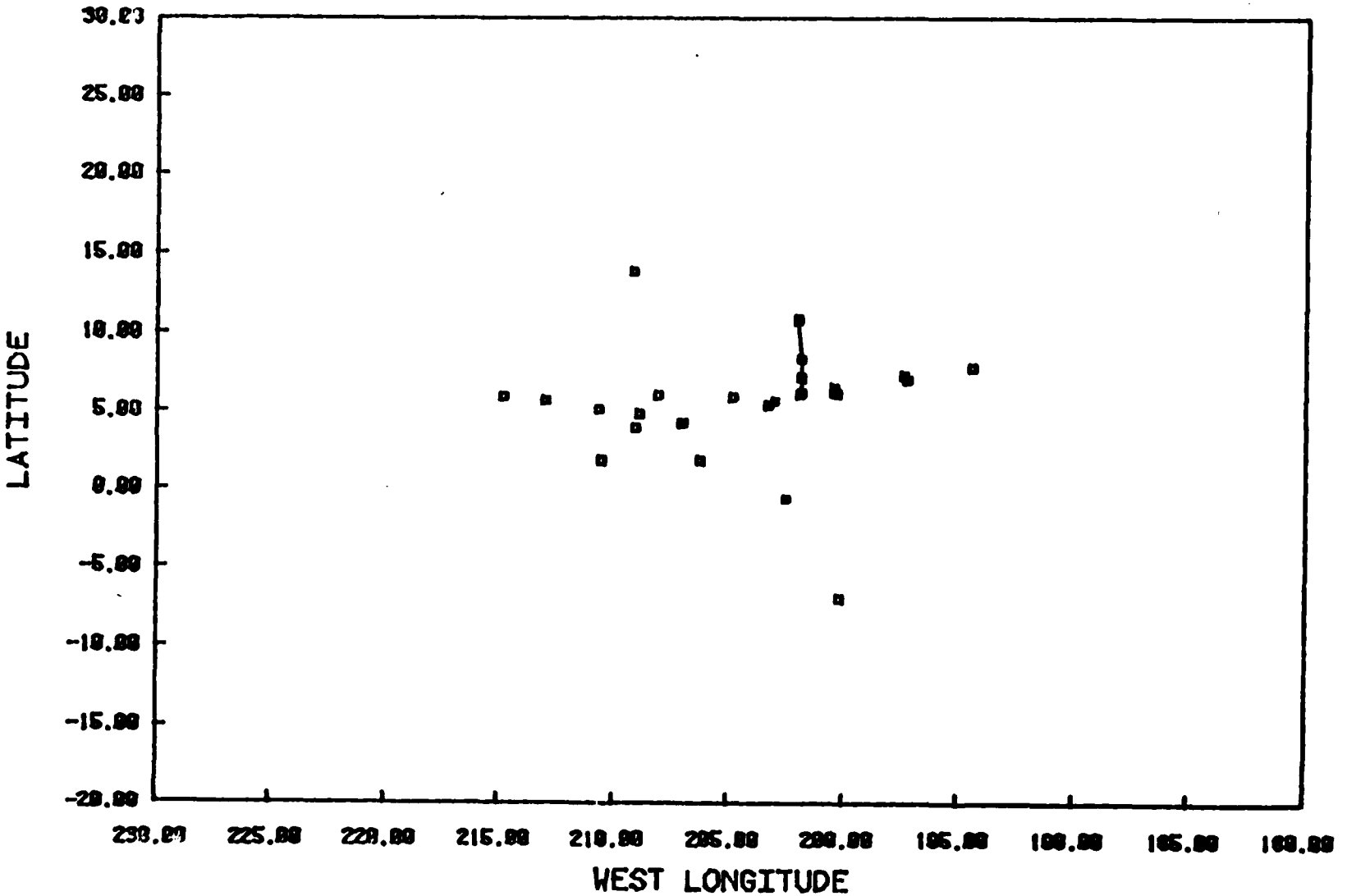

Figure 2-3. Potential correlation #2 (ORTIA/PARIA).

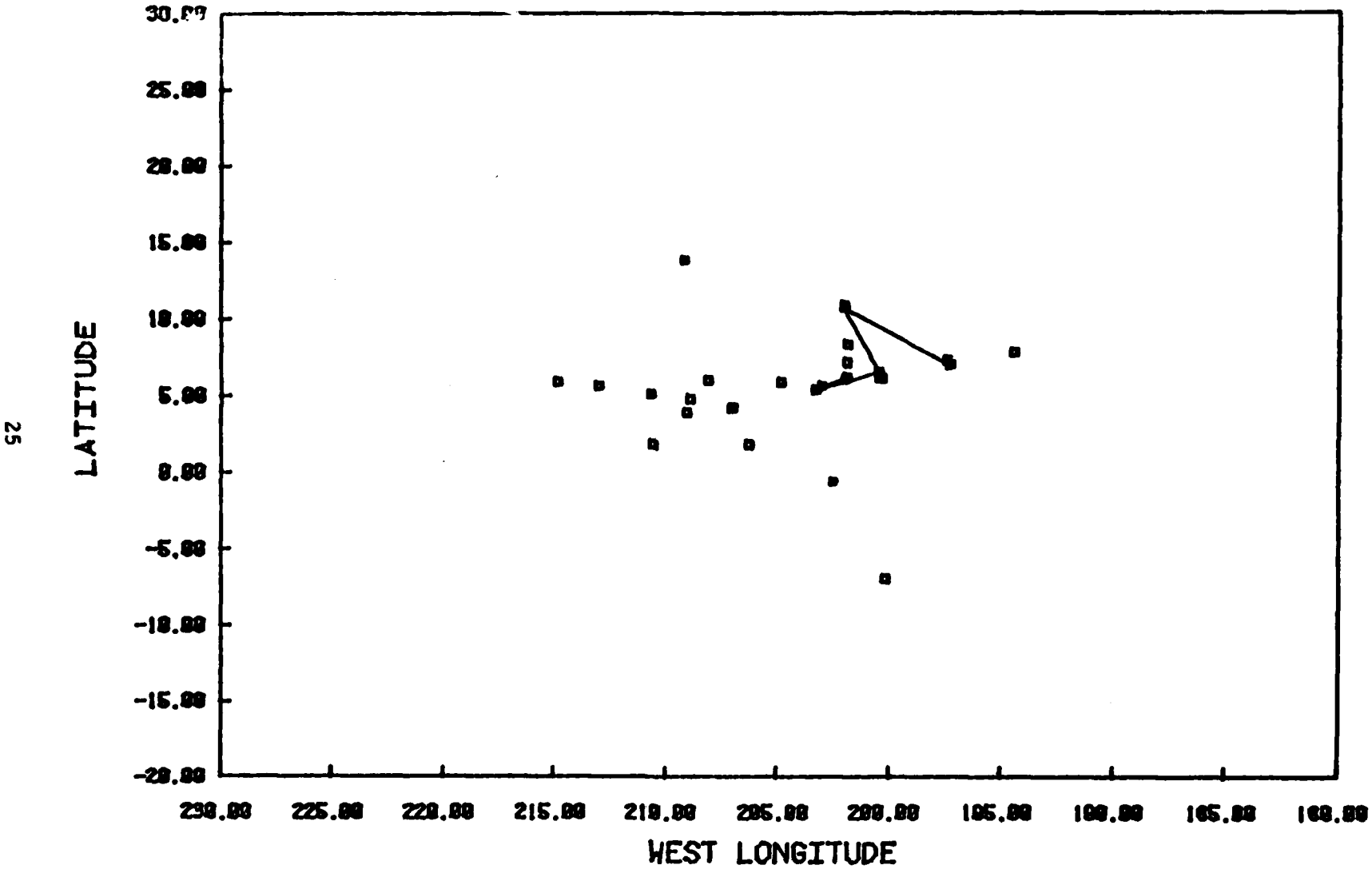

Figure 2-4. Potential correlation #3 (ORT1A/PAR1A).

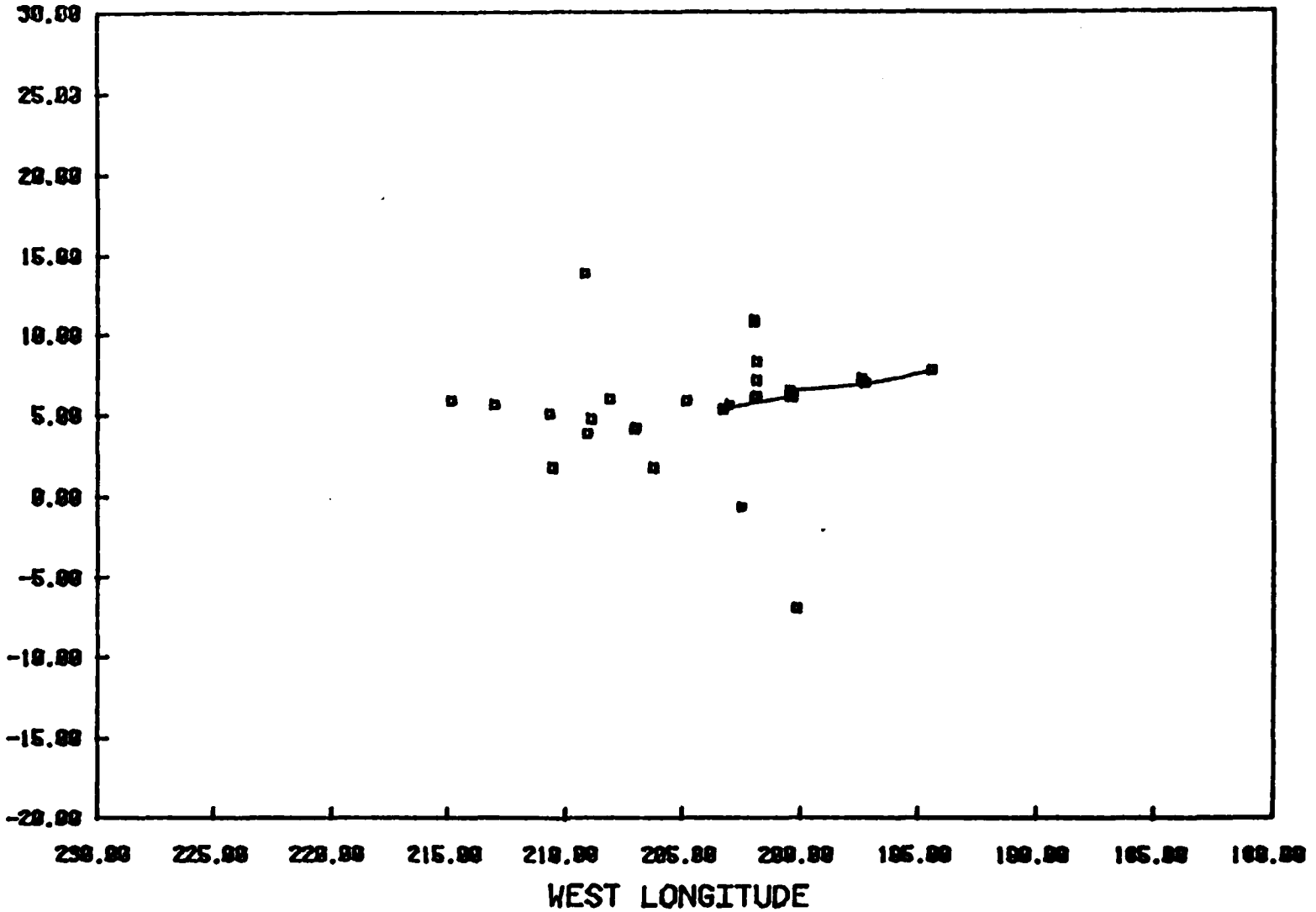

Figure 2-5. Potential correlation #4 (ORT1A/PAR1A).

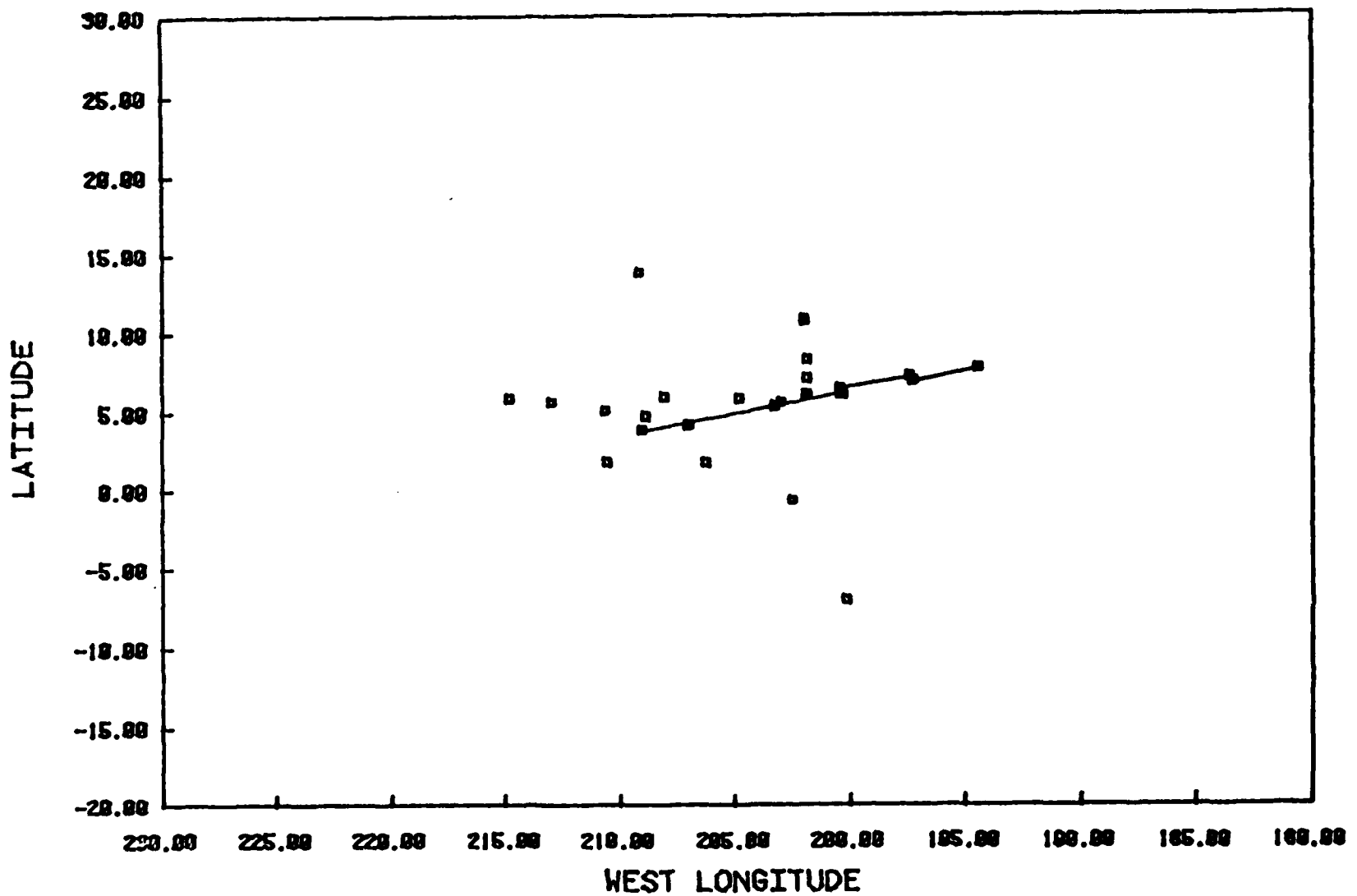

Figure 2-6. Potential correlation #5 (ORT1A/PAR1A).

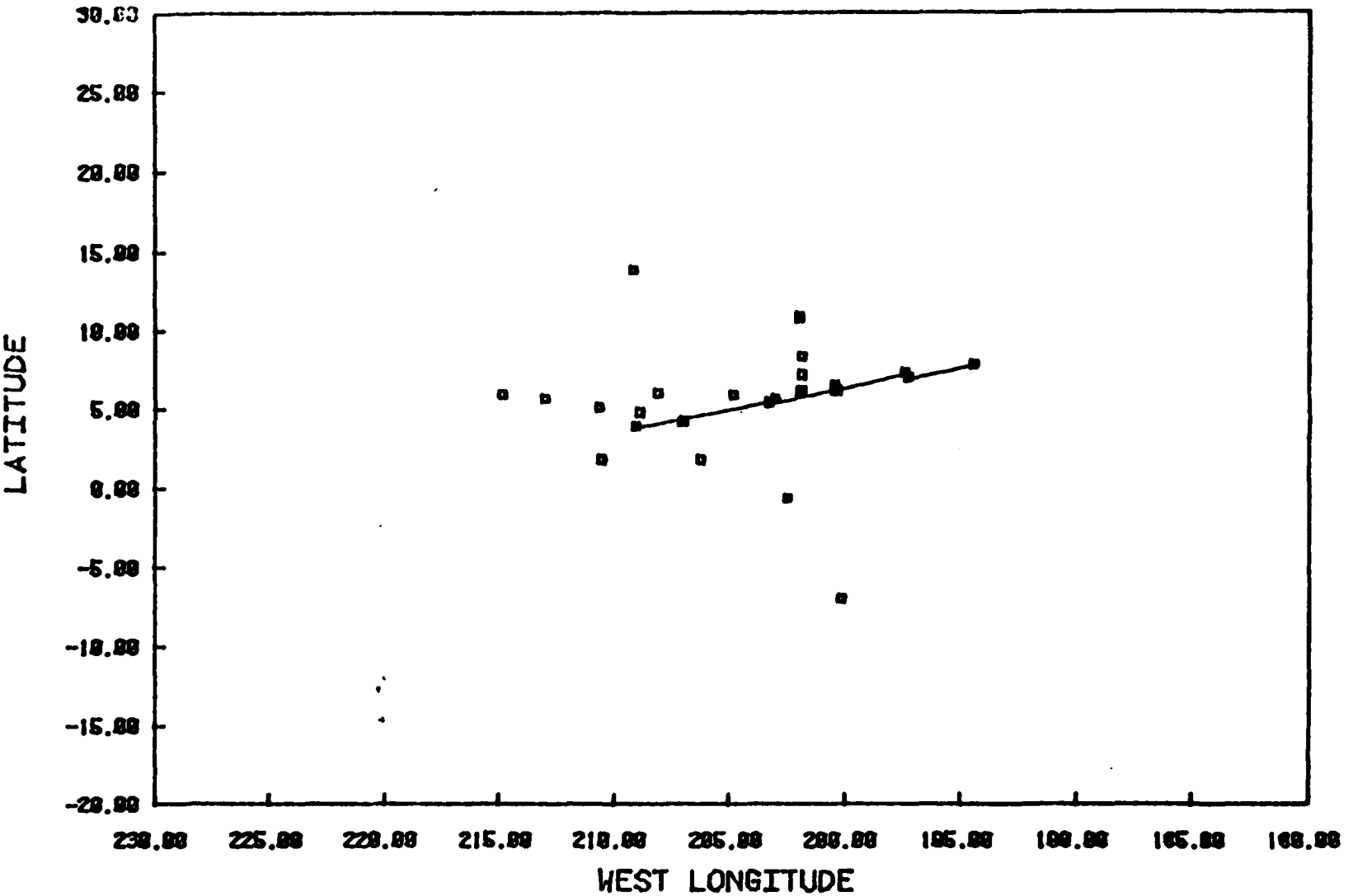

Figure 2-7. Potential correlation #6 (ORT1A/PAR1A).

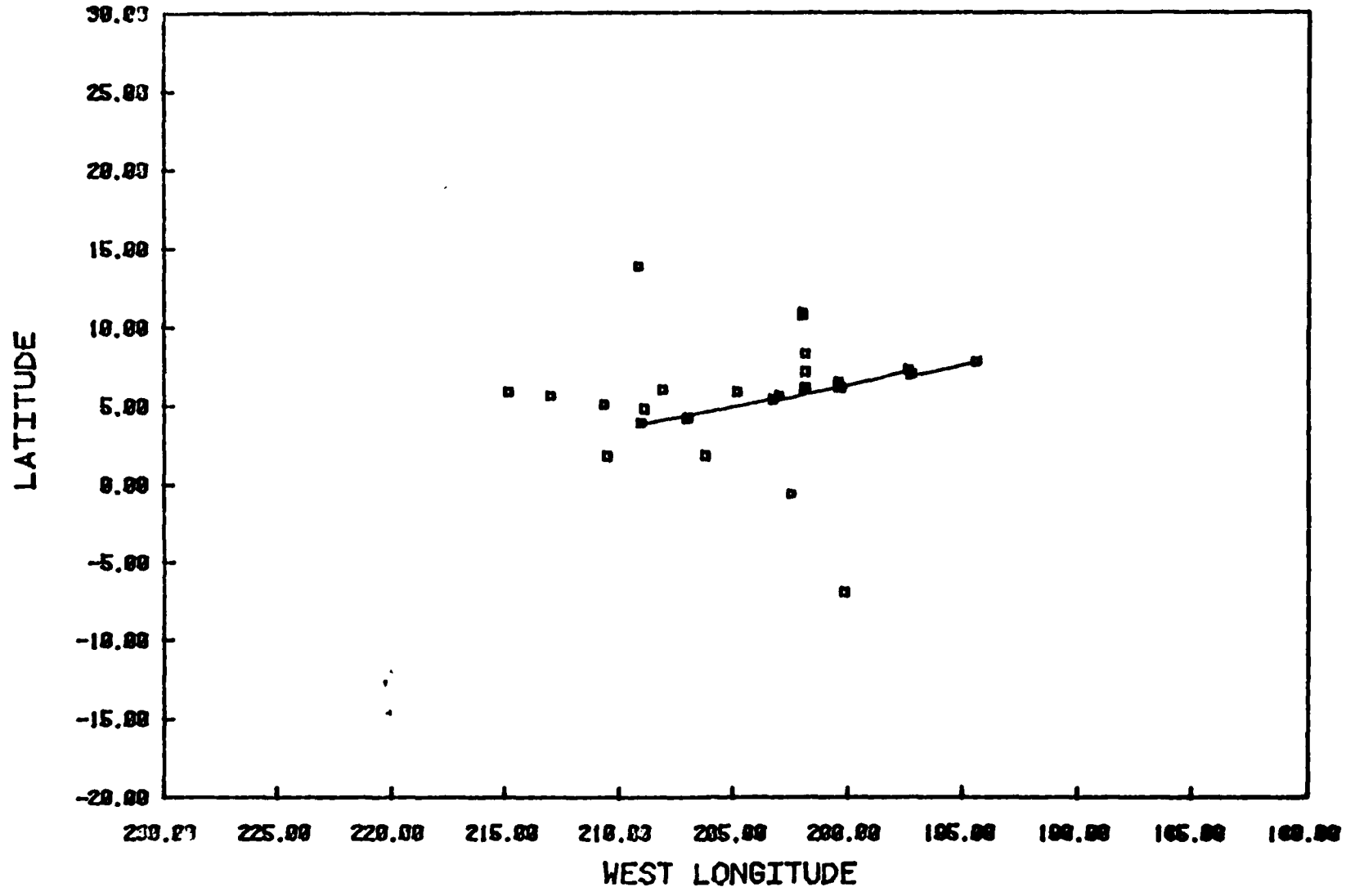

Figure 2-8. Potential correlation #7 (ORT1A/PAR1A).

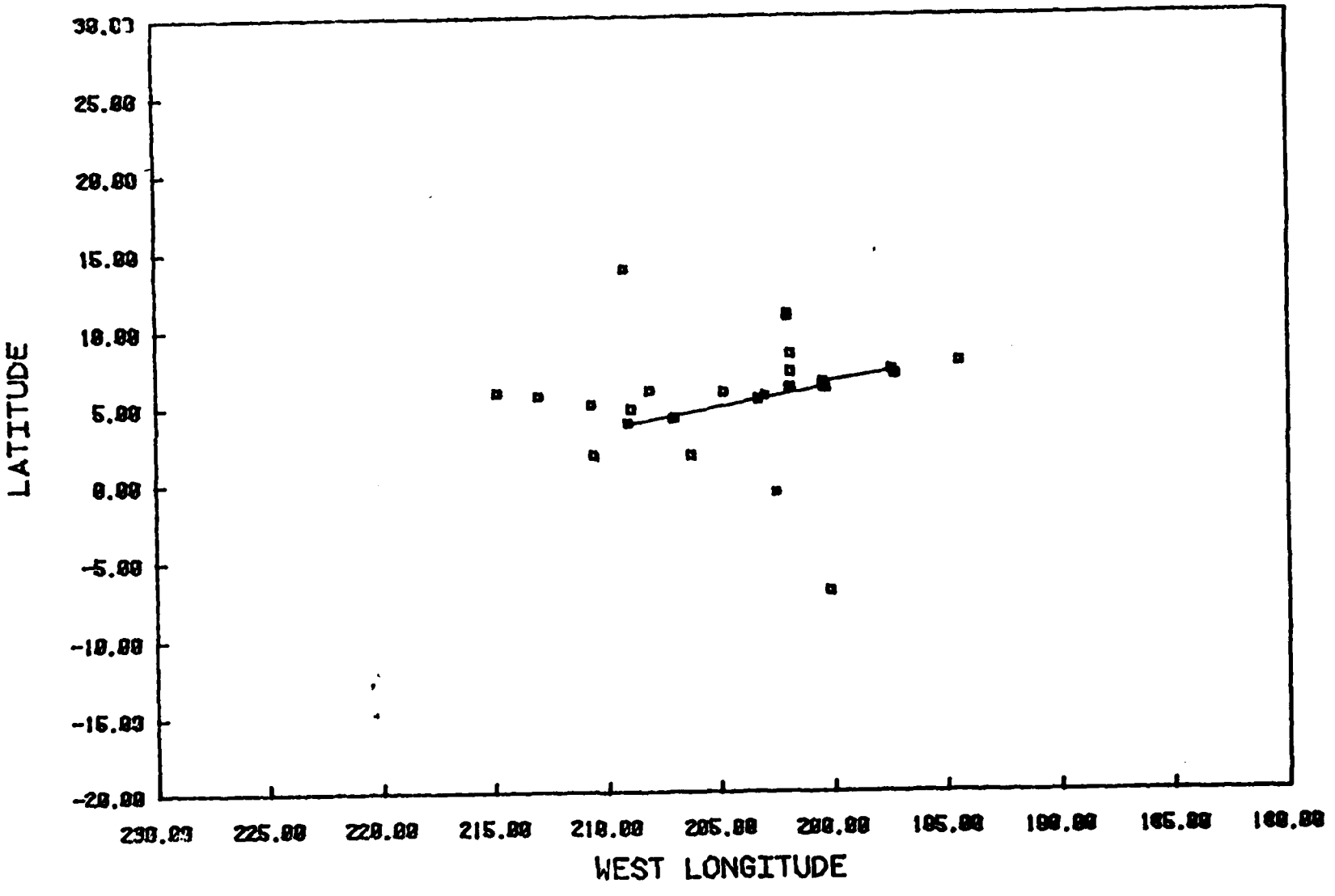

Figure 2-9. Potential correlation #8 (ORT1A/PAR1A).

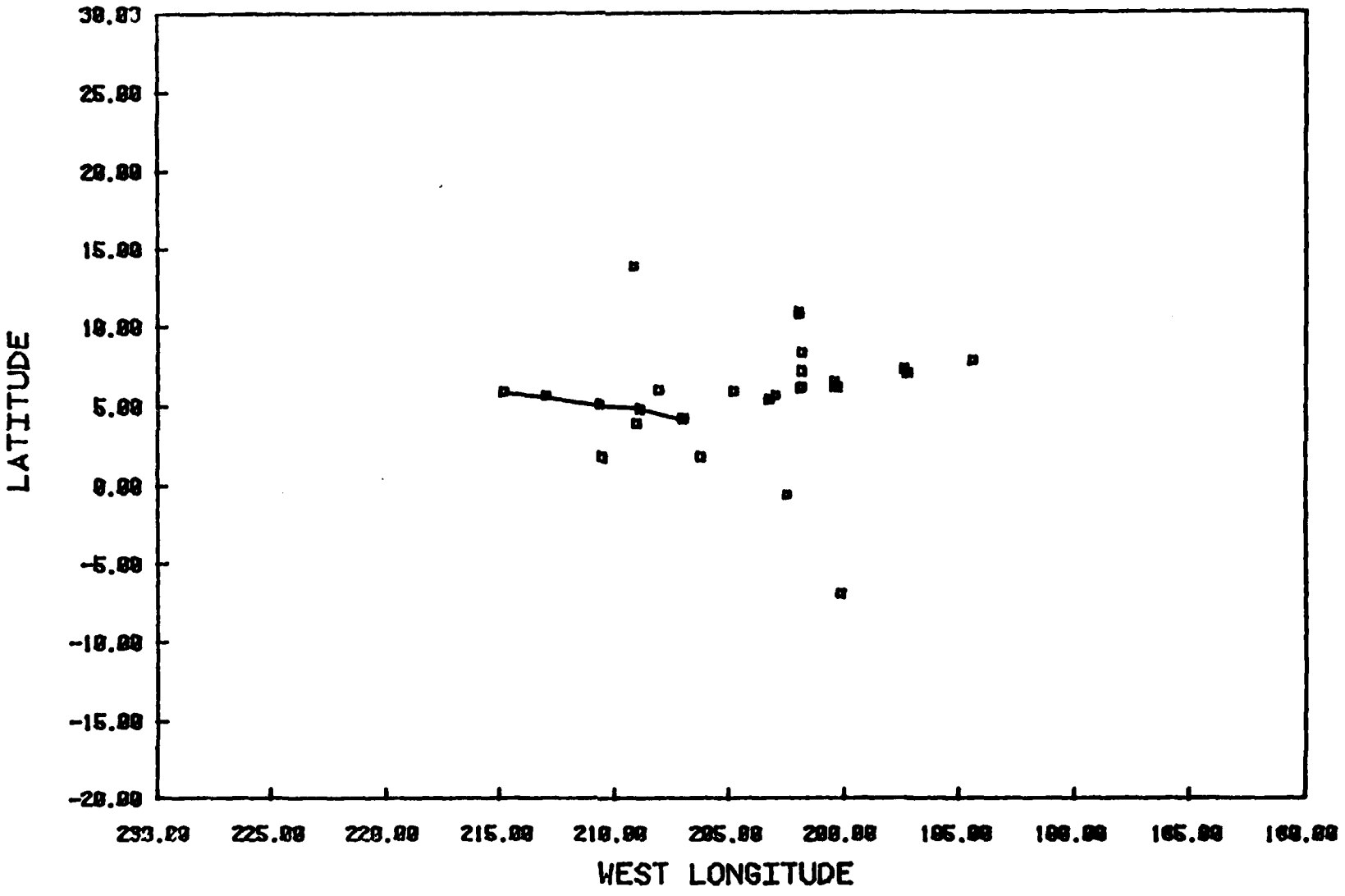

Figure 2-10. Potential correlation #9 (ORT1A/PAR1A).

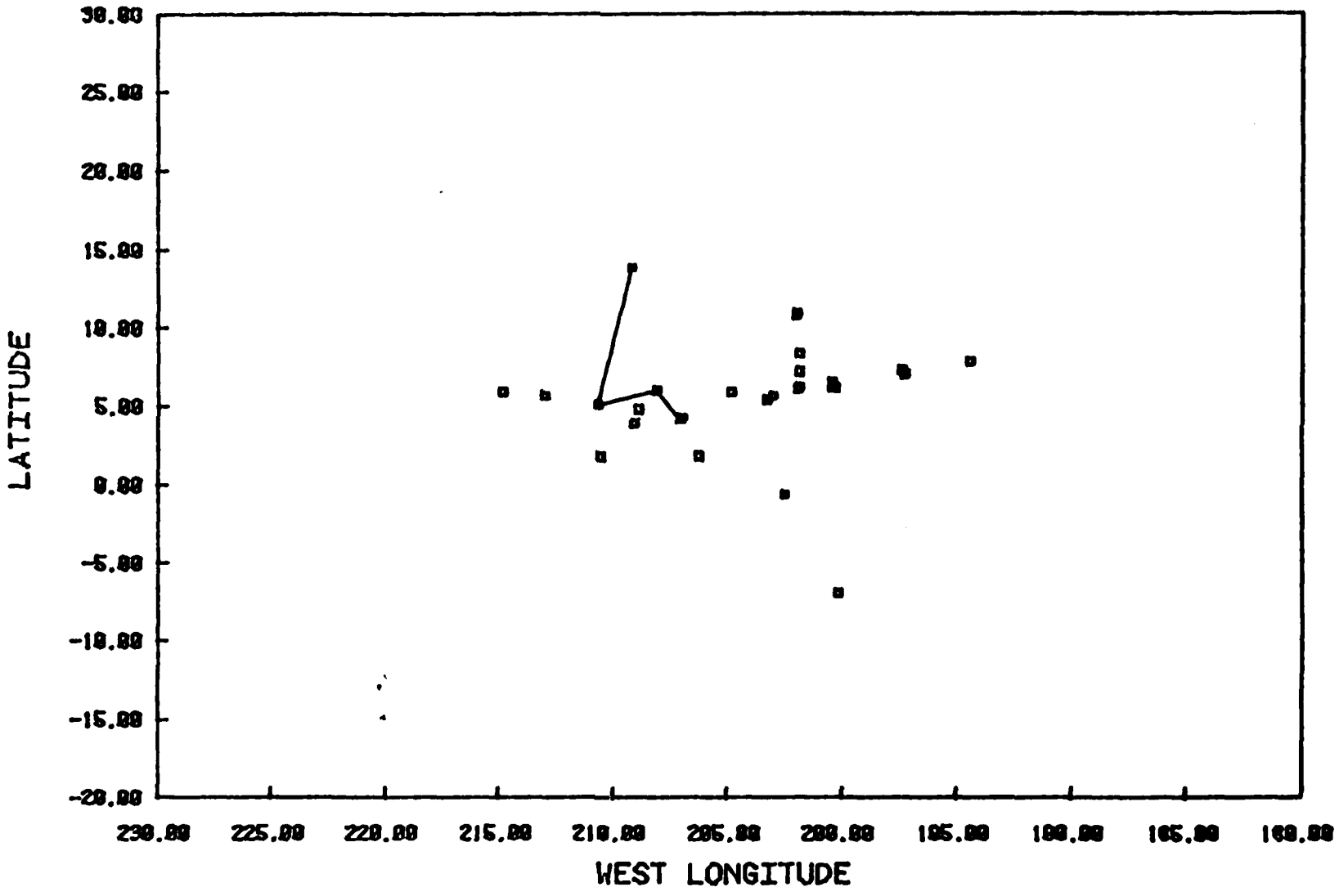

Figure 2-11. Potential correlation #10 (ORTIA/PARIA).

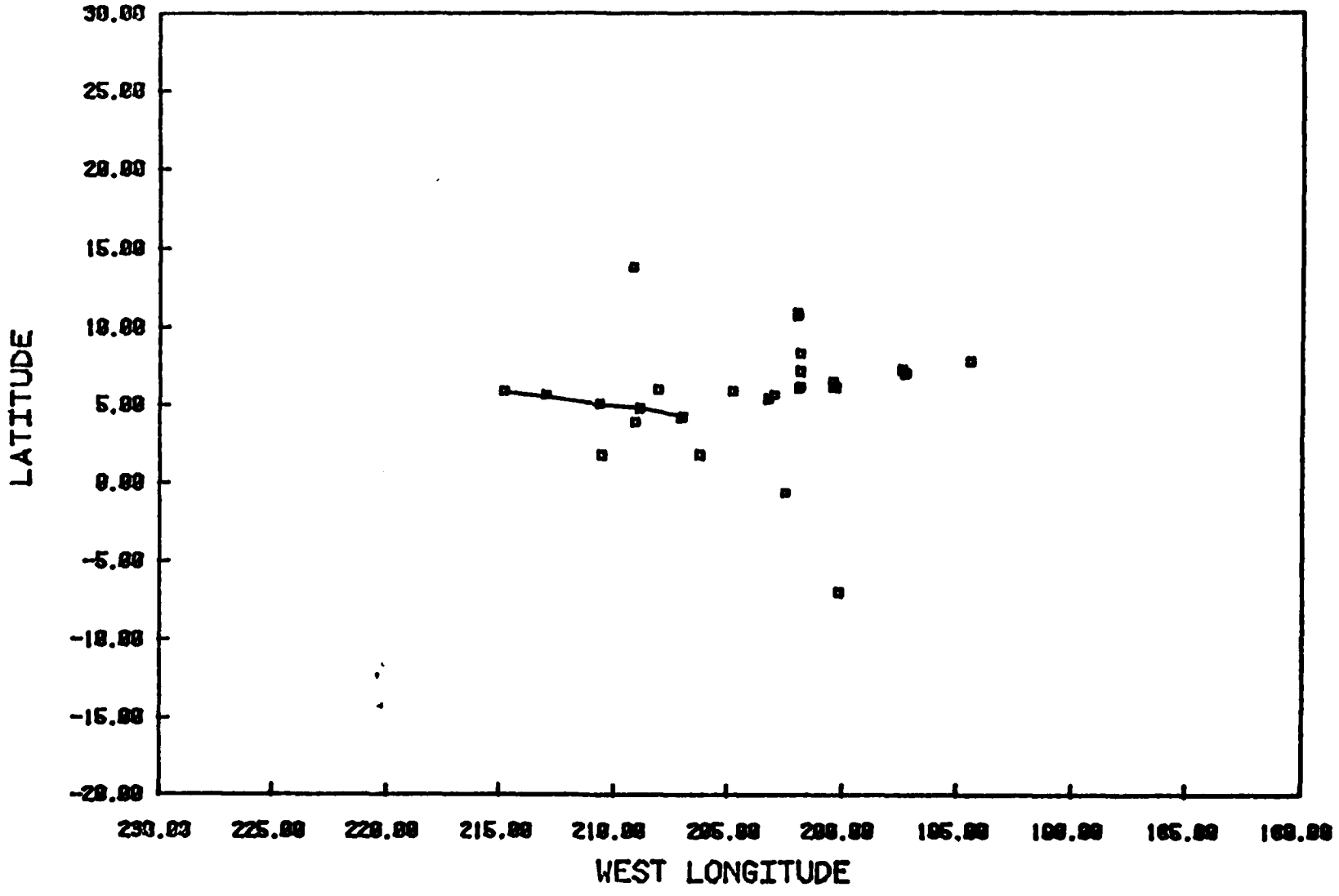

Figure 2-12. Potential correlation #11 (ORT1A/PAR1A).

Table 2-7 below summarizes the results of the backtracking Kalman filter on a correlation-by-correlation basis. Note that both Type 1 and Type 2 errors are mixed in with the set of correct correlations. No Type 3 errors were noted in either run.

Table 2-7. Summary of potential correlations constructed during Run #1.

Correl Number	Time	Data Point Number	Comments
1	.00000E+00 .00000E+00 .12000E+02 .24000E+02 .48000E+02 .48000E+02	22 20 23 24 25 21	Correct. Correlates Tracks #7 and #8.
2	.00000E+00 .00000E+00 .12000E+02 .24000E+02 .48000E+02 .48000E+02	20 22 23 24 21 25	Same as above. Note that data points were reordered due to coincidental time of report.
3	.00000E+00 .24000E+02 .36000E+02 .48000E+02 .48000E+02	20 7 8 21 9	Incorrect (Type 2 error).
4	.24000E+02 .24000E+02 .36000E+02 .36000E+02 .48000E+02 .48000E+02 .60000E+02	14 7 15 8 16 9 17	Incorrect (Type 1 error). Correlates Tracks #3 and #5, but leaves out Track #4.
5	.00000E+00 .24000E+02 .24000E+02 .36000E+02 .36000E+02	10 11 14 [illegible] 12 15	Correct. Correlates Tracks #3, #4, and #5.

Table 2-7. (Continued)

Correl Number	Time	Data Point Number	Comments
5	.00000E+00 .24000E+02 .24000E+02 .36000E+02 .36000E+02 .48000E+02 .48000E+02 .60000E+02	10 11 14 12 15 13 16 17	Incorrect (Type 1 error). Correlates Tracks #4 and #5, but leaves out Track #3.
7	.00000E+00 .24000E+02 .24000E+02 .24000E+02 .36000E+02 .36000E+02 .36000E+02 .48000E+02 .48000E+02 .48000E+02 .60000E+02	10 11 7 14 12 8 15 13 9 16 17	Same as Correlation 5. Note that data points were reordered due to coincidental time of report.
8	.00000E+00 .24000E+02 .24000E+02 .36000E+02 .36000E+02 .48000E+02 .48000E+02	10 11 7 12 8 13 9	Incorrect (Type 1 error). Correlates Tracks #3 and #4, but leaves out Track #5.
9	.12000E+02 .12000E+02 .24000E+02 .36000E+02 .48000E+02 .60000E+02	1 2 3 4 5 6	Correct. Correlates Tracks #1 and #2.
10	.12000E+02 .24000E+02 .36000E+02 .60000E+02	1 3 4 6	Incorrect (Type 2 error).
11	.12000E+02 .12000E+02 .24000E+02 .36000E+02 .48000E+02 .60000E+02	1 2 3 4 5 6	Same as Correlation 9. Note that data points were reordered due to coincidental time of report.

Note that in Table 2-7 each individual correlation consists of combinations of complete track files. For example, correlation 10 consists of data points {1, 26, 2, 27}, and we don't see correlations such as {1, 26, 2}. This particular problem structure is the defining characteristic of the track-to-track correlation problem. It arises because it is assumed that complete tracks (e.g., {1, 2} and {26, 27}) are constructed properly at the sensor level. (By contrast, in a sensor-level multitarget tracking problem, the key problem is to decide whether or not data points 1 and 2 are the same ship [1].)

The structure of the 0-1 integer program for k-track correlation can be illustrated by converting the potential correlations for Run #1 into the form of Equations (11) through (13), repeated here for convenience:

$$\max \; d^t \nu$$

subject to

$$B\nu \leq \mathbf{1}$$

ν binary .

For Run #1, this problem has the following form:

$$d = \begin{bmatrix} 130. \\ 130. \\ -1217. \\ 96. \\ 187. \\ 174. \\ 187. \\ 95. \\ 126. \\ -678. \\ 126. \end{bmatrix} \quad B = \begin{bmatrix} 0 & 0 & 0 & 0 & 0 & 0 & 0 & 0 & 1 & 1 & 1 \\ 0 & 0 & 0 & 0 & 0 & 0 & 0 & 0 & 1 & 0 & 1 \\ 0 & 0 & 1 & 1 & 1 & 0 & 1 & 1 & 0 & 0 & 0 \\ 0 & 0 & 0 & 0 & 1 & 1 & 1 & 1 & 0 & 0 & 0 \\ 0 & 0 & 0 & 1 & 1 & 1 & 1 & 0 & 0 & 1 & 0 \\ 0 & 0 & 0 & 0 & 0 & 0 & 0 & 0 & 0 & 0 & 0 \\ 1 & 1 & 1 & 0 & 0 & 0 & 0 & 0 & 0 & 0 & 0 \\ 1 & 1 & 0 & 0 & 0 & 0 & 0 & 0 & 0 & 0 & 0 \\ 0 & 0 & 0 & 0 & 0 & 0 & 0 & 0 & 0 & 0 & 0 \\ 0 & 0 & 0 & 0 & 0 & 0 & 0 & 0 & 0 & 0 & 0 \end{bmatrix}$$

Potential Correlation Number →

Track File Numbers ↓

The vector d has elements which correspond to the log-likelihood function (Equation (8)) for each potential correlation. Thus the first element of d is the numerical value of $\ell n\, p(\omega)$ evaluated at the last data point in Correlation 1.

Note that B is a 10x11 matrix (number of track files x number of potential correlations). B is made up of columns of zeros and ones, each column representing one particular correlation. For example, Column 1 in B represents Correlation 1, which consists of Tracks #7 and #8 (the 7th and 8th elements of the column are set to 1).

Closer examination of B reveals that the problem can be decomposed into a set of independent subproblems. By appropriately permuting columns of B, we have the equivalent matrix

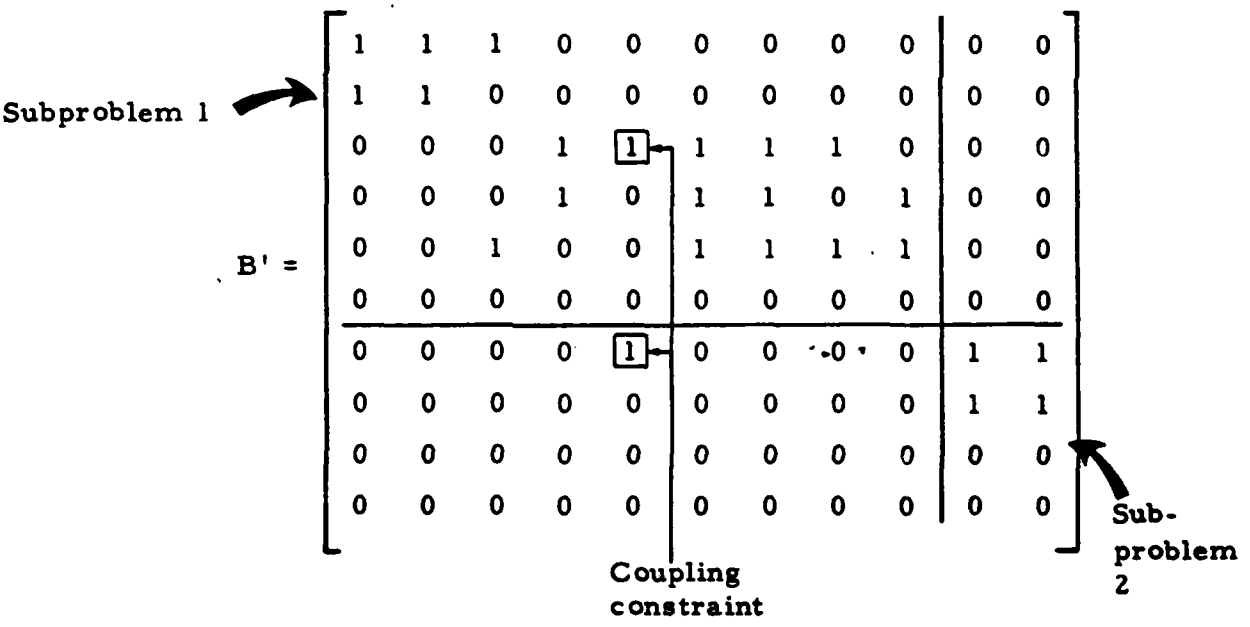

$$B' = \left[\begin{array}{cccccccccc|cc}
1 & 1 & 1 & 0 & 0 & 0 & 0 & 0 & 0 & 0 & 0 \\
1 & 1 & 0 & 0 & 0 & 0 & 0 & 0 & 0 & 0 & 0 \\
0 & 0 & 0 & 1 & \boxed{1} & 1 & 1 & 1 & 0 & 0 & 0 \\
0 & 0 & 0 & 1 & 0 & 1 & 1 & 0 & 1 & 0 & 0 \\
0 & 0 & 1 & 0 & 0 & 1 & 1 & 1 & 1 & 0 & 0 \\
0 & 0 & 0 & 0 & 0 & 0 & 0 & 0 & 0 & 0 & 0 \\
\hline
0 & 0 & 0 & 0 & \boxed{1} & 0 & 0 & 0 & 0 & 1 & 1 \\
0 & 0 & 0 & 0 & 0 & 0 & 0 & 0 & 0 & 1 & 1 \\
0 & 0 & 0 & 0 & 0 & 0 & 0 & 0 & 0 & 0 & 0 \\
0 & 0 & 0 & 0 & 0 & 0 & 0 & 0 & 0 & 0 & 0
\end{array}\right]$$

Thus B' is a decomposition of the original intersensor correlation problem into two subproblems, with one coupling constraint.

The structure of the problem is further reduced by column elimination. Let b^i be the i-th column of B. Then the j-th column of B can be eliminated if

$$b^i = b^j$$

and

$$d_i \geq d_j ,$$

where d_i is the i-th element of the cost vector d. Furthermore, the k-th column can be eliminated if $d_k \leq 0$. Finally, any row of zeros can be eliminated. Carrying out this process for B', we arrive at an integer program with maximum decoupling and minimum size (note that the coupling constraint was eliminated, and that Subproblem 1 was further decomposed):

Subproblem 1a

$$d'' = \begin{bmatrix} 126. \\ 95. \\ 187. \\ 96. \\ 174. \\ 130. \end{bmatrix}, \quad B'' = \left[\begin{array}{c|ccccc} 1 & 0 & 0 & 0 & 0 & 0 \\ \hline 1 & 0 & 0 & 0 & 0 & 0 \\ \hline 0 & 1 & 1 & 1 & 0 & 0 \\ 0 & 1 & 1 & 0 & 1 & 0 \\ 0 & 0 & 1 & 1 & 1 & 0 \\ \hline 0 & 0 & 0 & 0 & 0 & 1 \\ \hline 0 & 0 & 0 & 0 & 0 & 1 \end{array}\right]$$

Subproblem 1b

Subproblem 2

Application of these methods markedly decreases run time, which depends exponentially upon the size of B.

2.3 Algorithm Characteristics

The truth models and results of integer program processing for Runs #1 and 2 are shown graphically in Figures 2-13 through 2-16. As the figures indicate, in Run #1 the k-track correlation algorithm performed correctly. In Run #2, with sensors one order of magnitude less accurate (ratio of standard deviation of noise), one Type 1 error was made.

Note that the integer program is constrained to select from among the elements of potential correlation set D during the process of forming a complete picture of the surveillance area. Since Type 1, Type 2, and Type 3 errors can occur during the formation of the set D, the integer program is subject to errors of the same type.

The total run time requirement of the k-track correlation algorithm depends upon the run times of the two individual segments of the code: (1) the construction of potential correlations, and (2) the integer program. Of the two segments, the integer program is the most sensitive to program size. As Figure 2-17 indicates, the results for ten test cases indicate a reasonable growth in the back-tracking Kalman filter run time as the problem size increases. As Figure 2-18 indicates, the integer program exhibits a sustained exponential increase in run time as problem size increases. The underlying problem structure is such that the decoupling procedure mentioned in Section 2.2 above is critical for MSI problems where extremely large numbers of potential correlations are found.

In several cases, a suboptimal solution was returned by the integer program due to run time constraints placed on the code. In those cases where the maximum time limit resulted in a possibly sub-optimal solution, good accuracy was obtained. Thus it appears that good suboptimal solutions to the integer program can be obtained within a reasonable period of time for the types of data bases discussed in this paper.

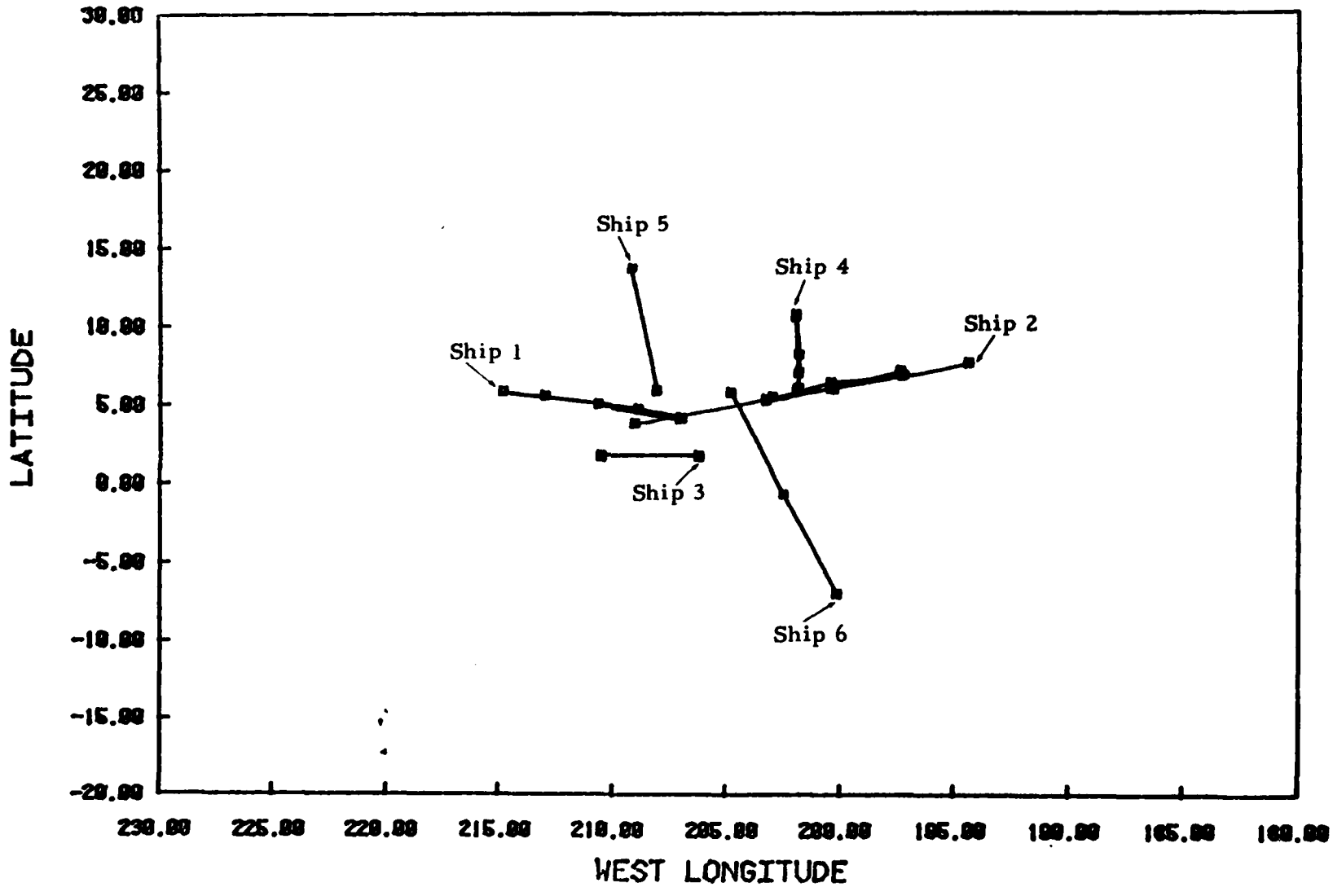

Figure 2-13. Actual tracks contained in synthetic data base ORT1A.

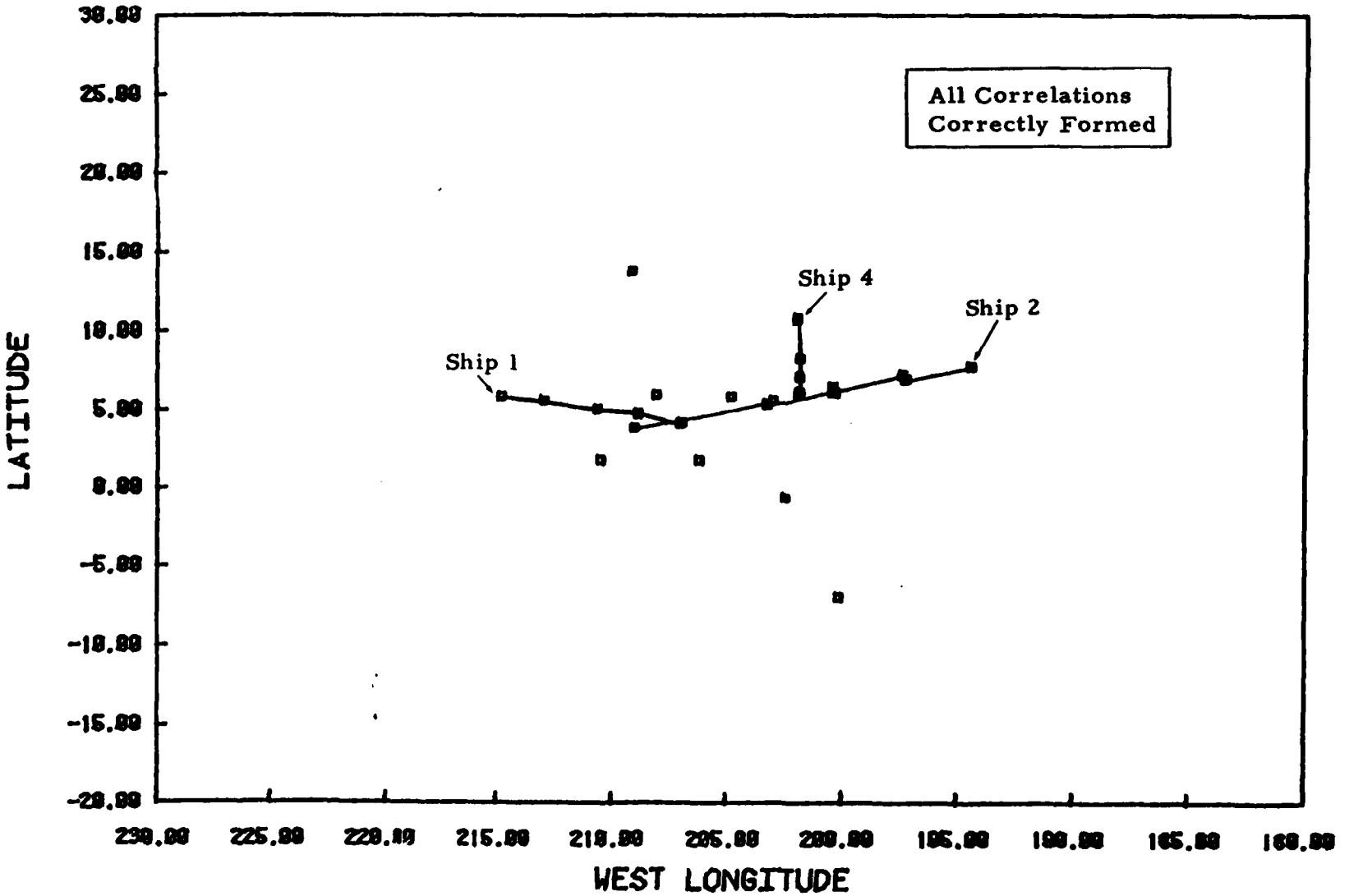

Figure 2-14. Correlated tracks produced by integer program (ORT1A/PAR1A).

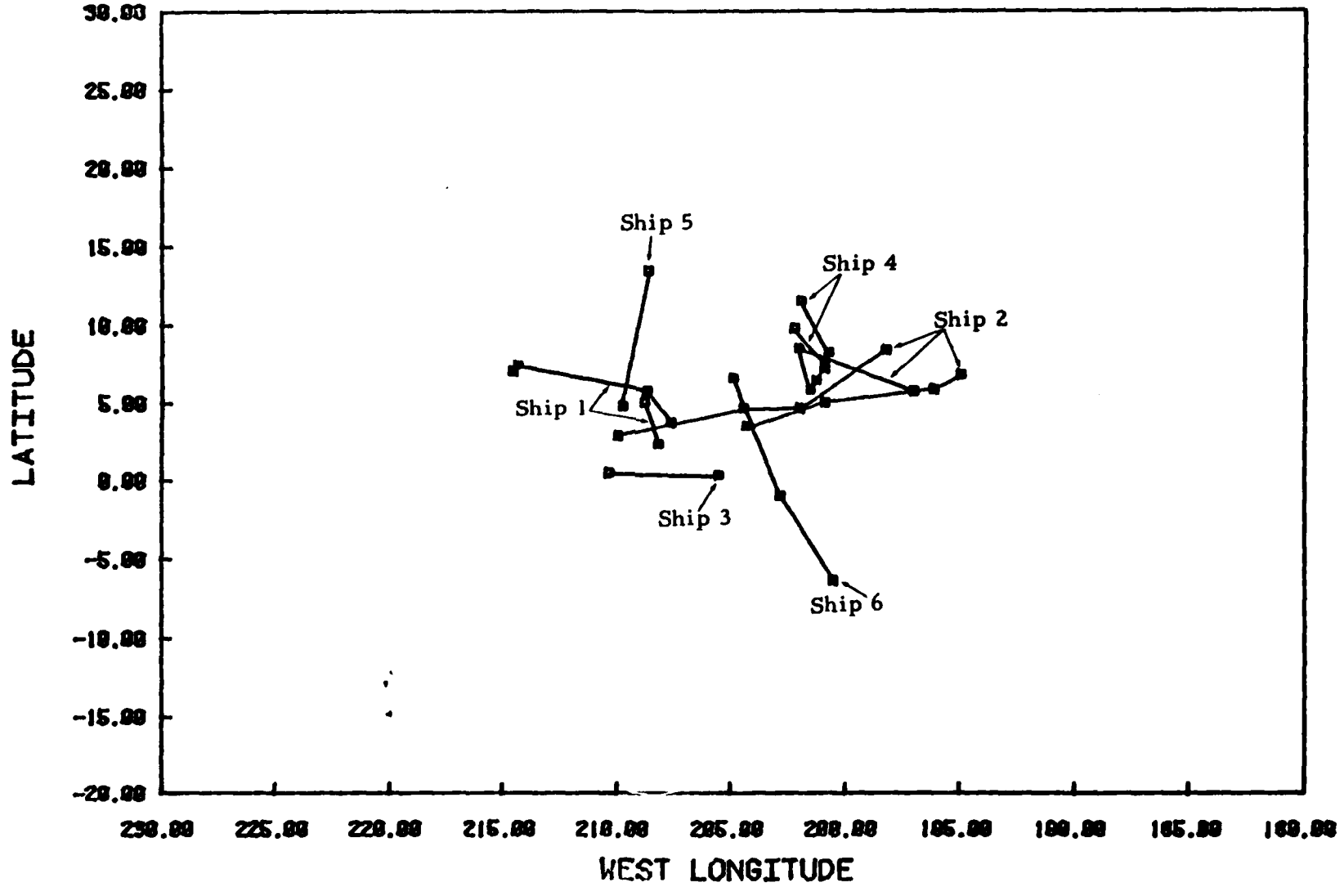

Figure 2-15. Actual tracks contained in synthetic data base ORT1B.

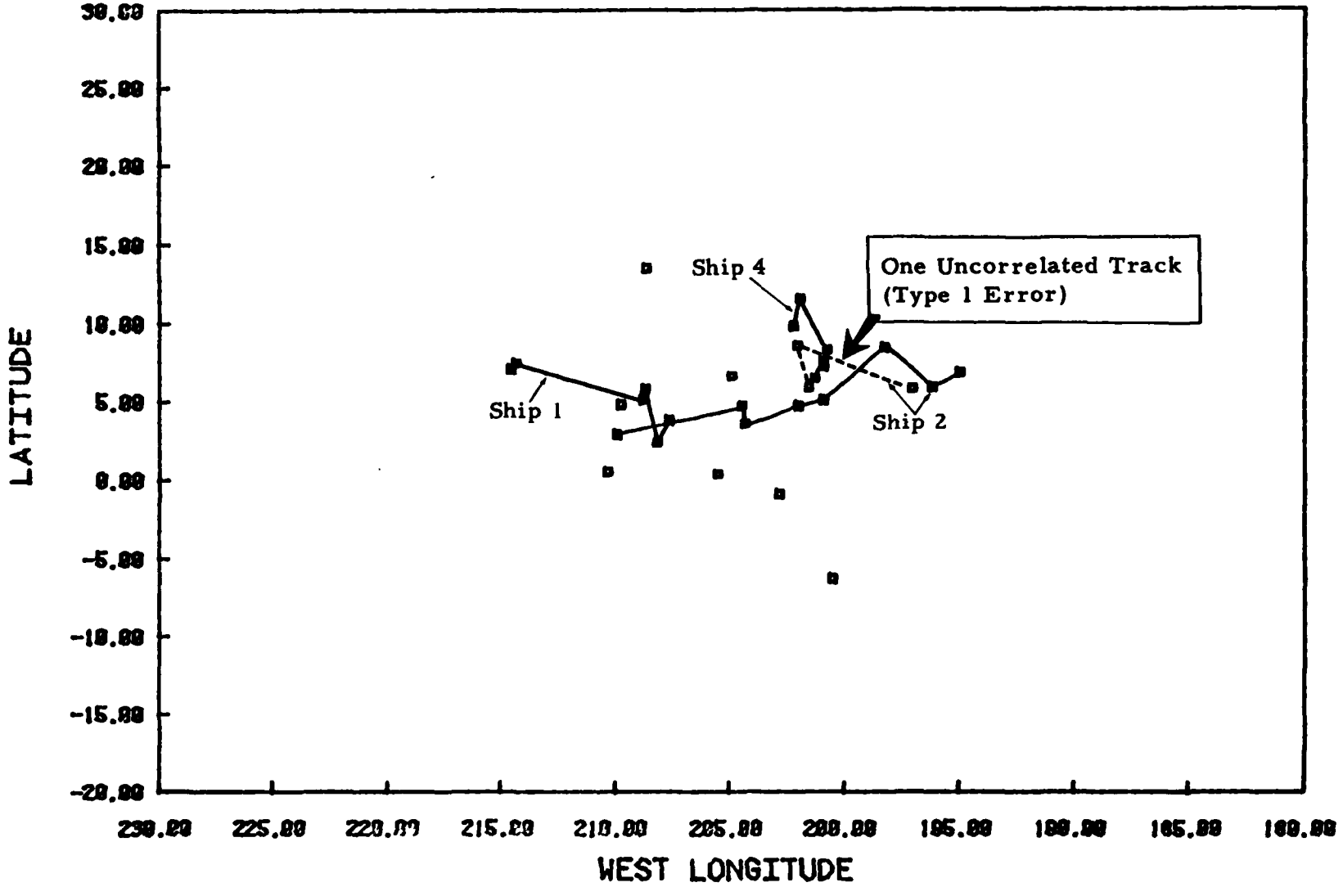

Figure 2-16. Correlated tracks produced by integer program (ORT1B/PAR1B).

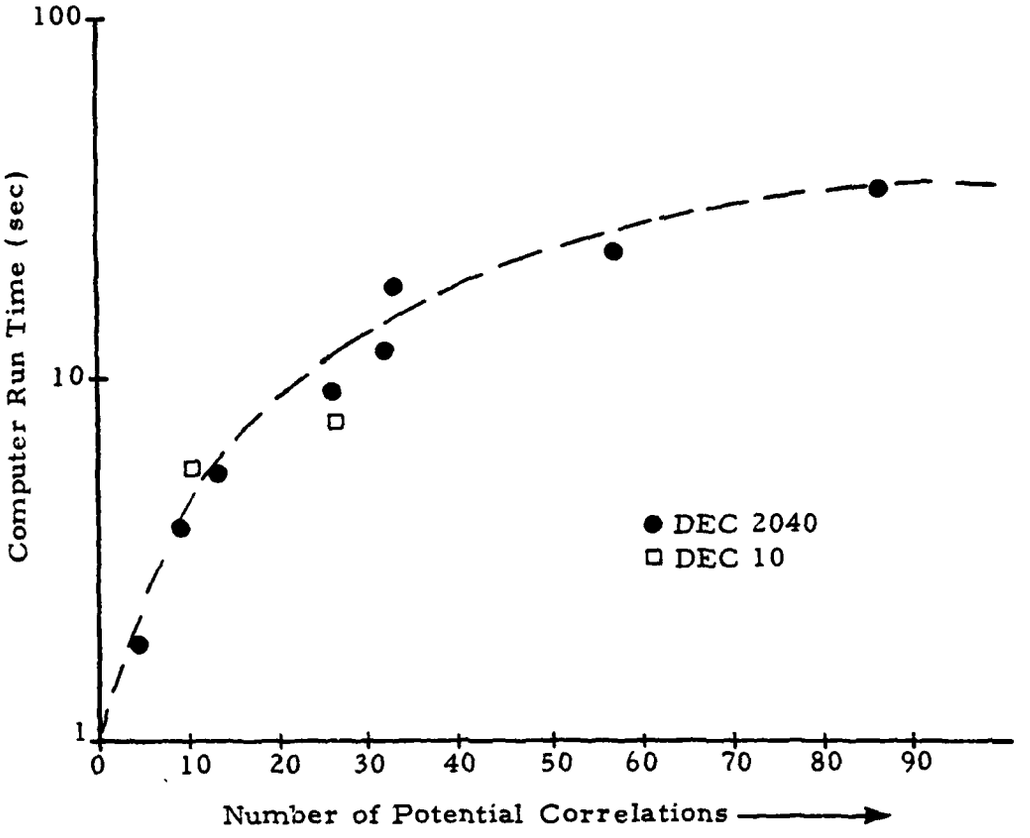

Figure 2-17. Run times for construction of set of potential correlations.

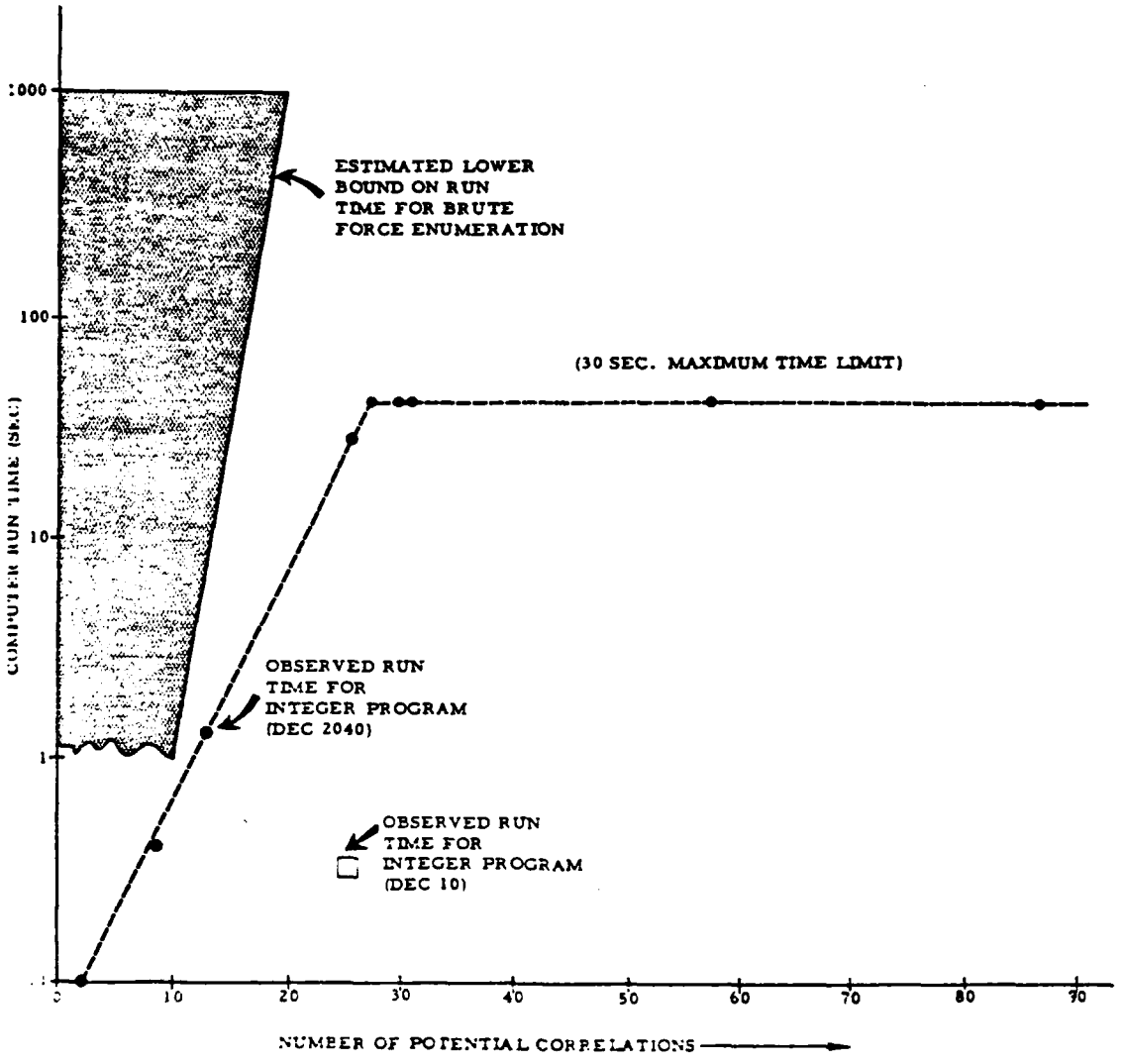

Figure 2-18. Run times for solution of Bayesian decision problem.

3.0 CONCLUSIONS

This paper summarizes a study which consisted of essentially two parts:

- initial development of a sophisticated intersensor (track-to-track) correlation algorithm
- preliminary analysis of the algorithm's characteristics when applied to synthetic data.

The primary finding of the paper is that an accurate picture of a large ocean surveillance area can be constructed automatically by the k-track correlation algorithm. This finding is substantiated by the analysis of synthetic data discussed in Section 2.

The structure of the algorithm is that of a Bayesian decision process, which by its very nature may produce some errors in the analysis of any particular data base. As noted above, these errors were minimal for the analysis performed herein. There is a critical need for parameter tuning against truth models before the algorithm can be trusted in an operational situation. Thus it is clear that substantial work remains before the promising results obtained during this short preliminary study can be broadly applied.

In the area of track-to-track correlation algorithm development, there remains a number of important issues yet to be resolved. A few of these are as follows:

- How large a problem can the integer program handle in real time after the decoupling procedure mentioned in Section 2.2 is implemented?
- Using the k-track correlation algorithm as a benchmark, how accurate are simpler suboptimal correlation algorithms (such as the pairwise algorithm mentioned in Section 1.2)?

- What is the impact on algorithm accuracy of Kalman filter mismatch (i.e., a mismatch between actual and assumed sensor accuracy)?
- What is the feasible operating regime for track-to-track correlation algorithms in terms of ship density?
- How sensitive is algorithm accuracy to intersensor bias? How accurately can intersensor alignment be carried out? Can we "bootstrap" the alignment as track-to-track correlation is carried out?
- What is the proper balance between real-time track-to-track correlation accuracy and the load on surveillance network communication links (how much data is enough for a given surveillance area)?

This partial list of important MSI issues yet to be resolved can of course be substantially expanded. Hopefully, the results of this short preliminary study of one specific correlation algorithm will resolve some of the complex issues surrounding automatic, accurate, real-time ocean surveillance.

REFERENCE

[1] C. L. Morefield, "Application of 0-1 Integer Programming to Multitarget Tracking Problems," IEEE Trans. Auto. Contr., Vol. AC-22, June, 1977, pp. 302-312.


DAT
FILM
5